Dissertation
submitted to the
Combined Faculties for the Natural Sciences and for Mathematics
of the Ruperto-Carola University of Heidelberg, Germany
for the degree of
Doctor of Natural Sciences

presented by

M.Sc, Ximing Ding
born in Dalian, China
Oral examination: 18. 12. 2017

Aging of human bone marrow – functional and epigenetic changes in senescent mesenchymal stromal cells

Referees: Dr. Judith B. Zaugg

Prof. Dr. Michael Boutros

Abstract

Aging is a complex process that is associated with changes in many parts of the body over the lifespan of an individual. In this work, various aspects of aging in the human bone marrow were investigated.

As the regenerative power of a tissue is linked to the potential of its stem cells to replace the accumulated damages, the aging process in somatic stem cells was studied focusing on the influence of the niche in regulating stem cell aging. The hematopoietic stem cells (HSC) together with elements that constitute the bone marrow niche were investigated as a model for somatic stem cell aging as HSCs are accessible in healthy human individuals. The subjects ranged from 20 to 60 years with a median age of 33.2 years.

From each bone marrow sample, the $CD34^+$ population as HSCs and four other cell subpopulations, lymphocytes and precursors (LYM), monocytes/macrophages precursors (MON), granulocytic (GRA), and erythroid precursors (ERP) were isolated by flow cytometry. The mesenchymal stromal cells (MSC) were isolated by *in vitro* culture. We found that the relative proportions, cell size as well as cell granularity of the major bone marrow constituents did not correlate with the biological age of the donors. However, further downstream analysis indicated that age-associated changes were prominent on protein level in HSCs as well as in other cell types of the niche such as MSCs.

The interactions between the HSCs and the niche were studied *in vitro* using a co-culture system of $CD34^+$ cells and mesenchymal stromal cells (MSC). As previous studies indicated that the supportive function of MSCs as well as their differentiation potentials towards adipocytes and osteocytes change significantly with age, we have examined the supportive ability of the undifferentiated MSCs versus adipogenically differentiated MSCs (ADI-MSCs) and osteogenically differentiated MSCs (OST-MSCs) for HSCs. We showed that MSCs, ADI-MSCs and OST-MSCs were able to support the proliferation of HSCs and maintain their primitive immunephenotype. Compared to undifferentiated MSCs and OST-MSCs, the co-culture with ADI-MSCs increased the proliferation of HSCs much stronger while still maintaining the HSCs at a high expression level of CD34.

As the impact of the MSCs on HSCs might be caused by epigenetic changes, the aging-associated alterations in the marrow niche were studied at the chromatin level. To this end, changes in chromatin accessibility were studied in MSCs by ATAC-seq. After establishing the protocol for performing ATAC-seq using primary MSCs, we studied the MSC samples derived from 16 healthy human subjects of different ages between 21 and 59 years. A set of 122,884 ATAC-seq peaks was identified. We have demonstrated that donor age is associated with alterations in open chromatin profiles. Moreover, at a false discovery rate of 5%, we could identify 4,579 differential chromatin accessible sites upon aging. A functional analysis of these sites showed enrichment of cell development and differentiation processes. Additionally, genes of the hippo signaling pathway, TGF-beta signaling pathway, cancer pathways and cell adhesion pathways were also found to be enriched. A motif enrichment analysis suggested that TATA box motifs and binding sites for transcription factors TFAP2C, KLF16, HIC1.p2, WT1 and MTF.p2 were enriched in promoter regions of differential chromatin accessible sites upon aging.

In conclusion, this study showed that the interplay with the stem cell niche controls HSC functions. The differentiation of MSCs affects the proliferation and stemness of HSCs *in vitro*. Furthermore, we have demonstrated that aging is associated with chromatin accessibility alterations in MSCs, which provides a foundation for further in-depth mechanistic analyses.

Zusammenfassung

Der Alterungsprozess ist ein komplexer Vorgang, der mit Änderungen in vielen Körperteilen im Laufe des menschlichen Lebens assoziiert ist. In der folgenden Arbeit wurden verschiedene Aspekte des Alterungsvorgangs im menschlichen Knochenmark untersucht.

Da die regenerative Kraft eines Gewebes verbunden ist mit dem Potential seiner Stammzellen, die angehäuften Schäden zu ersetzen, wurde der Alterungsprozess somatischer Stammzellen untersucht mit dem Fokus auf den Einfluss der Nische, die Stammzellalterung zu steuern. Aufgrund der Zugänglichkeit in gesunden Menschen wurden die hämatopoetischen Stammzellen zusammen mit anderen Bestandteilen der Knochenmarknische als ein allgemeines Modell für den Alterungsprozess somatischer Stammzellen untersucht. Die Probenspender waren im Alter von 20 bis 60 Jahren mit einem medianen Alter von 33.2 Jahren.

Für jede Knochenmarkprobe wurden die $CD34^+$ hämatopoetischen Stammzellen (HSC) und vier andere Zellpopulationen, Lymphozyten und Vorläufer (LYM), Monozyten/Makrophagen und Vorläufer (MON), Granulozytische (GRA) und erythroide Vorläufer (ERP) mittels Durchflusszytometrie isoliert. Die mesenchymalen Stromazellen (MSC) wurden durch *in vitro* Kultur isoliert. Wir fanden heraus, dass die relativen Anteile, Zellgröße sowie Zellgranularität der Knochenmarkbestandteile nicht mit dem biologischen Alter der Spender korrelierten. Weitere nachfolgende Analysen zeigten jedoch, dass die altersassoziierten Änderungen auf Proteinebene prominent waren, sowohl in HSCs als auch in anderen Zelltypen der Nische, wie zum Beispiel in MSCs.

Die Wechselwirkungen zwischen den hämatopoetischen Stammzellen und der Nische wurden in vitro untersucht mittels eines Kokultur-Systems bestehend aus $CD34^+$ hämatopoetischen Stammzellen und mesenchymalen Stromazellen. Da frühere Studien zeigten, dass sich sowohl die supportive Funktion als auch das adipogene und osteogene Differenzierungspotential der MSCs signifikant mit dem Alter ändern, wurden die supportiven Fähigkeiten der unbehandelten MSCs im Gegensatz zu adipogen-differenzierten MSCs (ADI-MSC) und osteogen-differenzierten MSCs (OST-MSC) untersucht. Wir konnten zeigen, dass MSCs, ADI-

MSCs und OST-MSCs sowohl die Proliferierung als auch den Erhalt des primitiven Immunphänotyps der HSCs unterstützten. Verglichen mit unbehandelten MSCs und OST-MSCs, hob die Kokultur mit ADI-MSCs die Proliferierung der HSCs viel stärker an während die Expression des CD34 Antigens gleichzeitig hoch blieb.

Da die Auswirkung der MSCs auf HSCs von den epigenetischen Änderungen erzeugt werden könnte, wurden die altersassoziierten Änderungen in der Knochenmarknische auf Chromatinebene untersucht. Die Änderungen der offenen Chromatin-Zugänglichkeit in MSCs wurden mittels ATAC-Sequenzierung (ATAC-seq) erforscht. Nach der Anpassung des Protokolls wurden MSC proben aus 16 gesunden Menschen unterschiedlichen Alters zwischen 21 und 59 Jahren analysiert. Aus dem erzeugten Datensatz wurde eine Reihe von 122.884 ATAC-seq Peaks identifiziert. Wir zeigten, dass das Spenderalter assoziiert war mit den Änderungen in den offenen ATAC-seq Chromatinprofilen. Außerdem konnten wir 4.579 altersdifferenzielle ATAC-seq Peaks mit einer False Discovery Rate von 5% identifizieren. Eine funktionale Anreicherungsanalyse der altersdifferentiellen ATAC-seq Peaks zeigte, dass Zellentwicklung und Differenzierungsprozesse angereichert waren. Zusätzlich waren die Gene der Hippo und TGF-beta Signalwege sowie Krebs- und Zelladhäsionssignalwege angereichert. Eine Motivanreicherungsanalyse deutete darauf hin, dass die TATA-box Motive und Bindungsstellen für Transkriptionsfaktoren TFAP2C, KLF16, HIC1.p2, WT1 sowie MTF.p2 in Promotorregionen der altersdifferentiellen Peaks angereichert waren.

Zusammenfassend zeigte diese Studie, dass das Zusammenspiel mit der Stammzellnische die HSC Funktionen steuert. Die Differenzierung der MSCs beeinflusst die Proliferierung und Stammzellfähigkeit der HSCs *in vitro*. Des weiteren zeigten wir, dass der Alterungsprozess assoziiert ist mit Änderungen der Chromatin-Zugänglichkeit in MSCs, was eine Grundlage für weitere mechanistische Analysen darstellt.

Acknowledgement

First of all, I would like to thank Drs. Anne-Claude Gavin and Anthony D. Ho for the supervision of my PhD project.

I would like to thank Dr. Anne-Claude Gavin for her guidance and inspiring enthusiasm in science. I have learnt a great deal from her.

I would like to thank Prof. Anthony D. Ho for enabling me to work on such an exciting and interdisciplinary project. I am grateful to his constant support and motivation.

I would like to express my gratitude to Dr. Judith Zaugg for reviewing this thesis and serving on the Thesis Advisory Committee over the years.

I would like to thank Prof. Michael Boutros for taking care of my PhD project from the University side by reviewing this thesis and serving on my Thesis Advisory Committee.

I would like to thank Dr. Wolfgang Huber and Prof. Jan Lohmann for their interests in this work and for getting on board with my Thesis Defense Committee.

I would like to thank the other members of my Thesis Advisory Committee, Drs. Martin Beck and Alexander Aulehla for their very helpful scientific discussions.

The group of Prof. Ho at University Hospital Heidelberg provided a wonderful niche to study stem cells. I would like to thank Patrick for the introduction into the fascinating field of stem cell biology. Rainer is a good friend who helped me a lot both scientifically and privately. Anke provided particularly a great support both in the lab and privately. A thank you goes to Angela who gave me many good advices based on her long years' experience. Dr. Eckstein was always happy to share his knowledge on flow cytometry.

I would like to thank all the past and present members of the Gavin laboratory. Special thanks go to the SystemAge team: Marco has taught me a great deal about mass spectrometry. Fei and Noorie have been close companions on this journey. I would like to thank Matt for reading though my thesis and teaching me how to perform network analysis. Many special thanks go to Cihan who read my thesis and

gave me many great ideas. I’d like to thank Joanna, Charlotte, Katharina, Enric and Antonella for providing a wonderful working atmosphere in the lab.

I would like to thank Mariana from the Zaugg group for great collaboration on the ATAC-seq project. I also enjoyed the inspiring scientific discussions with Ivan and Christian.

I would like to thank members of the EMBL FACS Core Facility, Drs. Alexis Perez Malte Paulsen for sharing with me their expertise in flow cytometry.

I would like to thank the EMBL Genome Core Facility, Dr. Vladimir Benes and Paul Collier for their support in the ATAC-seq part of my project.

The past four years have passed in the blink of an eye. Looking back, there were good times, there were hard times, but there were never bad times. I was fortunate to get supported by so many great friends both at EMBL and at University Hospital. I am deeply grateful to that.

Finally I would like to thank my parents for their unconditional support of my PhD work.

Table of Contents

1. Introduction

1.1 Outline of the thesis

Bone marrow is the site of blood formation in postpartum human life. The hematopoietic stem cells (HSCs) residing in the bone marrow are supported and regulated by the surrounding microenvironment of the bone marrow. As the regeneration of the blood system is linked to the potential of HSCs to replace the corresponding damaged cells and tissues, one could argue that the blood system is as old as its stem cells (Ho *et al.*, 2005).

In this thesis, my goal is to investigate the molecular signatures of aging in the hematopoietic stem cell niche:

(1) Characterize relative quantitative and morphologic changes upon aging in the major constituents of the human bone marrow using flow cytometry.

(2) Study interactions between hematopoietic stem cells and aged stem cell niche using an *in vitro* niche model.

(3) Define the chromatin accessibility landscape underlying aging stem cell niche using ATAC-seq.

This work was performed in the research groups of Prof. Anthony D. Ho and Dr. Anne-Claude Gavin. The ATAC-seq project was performed in collaboration with the research group of Dr. Judith Zaugg.

The “Introduction” chapter describes the background of the thesis, where biological concepts relevant for this study are first introduced. As an integral part of the thesis, chromatin accessibility and its recent profiling methods are also discussed in the context of aging.

In the chapter “Materials and Methods”, all experiments performed in this study are depicted, including optimizations or adaptions, which differ from the standard protocols.

In chapter “Results”, I first illustrate the alterations in the major constituents of the bone marrow with age from flow cytometry data. I then demonstrate interactions between HSCs and the niche *in vitro* using a co-culture system of HSCs and undifferentiated MSCs, adipogenically differentiated MSCs and osteogenically differentiated MSCs. Lastly, I studied the changes in the epigenetic landscape of the aging MSCs using ATAC-seq. Genome-wide profiles and findings for variations in chromatin accessibility are presented and discussed.

In “Discussion and Outlook”, the significance of our results in relationship to those of other authors in the literature is deliberated. The relevant conclusions that we can derive from our results are discussed. Potentials for further analysis and future research work are proposed with the aim to obtain a more holistic understanding of the aging process both in HSCs as well as in the bone marrow niche.

1.2 The human bone marrow and hematopoiesis

In adult humans, bone marrow is the site of blood formation (hematopoiesis). The bone marrow can be divided into red and yellow marrow (Bain *et al.*, 2009). The red marrow contains predominantly hematopoietic cells whereas the yellow marrow is largely adipose tissue. The ratio between hematopoietic cells to fat has been used to estimate bone marrow cellularity. This ratio decreases with age. In newborns, virtually the entire bone cavity is filled by red marrow. With age, the ratio between red and fatty marrow is gradually shifted in favor of the latter. Despite this general observation, there is considerable individual variability in the distribution of red and yellow marrow (Hashimoto, 1962). According to the demand for production of blood cells, the red marrow can expand. In addition to the hematopoietic cells, the bone marrow also consists of many stromal and supportive elements such as mesenchymal cells, fibroblasts, osteocytes and adipocytes. Together with the hematopoietic stem and progenitor cells, these cellular subpopulations constitute the so-called hematopoietic stem cell compartment which is responsible for the maintenance and regulation of hematopoiesis.

1.3 Hematopoietic stem cell compartment

The hematopoietic compartment consists of hematopoietic stem cells (HSC) and their progenitors, as well as cells of the bone marrow microenvironment referred to as the niche. The interactions between stem cells and the niche are important for the maintenance of biological functions in the bone marrow.

1.3.1 Hematopoietic stem and progenitor cells

Hematopoietic stem cells (HSC) are multipotent, thus they can maintain their cell number by proliferation as well as differentiate into all functional cell types of the blood (Seita *et al.*, 2010). This unique characteristic of stem cells, *i.e.* both self-

renewal and differentiation is achieved by a precise regulation of asymmetric versus symmetric divisions of the cells (Ho *et al.*, 2007; Seita *et al.*, 2010). The division into two daughter cells both with stem cell characteristics is called symmetrical division whereas the asymmetrical division results in one daughter cell with stem cell characteristics and the other one destined to give rise to more mature progenitors with subsequently more limited self-renewal capacity (Ho *et al.*, 2007; Seita *et al.*, 2010). After a number of divisions, mature and functional erythrocytes, monocytes and granulocytes, and megakaryocytes are derived from the common myeloid progenitors. The lymphoid lineage differentiation leads to the formation of T- , B-lymphocytes and natural killer cells (Seita *et al.*, 2010) (Figure 1).

The existence of HSCs in the bone marrow was first proven by Till and McCulloch in the early 1960s. In a mouse transplantation assay, they could observe that some bone marrow cells injected into irradiated mice could form proliferating colonies in the spleen (Till *et al.*, 1961). Some of these cells were able to build up the entire blood system when they were injected into secondary hosts in serial transplantation models (Siminovitch *et al.*, 1963).

The isolation and characterization of HSCs are commonly based on the cluster of differentiation (CD) antigens expressed on the cell surface. The surface antigen CD34 is currently the most important marker to characterize human HSCs (Civin *et al.*, 1984; Katz *et al.*, 1985). CD34 represents a surrogate marker for a population that is enriched for hematopoietic stem and progenitor cells with a significant percentage of HSCs (Giebel *et al.*, 2008). The $CD34^+$ cell population is, for the purpose of this study, defined as HSC (Figure 1).

Due to the fact that CD34 enriched cell population is heterogeneous, additional markers such as CD38 are frequently used to identify more primitive stem cell populations (Sutherland *et al.*, 1989; Weilbaecher *et al.*, 1991; Petzer *et al.*, 1996). In addition to the expression of cell surface markers, HSCs can also be characterized based on their division kinetics. Wagner *et al.* and Huang *et al.* examined the immunephenotypes of slow and fast dividing HSCs which were both derived from the $CD34^+/CD38^-$ population and could show that HSC stemness was associated with the slow dividing cell population (Huang *et al.*, 1999; Wagner *et al.*, 2004).

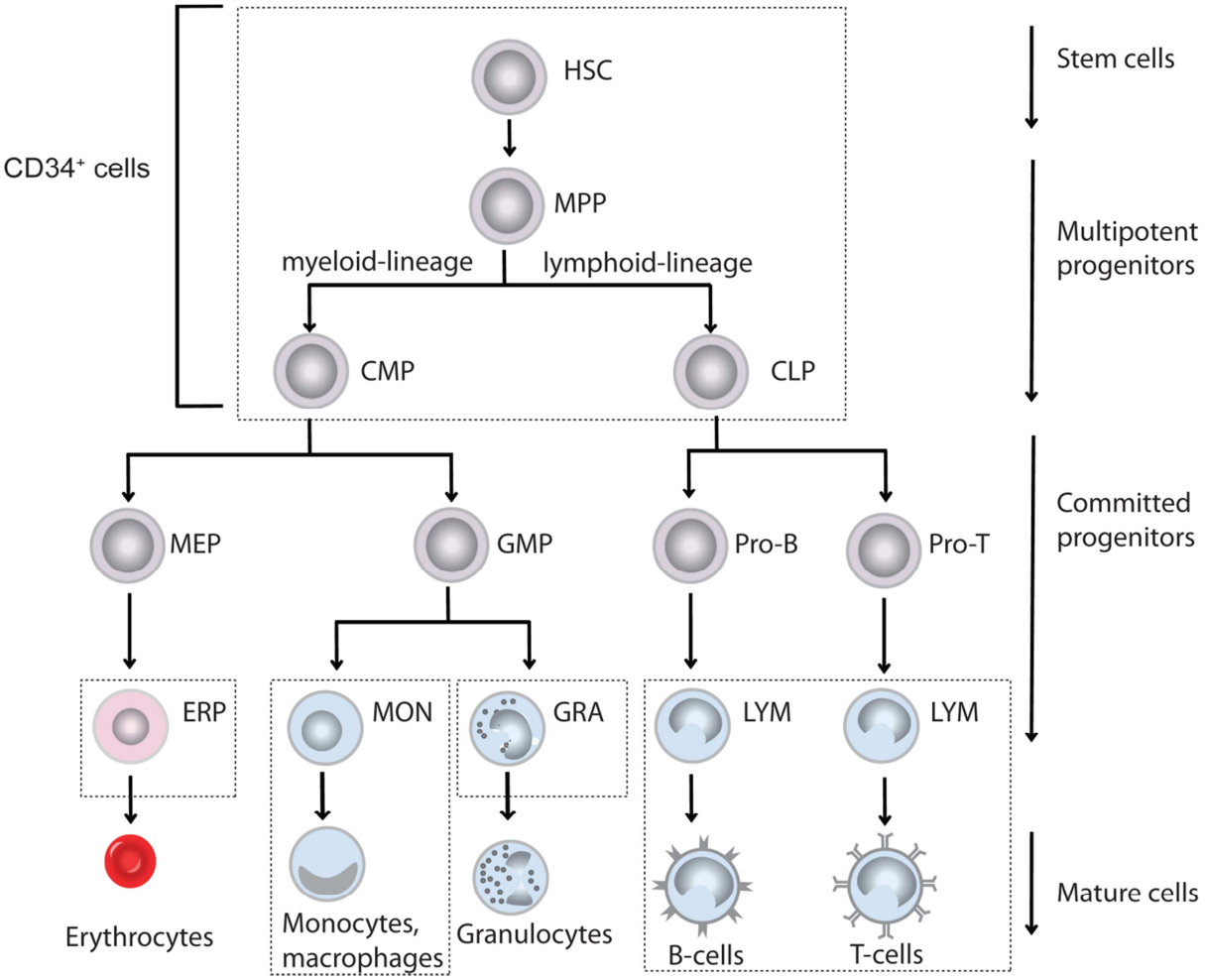

Figure 1 A simplified overview of human hematopoiesis. Hematopoietic stem and progenitor cells give rise to both the myeloid and lymphoid lineages of blood cells. HSC, hematopoietic stem cell; MPP, multipotent progenitor; CMP, common myeloid progenitor; CLP, common lymphoid progenitor; MEP, megakaryocyte and erythroid progenitor; GMP, granulocyte−macrophage progenitor; Pro-B, pro-B cell; Pro-T, pro-T cell; ERP, erythroid precursors; MON, monocytes, macrophages and restricted precursors; GRA, granulocytic precursors; LYM, lymphocytes and restricted precursors. Cell types isolated and studied in the course of the project are marked by dashed boxes. Figure was adapted from Larsson *et al.* (Larsson *et al.*, 2005).

1.3.2 The hematopoietic stem cell niche

The bone marrow niche provides a specialized microenvironment for the regulation of HSCs (Nakamura-Ishizu *et al.*, 2014). The interactions between the stem cells and the niche are mainly based on three mechanisms: signaling through cytokines, direct cell-cell interactions and contacts to the extracellular niche matrix (Moore, 2006).

The concept of stem cell niche was first proposed by Schofield as physiologically constrained microenvironment in which the stem cells reside (Schofield, 1978). In the bone marrow, precursor cells of both lymphoid and myeloid lineages as well as stromal cells play important roles in the regulation of HSC fate (Wilson *et al.*, 2006). In the present study, the entire population of the bone marrow mononuclear cells (cells with single nucleus) was isolated as constituents of the HSC niche. This includes lymphocytes and restricted precursors (LYM), monocytes, macrophages and restricted precursors (MON), granulocytic precursors (GRA) and erythroid precursors (ERP). In addition to the hematopoietic cells, one major component of the bone marrow supportive stroma mesenchymal stromal cells (MSCs) were isolated and expanded by *in vitro* culture.

Results derived from animal models showed that *in vivo*, the hematopoietic compartment can be functionally separated into two types – the endosteal (also called as osteoblastic) niche and the perivascular niche (Nakamura-Ishizu *et al.*, 2013). The endosteal niche is located close to the endosteum of the bone with low oxygen and nutrient supply. The major constituents of the niche are osteoblasts and mesenchymal stromal cells, which are osteoblast precursors (Nakamura-Ishizu *et al.*, 2013). The osteoblasts secrete a number of cytokines including M-SCF, RANKL, Il7 and c-FMS regulating the lymphoid and osteoclast development. A subpopulation of the osteoblasts expressing cell adhesion protein N-cadherin (spindle-shaped N-Cadherin^{+} CD45^{-} osteoblastic cells, SNO) maintains the quiescent state of HSCs by cell-cell contacts (Zhang *et al.*, 2003). The vascular niche is located close to the blood vessels. It mainly consists of endothelial cells of sinusoidal vessels, which support the proliferation and differentiation of HSCs (Kopp *et al.*, 2005). HSCs in the vascular niche are subjected to high oxygen and nutrient concentrations. Due to its close proximity to the vascular system, the vascular niche probably also supports the trans-endothelial migration of HSCs from the bone marrow into the perivascular blood system (Lapidot *et al.*, 2005).

1.3.3 HSC homing and mobilization

Albeit the HSCs principally reside in the bone marrow, they might migrate from the bone marrow niche to the peripheral blood system. The natural release of HSCs into the peripheral blood can occur as response to blood loss, inflammation or injury induced by chemotherapy or irradiation (Lapidot *et al.*, 2005). *Vice versa*, the migration of HSCs from the circulation back to the bone marrow niche is called homing. The processes of homing and mobilization are regulated by mechanisms of reversible cell-cell contacts and trans-endothelial migration (Lapidot *et al.*, 2005). The most well-studied mechanism in the processes of HSC homing and mobilization is the interaction between the cytokine SDF-1 (stromal cell-derived factor 1) with its receptor CXCR4. The osteoblasts and stromal cells of the bone marrow niche secrete SDF-1 into the blood system. This signal is sensed by HSCs through the CXCR4 receptors on the cell surface. Along the increasing concentration gradient of SDF-1, the HSCs are able to migrate back into the bone marrow (Lapidot *et al.*, 2005). The trans-endothelial migration of the HSCs through the blood-marrow barrier is enabled by a group of adhesion proteins such as selectin E and P, integrin alpha 4 and 5, lFA1 (lymphocyte function-associated antigen-1), CD44 and the Rho GTPase Rac 1 and 2 (Kopp *et al.*, 2005; Lapidot *et al.*, 2005).

The HSCs can be mobilized into the peripheral blood by stress such as at the time of recovery after chemotherapy. The mobilization could be induced by the compound G-CSF (granulocyte-colony stimulating factor) which activates the cleavage of SDF-1 by proteases such as elastase, cathepsin G, MMP-2 and MMP9 (Jansen *et al.*, 2005). The CXCR4 antagonist AMD3100 is also capable of inducing migration of the HSCs in the bone marrow (De Clercq, 2003). The understanding of the mobilization and homing processes has led to advancements in clinical stem cell transplantation techniques. HSCs used for transplantation treatments against leukemia were initially isolated from the bone marrow. Since 1985, the sampling of HSCs for clinical stem cell transplantations has been primarily isolated from mobilized peripheral blood due to better treatment effects resulting in better reconstitution of the bone marrow (Ho *et al.*, 2000). Within a decade, mobilized peripheral blood has replaced bone marrow for the vast majority of autologous transplant procedures (Ho *et al.*, 2000).

1.3.4 Aging of the human hematopoietic stem cell compartment

The regenerative potential of a tissue decreases upon aging. For the blood system, the regeneration depends on the hematopoietic stem cell compartment in the bone marrow (Ho *et al.*, 2005; Wagner *et al.*, 2009). Aging is a gradual and cumulative process which varies between individuals, the most commonly observed phenotypes associated with physiological aging focus on the primitive hematopoietic stem cell (HSC) population (Geiger *et al.*, 2013) (Figure 2).

It was observed based on studies mostly in mouse models and a few in humans that the number of HSCs identified with cell surface markers increased by two- to ten-fold in aged human bone marrows (Rossi *et al.*, 2005; Chambers and Goodell, 2007; Beerman *et al.*, 2017). Some of the authors suggested that the increase in HSC number might counteract the functional decline of an aged blood system by a higher level of blood cell regeneration. Experimental data could not, however, support this hypothesis. Mouse transplantation assays demonstrated that aged HSCs exhibited a diminished regenerative potential (Sudo *et al.*, 2000). Despite the increased cell number, the regenerative capacity of the entire HSC pool was reduced in aged individuals. The presence of $CD34^+$ HSCs in high numbers might be due to an increased frequency of symmetric cell divisions leading to impaired regeneration potential of the daughter cells (Sudo *et al.*, 2000). Moreover, the aged HSCs exhibited diminished responsiveness to cytokines secreted when transplanting aged HSCs into young recipients in the mouse model suggesting that HSC-intrinsic mechanisms are more responsible for this aging phenotype (Rossi *et al.*, 2005).

The second commonly observed phenotype is skewed differentiation potential of aged HSCs towards myeloid lineage. Aged HSCs tend to differentiate more into cells of myeloid lineage whereas the output of lymphoid-lineage cells is decreased (Beerman *et al.*, 2017). Comparing to young HSCs, the absolute number of myeloid cells formed by aged HSCs is increased (Beerman *et al.*, 2017). However, despite the increased cell quantity, the biological function of the produced myeloid cells is reduced (Signer *et al.*, 2007). The lymphoid to myeloid lineage skewing might be caused by changes in HSC differentiation or by altered proliferation of myeloid and lymphoid precursors. Other authors applied the single-cell technique to study the functional heterogeneity in the primitive HSC population. They showed that the

differentiation potential of cells in the primitive HSC population varied strongly from each other (Muller-Sieburg *et al.*, 2006; Benz *et al.*, 2012). Some HSC subtypes tended to differentiate into myeloid cells and were thus myeloid-biased, some cells were balanced whereas some other cells were lymphoid-biased. The observed lineage skewing might also be caused by the different composition of the HSC subtypes upon aging (Muller-Sieburg *et al.*, 2006). In conclusion, the lineage skewing phenotype might be caused both by changes in the HSC pool composition as well as by alterations in the differentiation potential at a cellular level in the individual HSCs (Challen *et al.*, 2010; Dykstra *et al.*, 2011).

The third phenotype associated with aging HSCs is the diminished homing and mobilization property (Köhler *et al.*, 2009). It was shown that young and aged HSCs have distinct selectivity for the bone marrow niche *in vivo*. Aged HSCs tend to home to a bone marrow niche at a position more distant to the endosteum bone (Köhler *et al.*, 2009). *In vitro* studies showed that aged HSCs exhibit increased mobilization compared to young cells (Florian *et al.*, 2012).

Consistent with the lineage skewing previously described, Rossi *el al.* observed in aged HSCs a down-regulation of lymphoid-specific genes and up-regulation of myeloid-specific genes such as RUNX1, which could possibly explain the lineage skewing phenotype (Rossi *et al.*, 2005). Beside common mechanisms of aging such as oxidative damage by reactive oxygen species (ROS) (Ito *et al.*, 2004), DNA damage accumulation and telomere shortening (Rossi *et al.*, 2008), the epigenetic mechanisms also play an important role for aging HSCs (Chambers *et al.*, 2007).

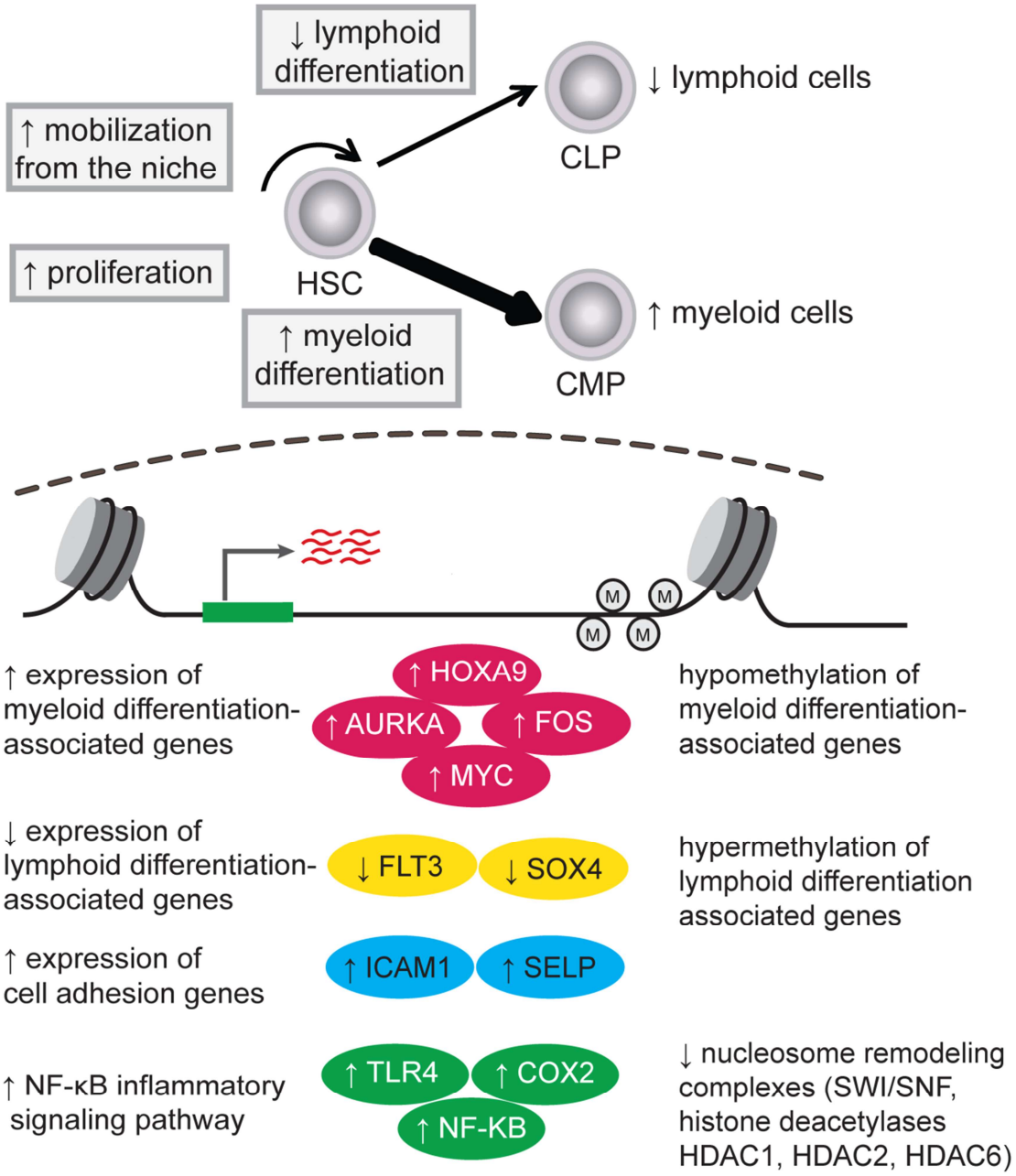

Figure 2 Commonly known aging phenotypes and intrinsic mechanisms in human HSCs. In aged HSCs, an increased differentiation potential towards cells of myeloid lineage and a decreased potential towards cells of lymphoid lineage were commonly observed. Moreover, the rate of proliferation and mobilization from the niche increased upon aging. On transcriptome level, the expression of genes associated to myeloid differentiation (HOXA9, AURKA, FOS, MYC) increased while decreased expression was observed for genes associated to lymphoid differentiation (FLT3, SOX4). The expression of cell adhesion genes ICAM1 and SELP increased in aged HSCs. The genes of the NF-κB inflammatory signaling pathway (TLR4, COX2, NF-κB) were also up-regulated upon aging. On epigenetic level, the genes associated to myeloid differentiation were hypomethylated whereas genes associated to lymphoid differentiation were hypermethylated. Furthermore, the nucleosome remodeling complexes SWI/SNF and histone deacetylases were down-regulated upon aging. CLP, common lymphoid progenitors; CMP, common myeloid progenitors.

Isabelle Hellwig, a former colleague from the research group of Dr. Anthony D. Ho studied methylation changes in $CD34^+$ HSCs from donors of different ages. She found 192 CpG dinucleotides with significantly increased methylation whereas a loss of methylation was measured at 350 CpG sites upon aging. The aging-related hypomethylation showed high analogy with the hypomethylation of myeloid differentiation-associated genes, suggesting that DNA-methylation changes contribute to the myeloid lineage skewing observed in aged HSCs (Bocker *et al.*, 2011; Winnefeld *et al.*, 2012). Beyond that study, changes in DNA methylation patterns upon aging were also reported by other groups (Bocker *et al.*, 2011; Hogart *et al.*, 2012; Beerman *et al.*, 2013).

Modifiers of the chromatin structure were also shown to change upon aging. Chambers and colleagues observed a general down regulation of genes related to chromatin remodeling SWI/SNF complex and histone deacetylases HDAC1, HDAC2 and HDAC6 (Chambers *et al.*, 2007). Moreover, it was observed in aged HSCs that multiple members of the polycomb repressive complexes PRC1 and PRC2 are differentially regulated (Klauke *et al.*, 2011). The reason for the altered epigenetic status might be due to failures of DNA methyl transferases (DNMTs), histone methyltransfereases and acetyltransferases to pass on the HSC-specific epigenetic information to the newly synthesized DNA strands of the daughter HSCs upon cell proliferation (Rando *et al.*, 2012).

Niche-derived factors also contribute to the aging phenotypes of HSCs. As previously described, SDF1 is an important protein factor for HSC homing produced by osteoblasts and MSCs in the bone marrow niche. As the fat content increases with age, the blood plasma level of SDF1 decreases, resulting in altered homing and mobilization behavior in aged HSCs. The enhanced adipogenesis might be due to the lineage skewing of MSCs towards adipogenic differentiation upon aging (Tuljapurkar *et al.*, 2011; Kubo *et al.*, 2012).

In conclusion, an aging stem cell niche in the bone marrow affects the physiology of HSCs in many different aspects (Figure 2). One of the most important cell types of the niche is the mesenchymal stromal cell.

1.4 Mesenchymal stromal cells

Mesenchymal stromal cells (MSCs) are cells of mesenchymal origin which are found in the bone marrow, adipose and muscle tissues, brain and vascular vessels (Dominici *et al.*, 2006). This cell type was initially discovered and characterized by Friedenstein and colleagues early 1970s (Friedenstein *et al.*, 1976). The mesenchymal stromal cells are alternatively called “mesenchymal stem cells” due to their ability to differentiate into osteocytes (bone cells), adipocytes (fat cells) and chondrocytes (cartilage cells) (Pittenger, 1999) (Figure 3). The MSCs are commonly characterized by their plastic adherent growth, immunophenotype and *in vitro* differentiation potential (Horwitz *et al.*, 2005). Thus far, there is no specific cell surface marker that could be used to specifically identify MSCs. To characterize MSCs, a combination of several markers was suggested such as CD90, CD73 and CD105. In addition, markers such as CD45 and CD34 are required to be absent (Dominici *et al.*, 2006).

The multipotency of MSCs can be confirmed *in vitro* by 21 days of differentiation. There are significant microscopic changes in the cell morphology during the differentiation process. Adipogenically differentiated MSCs contain vacuoles filled with triglycerides, osteogenically differentiated cells are characterized by calcium phosphate and inorganic hydroxyapatite precipitates whereas chondrogenically differentiated cells show strong secretion of extracellular mucopolysaccharides (Figure 3). The adipogenic and osteogenic differentiation of MSCs could be demonstrated reproducibly *in vitro* by exposing the MSCs to the respective media containing differentiation agents. During the adipogenic differentiation, a set of genes are highly expressed such as peroxisome proliferator-activated receptor gamma 2 (PPARγ 2), CCAAT/enhancer binding protein alpha (C/EBPα) and fatty acid binding protein 4 (FABP4). During the osteogenic differentiation, osteopontin, osteocalcin and runt-related transcription factor 2 (RUNX2) are strongly expressed (Siersbaek *et al.*, 2010; Polini *et al.*, 2011; Rippo *et al.*, 2013).

Due to strong population heterogeneity and the lack of a unique immunephenotype, the usage of a standardized protocol for isolating MSCs is crucial for the experimental design. *In vitro* studies indicated that isolation and culture conditions

have a strong influence on the molecular phenotypes of MSCs. It might lead to misinterpretations of experimental results if they are not kept constant for all samples within one experiment (Wagner *et al.*, 2007). Especially the composition and concentration of the culture medium affect strongly the differentiation potential of MSCs (Wagner *et al.*, 2007).

All MSC samples used in the present study were derived from the bone marrow of healthy human individuals. The same type of maintenance medium (7th medium) was used for isolation, maintenance and expansion of the cells (details described in Methods and Materials).

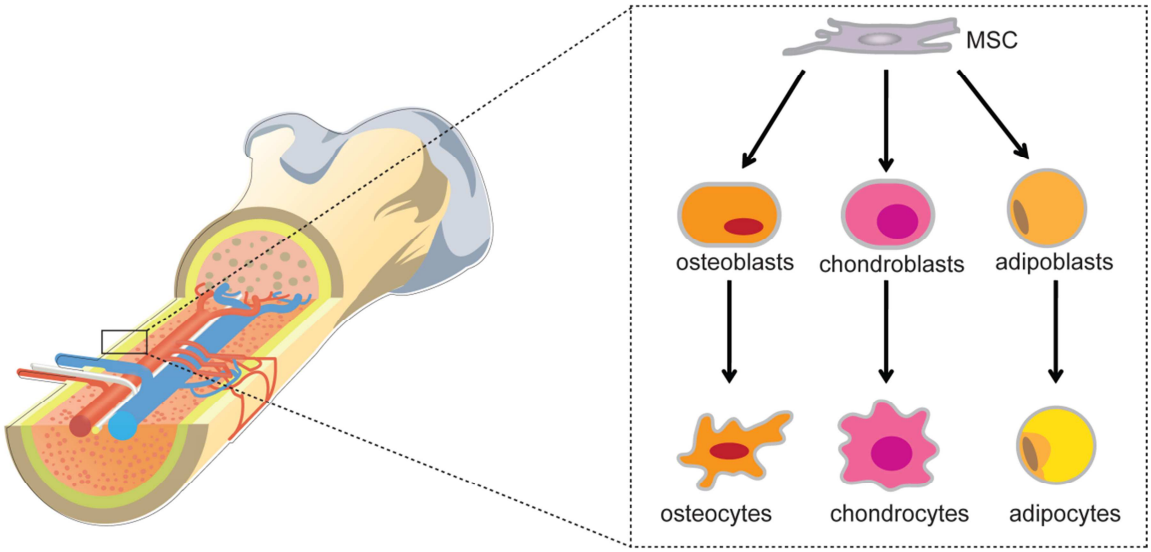

Figure 3 Bone marrow derived mesenchymal stromal cells (MSC) possess the ability to self-renew as well as to differentiate. The MSCs located in proximity to the bone can be differentiated into osteoblasts, chondroblasts and adipoblasts which further maturate into osteocytes, chondrocytes and adipocytes. The figure was adapted from Verovskaya *et al.* and Frenette *et al.* (Frenette *et al.*, 2013; Verovskaya *et al.*, 2017).

1.4.1 Interactions of MSCs with other cell types

MSCs can interact with other cell types through cytokines or cell-cell contacts. For example, it was shown that MSCs secrete a set of cytokines such as EGF, VEGF-α, IGF-1, KGF, Angiopoietin-1 and SDF-1, which affect the proliferation and migration of endothelial cells and hematopoietic cells upon *in vitro* co-culture (Wagner *et al.*, 2008). Additionally, MSCs exert a modulatory function on the innate and adaptive immune system by modulating the proliferation and migration of T- and B-cells, NK-cells, dendritic cells, neutrophils and monocytes. These influences can be exerted by cell-cell contacts or secreted cytokines such as nitrogen oxide, interleukin, prostaglandin E2 and interferon-gamma (Shi *et al.*, 2011; Le Blanc *et al.*, 2012). *In vivo* MSCs are able to increase angiogenesis and improve wound healing by recruiting endothelial cells (Sensebé *et al.*, 2010). Furthermore, MSCs interact via cell surface receptors such as integrin beta 1 with hematopoietic stem cells (Walenda *et al.*, 2010). As feeder cells, MSCs can promote the proliferation as well as the maintenance of HSC stemness *ex vivo*. Based on this property, an *in vitro* HSC-MSCs co-culture system was established to study the interactions between the niche and hematopoietic stem cells (Docheva *et al.*, 2007; Huang *et al.*, 2007; Méndez-Ferrer *et al.*, 2010; Walenda *et al.*, 2010).

1.4.2 HSC-MSC *in vitro* co-culture system

The HSC-MSC *in vitro* co-culture system serves as a surrogate model to study the cross-talks between HSCs and the bone marrow niche. As described above, osteoblasts and MSCs are essential constituents of the endosteal niche *in vivo*. In the murine system, it was shown that the majority of the bone marrow stromal cells are derived from MSCs (Muguruma *et al.*, 2006; Wang *et al.*, 2006). Moreover, the MSCs express typical niche-derived factors such as SDF-1, VCAM-1, SCF, osteopontin and angiopoietin-1 (Nilsson *et al.*, 2005). Either through direct cell-cell contact or as secreted cytokines, these factors affect the physiology of HSCs. The cytokine SDF-1 regulates HSC migration to the bone marrow niche (Ponomaryov *et al.*, 2000); vascular cell adhesion molecule-1 (VCAM-1) mediates MSC-HSC adhesion (Simmons *et al.*, 1992; Papayannopoulou *et al.*, 1995); stem cell factor (SCF) maintains HSC quiescence and niche retention (Kent *et al.*, 2008); angiopoietin-1,

osteopontin and thrombopoietin-1 contribute to the maintenance of HSC quiescence (Arai *et al.*, 2004; Nilsson *et al.*, 2005; Stier *et al.*, 2005; Qian *et al.*, 2007; Yoshihara *et al.*, 2007). Based on the flexibility of this model, efforts were made to study the effects of an aging bone marrow niche on the phosphorylation of HSC proteome (Karimbocus, 2016). Using the method of stable isotope-labeling with amino acids (SILAC), the MSCs and HSCs in the co-culture were labeled with heavy and light amino acids, respectively (Mann, 2006). Protocols were established to study the early phosphorylation events upon MSC and HSC co-culture (Karimbocus, 2016).

1.4.3 Clinical applications of MSCs

Beyond serving as bone marrow niche, there is a wide range of potential clinical applications for human MSCs (Sensebé *et al.*, 2010). The therapeutic usages of MSCs are widely explored due to their differentiation potential, regeneration promoting properties and suppressive influences of the immune system (Sensebé *et al.*, 2010). MSCs are used in tissue engineering of bones, cartilages and connective tissues due to their potential to differentiate into osteoblasts and cartilage cells. Taking advantage of their positive effects on proliferation and differentiation of endogenous cardiac stem cells, MSCs are also applied in cardiovascular diseases (Sensebé *et al.*, 2010). The immunosuppressive properties of the MSCs have led to several studies on the treatment of graft-vs.-host disease (GvHD) or multiple sclerosis (Le Blanc *et al.*, 2012). Possible risks for clinical applications in these areas are immortalization or the transformation of MSCs *in vivo* (Frenette *et al.*, 2013). The attempt to use MSCs as feeder cells for HSC expansion in a clinical context bears a great potential. However, for possible therapeutic applications, it is crucial to understand the physiology and proliferation behavior of MSCs, especially with regard to aging and replicative senescence.

1.4.4 Aging of MSCs

All cells of the human body are subjected to aging. For human bone marrow MSCs, one differentiates between the biological aging process *in vivo* and the replicative senescence *in vitro* (Ho *et al.*, 2005). Phenotypes of *in vivo* aging are determined by the chronological age of the sample donors while replicative senescence is characterized by the number of cell divisions *in vitro*. Several studies indicated that the differentiation potential of MSCs seems to change with age (Figure 4). Stenderup and colleagues studied the osteogenic differentiation of MSCs and showed that aging is associated with decreased proliferative capacity of osteoprogenitor cells, suggesting that the decreased osteoblastic cell number leads to age-related decrease in bone formation (Stenderup *et al.*, 2003). By studying specific molecular markers for osteogenic and adipogenic differentiations, it was demonstrated in mouse that the intrinsic differentiation potential of MSCs shifts towards adipogenic differentiation with age. The expression of the transcription factor PPAR-gamma 2, which negatively regulates osteoblast development and positively regulates marrow adipocyte differentiation increases with age. The expressions of osteoblast-specific transcription factors such as RUNX2 and DLX5 decrease in aged MSCs. The expression of the osteoblast-specific markers such as collagen and osteocalcin decreases in aged MSCs as well (Moerman *et al.*, 2004). It was further shown that the expressions of different components of the Wnt and TGF-beta/BMP signaling pathways are altered upon aging which might cause enhanced adipogenesis (Ross, 2000; Moerman *et al.*, 2004). Moreover, the supportive function of MSCs for HSCs was also reported to decrease upon aging (Sethe *et al.*, 2006) (Figure 4). The secretion of the cytokine SDF-1 (stromal cell-derived factor 1) regulating the processes of HSC homing to the niche was reported to decrease in aged MSCs (Wagner *et al.*, 2009). The secreted SDF-1 is sensed by HSCs through the CXCR4 receptors on the cell surface. Along the increasing concentration gradient of SDF-1, the HSCs are able to migrate back to the bone marrow niche (Lapidot *et al.*, 2005).

The replicative senescence is characterized by morphological changes and decreased potential of proliferation and differentiation. This phenomenon was first described 40 years ago by Leonard Hayflick thus the limit of cell divisions is called the Hayflick-Limit (Hayflick *et al.*, 1961; Hayflick, 1965). In replicative senescent

MSCs, the cells become larger and more granular after 20 to 50 population doublings depending on culture conditions. Meanwhile, the activity of beta-galactosidase and the cell apoptosis rate are significantly increased (Zhou *et al.*, 2008). However, to what extend the replicative senescence reflects the aging process *in vivo* is still an area of active research.

The epigenetic regulations are crucial for aging in MSCs. Wolfgang Wagner, a previous colleague in the research group of Dr. Anthony D. Ho, studied DNA methylation pattern in MSCs derived from old and young human donors. Using a human methylation microarray-based technology, it was shown that methylation patterns were maintained throughout aging but highly significant differences were observed at specific CpG sites (Bork *et al.*, 2010). In terms of CpG islands – 295 CpGs were hypermethylated whereas 349 CpGs were hypomethylated upon aging. Many of these differences were observed in homeobox genes such as HOXA2, HOXA5 and HOXA6 as well as genes involved in cell differentiation such as RUNX2, DLX5, MGMT and BMP4 (Bork *et al.*, 2010). The main transcription factors for osteoblast differentiation RUNX2 and DLX5 were observed to be hypermethylated upon aging, which is in line with the previously observed decreased expressions of RUNX2 and DLX5 (Moerman *et al.*, 2004; Bork *et al.*, 2010). Some of the methylation changes in aged MSCs were in consistence with MSCs undergone multiple passages indicating a possible correlation between biological aging and replicative senescence (Bork *et al.*, 2010). However, despite the changes in homeobox genes and genes responsible for cell differentiation described above, a holistic understanding of the changing regulatory landscape in human MSCs upon aging still requires investigations on multiple molecular levels.

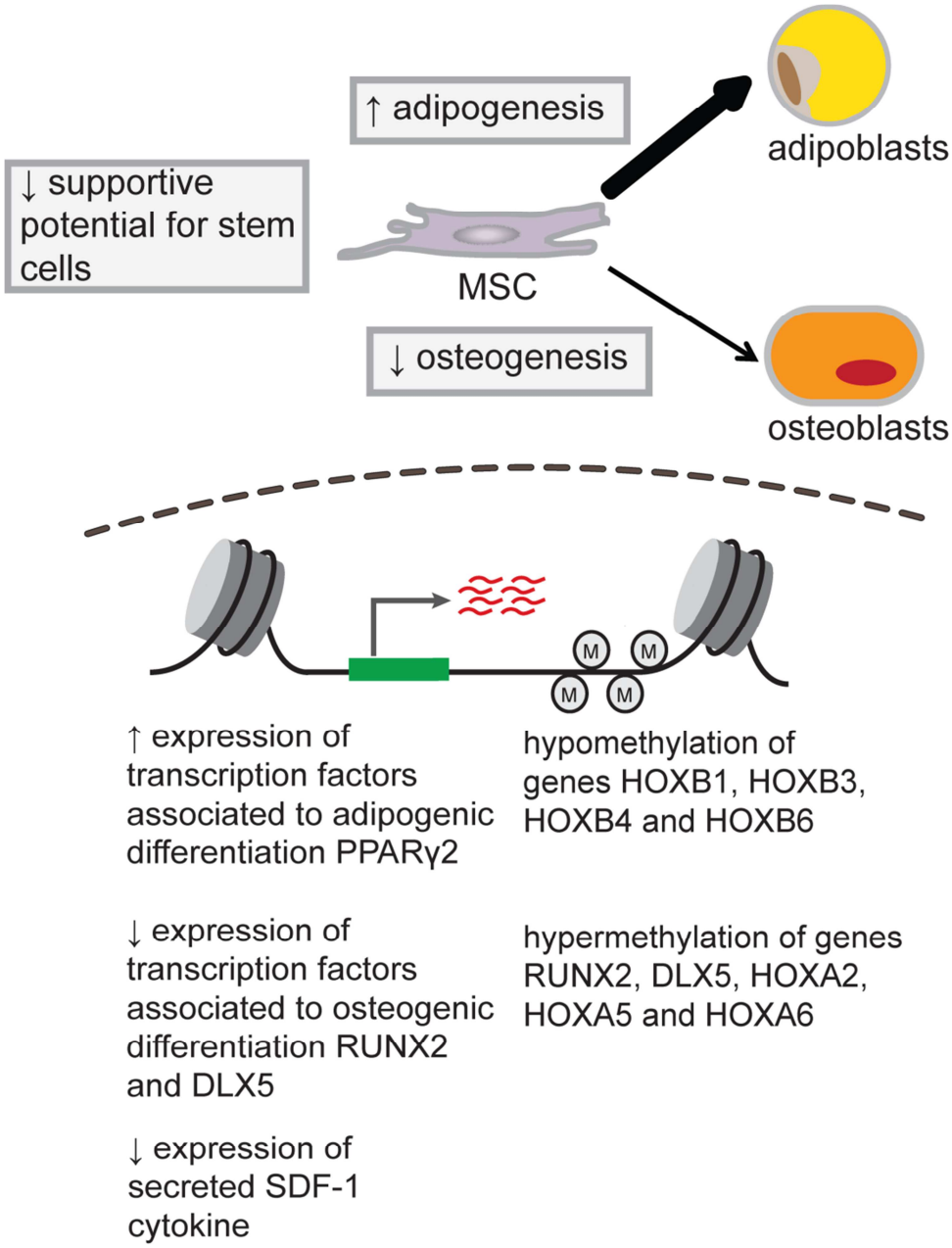

Figure 4 Commonly known aging phenotypes and intrinsic mechanisms in human MSCs. In aged MSCs, an increased differentiation potential towards adipocytes and a decreased potential towards osteocytes were observed. A decrease in the supportive potential for hematopoietic stem cells (HSCs) was shown in co-culture experiments. On transcriptome level, the expression of transcription factors associated to adipogenic differentiation (PPARγ2) increased while decreased expression was observed for transcription factors associated to osteogenic differentiation (RUNX2, DLX5). The expression level of secreted cytokine SDF-1 regulating HSC migration decreased in aged MSCs. On epigenetic level, the genes associated to osteogenic differentiation (RUNX2, DLX5) and homeobox genes (HOXA 2, 5 and 6) were hypermethylated in aged MSCs. The homeobox genes (HOXB 1, 3, 4 and 6) were hypomethylated upon aging in MSCs.

1.5 Epigenetic regulation in human cells

1.5.1 Transcriptional regulatory landscape in human

Gene expression is the process that converts the information embedded in a DNA template into an RNA molecule. The regulation of gene expression, both in time and space, is fundamental for many biological processes such as homeostasis, development and responses to environmental cues. In eukaryotes, the first step of gene expression, transcription, is carried out by three types of RNA polymerases. RNA polymerases I and III transcribe the genes encoding transfer RNA, ribosomal RNA, and various small RNAs. RNA polymerase II transcribes all protein encoding genes (Alberts *et al.*, 2015). The mechanisms regulating transcription activity are mainly achieved through the signals for the initiation of transcription encoded in the DNA template and the exposure of this genetic signal.

In the nucleus, eukaryotic genetic material is wrapped around complexes of histone proteins in the form of chromatin (Alberts *et al.*, 2015). The accessibility of the condensed DNA is therefore crucial for gene expression control. The initiation of gene expression starts with the relaxation of compact chromatin in regulatory regions. The initial modification of chromatin structure is commonly carried out by chromatin remodeling complexes, modification of histones and sometimes binding of the so-called pioneer transcription factors (Kouzarides, 2007).

The opening of compact chromatin leads to the exposure of transcription factors to *cis*-regulatory modules (CRM), which are genomic regions containing regulatory information (Armstrong, 2013). The CRMs can be located in close proximity or at large distance to the target gene. The transcriptional factors (TFs) bind to transcription factor binding sites (TFBS). They interact via co-factors to recruit and stabilize the transcription initiation complex to the promoter, upstream of the transcription start site (TSS). The transcription of the target gene is then initiated by the transcription initiation complex (Figure 5).

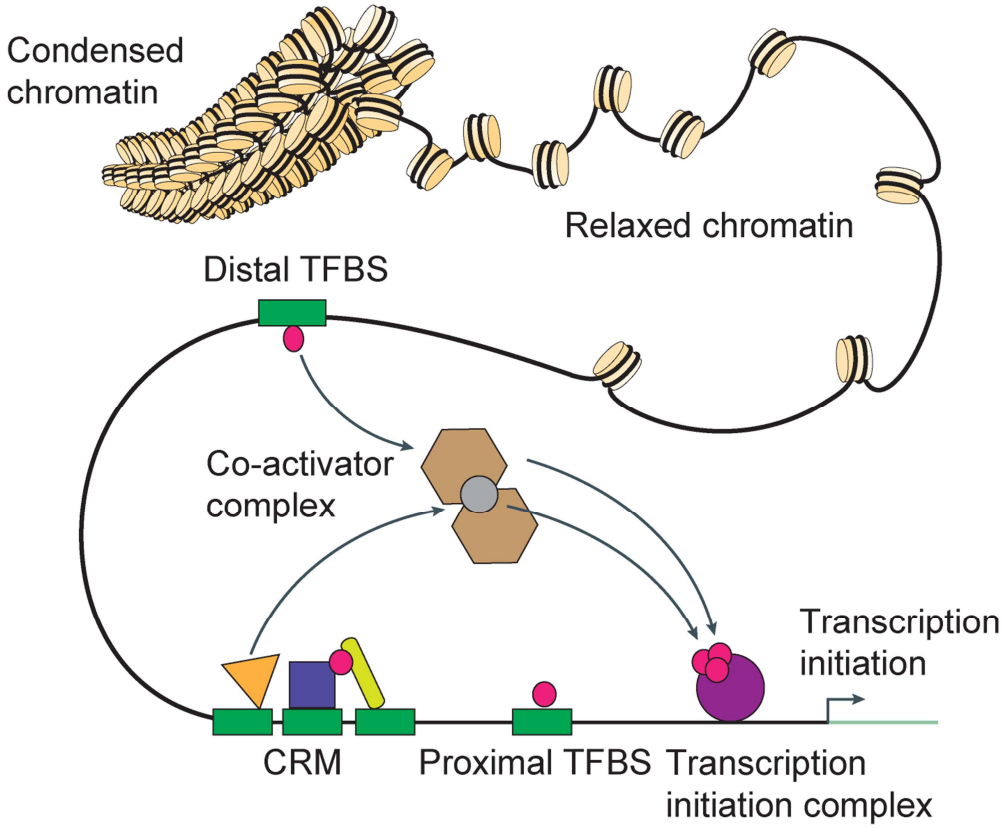

Figure 5 Overview of transcriptional regulation in eukaryotes. Condensed chromatin relaxes and transcription factors (TFs) bind transcription factor binding sites (TFBS) in both distal and proximal *cis*-regulatory modules (CRMs). Bound TFs interact with co-factors to stabilize the transcription initiation complex to the promoter region enabling gene expression. Figure was adapted from Wasserman *et al.* (Wasserman *et al.*, 2004).

1.5.2 Importance of chromatin accessibility for gene expression

The chromosome is the compact form of chromatin which consists of DNA and histone proteins (Armstrong, 2013). The basic unit of chromatin is the nucleosome. It consists of 147 bp of DNA wrapped around a protein octamer composed of four core histones (H3, H4, H2A and H2B). The positioning of the nucleosome is crucial for the regulation of transcription, as DNA wrapped around histones is less accessible than the naked DNA (Kaplan *et al.*, 2011; Li *et al.*, 2011). Previous studies also indicated that chromatin accessibility is correlated with the rate of transcriptional initiation at promoters suggesting that a low nucleosome occupancy at transcriptional start sites (TSS) is associated with transcriptional activation (Lee *et al.*, 2004; Shu *et al.*, 2011).

Several mechanisms could lead to chromatin accessibility changes. Conformational changes in chromatin structure lead to unwrapping of the nucleosomal DNA, allowing transcription factor binding. Changes in nucleosome occupancy can either occur through chromatin remodeling by altering the DNA-histone interaction non-covalently or through chromatin modification which mainly introduces covalent modifications on histone tails. Chromatin remodeling in human is mainly mediated by ATP-dependent SWF/SNF protein complex (Segal *et al.*, 2009).

Despite many contradictory observations, in most organisms, a general model of heterochromatin loss upon aging is proposed (Tsurumi *et al.*, 2012). In this model, a relaxation of heterochromatin due to down regulation of heterochromatin-silencing proteins may cause cellular dysfunctions with age (Pollina *et al.*, 2011; Tsurumi *et al.*, 2012). Changes in chromatin accessibility are important for the epigenetic regulation of the aging process. One prominent mechanism is the post-translational modification of histone tails.

1.5.3 Regulation of gene expression by modifications of histone tails

The N-terminus of histone tails are mainly modified by acetylation, methylation, phosphorylation and ubiquitylation. These modifications can either facilitate the ATP-dependent chromatin remodeling by SWF/SNF protein or alter directly the stability of contacts between DNA and nucleosomes (Armstrong, 2013). In the field of human aging, methylation and acetylation of lysines on histone H3 are the best-studied post-translational modifications.

Histone methylation is associated with either active or repressed genome regions depending on the residue and level of methylation. The methylation status is regulated by histone methyltransferases and demethylases. The monomethylation of histone H3 (H3K4me1) is enriched downstream of promoters; dimethylation (H3K4me2) is enriched in enhancer and promoter regions; whereas the trimethylation (H3K4me3) is enriched in promoter regions and involved in transcriptional activation (Heintzman *et al.*, 2007). In human fibroblast cells and murine HSCs, new regions of H3K4me3 emerged upon aging (Shah *et al.*, 2013; Sun *et al.*, 2014). H3K27me3 is

associated with the repressive state of chromatin (Creyghton *et al.*, 2010). Lysine 27 is methylated by polycomb repressive complex 2 (PRC2) and recognized by polycomb repressive complex 1 (PRC1), which in turn silences the gene expression by ubiquitylating histone H2A (Simon *et al.*, 2013). Increased H3K27me3 was shown in *C. elegans* with extended longevity (Ni *et al.*, 2012). In aged human fibroblast cells, a decrease in H3K27me3 level was observed (Shah *et al.*, 2013). In *Drosophila*, a decrease in H3K27me3 level was associated with aging (Siebold *et al.*, 2010). Taking those observations together, one can conclude that different H3K27me3 regulators may influence lifespans through specific loci in specific cell types and organisms (Pollina *et al.*, 2011).

1.5.4 Genome-wide sequencing methods to study chromatin accessibility

Due to the great importance of chromatin openness to the biological functions of the cells, many different methods have been developed to profile chromatin accessibility on a genome-wide scale. ATAC-seq is a recently introduced method to map chromatin accessibility genome-wide (Figure 6A). It stands for “Assay of Transposase Accessible Chromatin with Sequencing” (Buenrostro *et al.*, 2013). The method is based on the property of the transposase Tn5 to randomly integrate into open chromatin regions (Adey *et al.*, 2010). A hyperactive form of Tn5 is used in ATAC-seq to insert sequencing adaptors randomly to the open chromatin regions. This process is referred to as tagmentation (Figure 6A). A sequencing library is prepared by PCR-amplifying the tagmented DNA fragments. The library is then sequenced on the next-generation sequencing platforms from both ends of the DNA fragment (paired-end sequencing) (Buenrostro *et al.*, 2013).

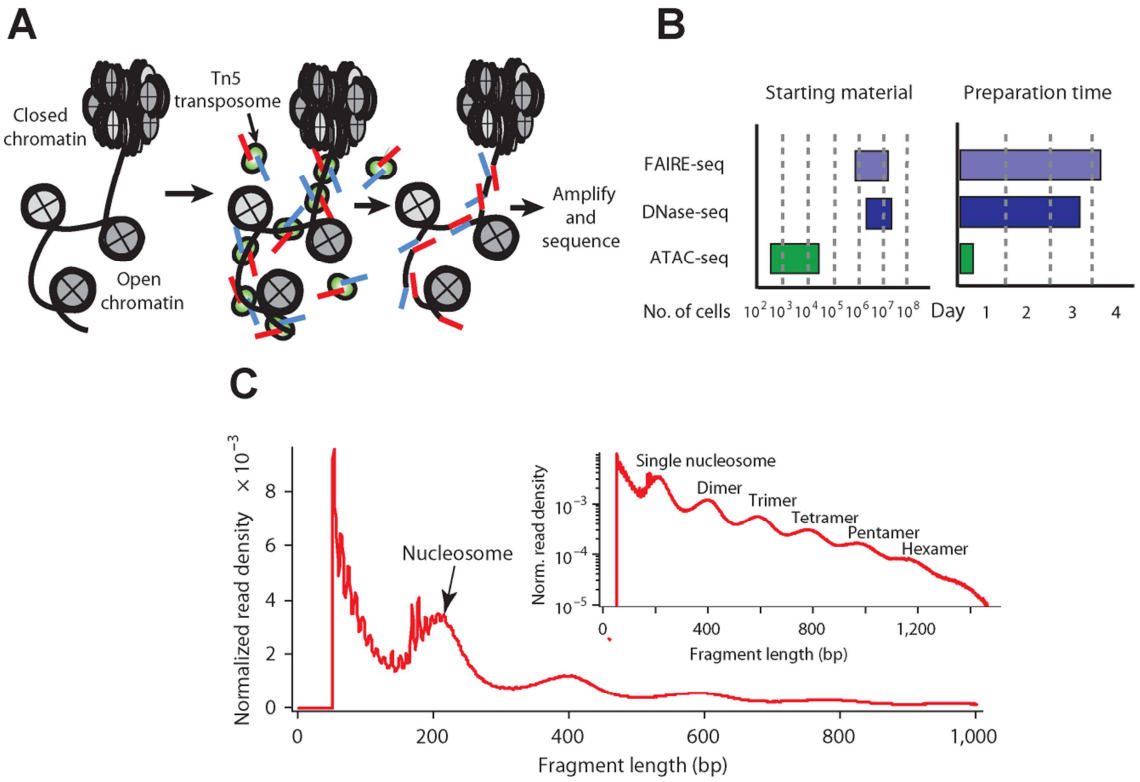

Figure 6 ATAC-seq is a method to probe chromatin accessibility genome-wide. **(A)** A hyperactive Tn5 transposase inserts sequencing adaptors into the open regions of the genome. The tagmented DNA fragments are PCR-amplified and sequenced from both ends. **(B)** Advantages of ATAC-seq (green) compared to FAIRE-seq (light blue) and DNase seq (dark blue) are the small amounts of starting material required and short sample preparation time. No. of cells (number of cells) **(C)** Fragment size distribution of ATAC-seq library shows a periodicity of approximately 200 bp indicating that many fragments are protected by the nucleosomes. Figures were adapted from Buenrostro *et al.* (Buenrostro *et al.*, 2013).

Sequencing reads can be subsequently used to infer nucleosome positions, chromatin regions of increased accessibility, as well as to predict transcription factor binding from a standard sample size of 500 – 50,000 cells (Buenrostro *et al.*, 2013). Recent publications also showed that this method is compatible with single cell microfluidic set-ups as well (Buenrostro *et al.*, 2015)

Clear advantages of ATAC-seq compared to established sequencing methods such as DNase-seq or FAIRE-seq (Formaldehyde-Assisted Isolation of Regulatory Elements-Sequencing) for assaying chromatin accessibility genome-wide lie in the small amount of cell material needed for library preparation as well the short library preparation time (Figure 6B). Working with clinical samples, rare cellular subtypes like *e.g.* $CD34^{+}/CD38^{-}$ human HSCs often cannot be isolated in adequate amounts for methods like DNase-seq or FAIRE-seq. Another advantage of the small amount of starting material is that important biological heterogeneity in cellular populations is

not averaged out in the cell population (Buenrostro *et al.*, 2013). The ATAC-seq paired-end reads produce detailed information about nucleosome packing and positioning (Buenrostro *et al.*, 2013). The size distribution of the ATAC-seq sequencing fragments indicates a periodicity of approximately 200 bp indicating that many fragments are protected by the nucleosomes (Figure 6C).

This method was applied to a variety of biological questions. By overlaying ChIP-seq data with ATAC-seq data, dynamics of four chromatin modifications across 16 stages of murine hematopoietic differentiation were profiled (Lara-Astiaso *et al.*, 2014). Among the 48,415 enhancer regions characterized, 17,035 lineage-specific enhancers are involved in the lineage commitment of hematopoietic differentiation (Lara-Astiaso *et al.*, 2014). By studying primary $CD4^+$ T cells isolated from healthy individuals, Qu and colleagues found gender to be a major contributor to the variation in chromatin accessibility profiles (Qu *et al.*, 2015). They also revealed novel elements that escape X chromosome inactivation and predicted gender-specific gene regulatory networks across autosomes (Qu *et al.*, 2015).

However, despite the large number of studies on chromatin accessibility dynamics, none of the studies were carried out in the field of human bone marrow aging. To understand the aging process of human hematopoietic stem cell niche, it is important to characterize the open chromatin profiles of the bone marrow-derived MSCs.

2. Experimental design

In the course of this PhD project, 59 bone marrow aspirate samples derived from healthy individuals between age 20 and 60 were collected and characterized by flow cytometry. I studied the age-associated proportional, morphological and immunophenotypic changes of the major bone marrow constituents comprising of hematopoietic stem cells (HSC), lymphocytes and restricted precursors (LYM), monocytes, macrophages and restricted precursors (MON), granulocytic precursors (GRA) and erythroid precursors (ERP).

The interactions between HSCs and the niche were studied *in vitro* using a co-culture system of HSCs and MSCs. As the supportive functions and the differentiation potentials towards adipocytes and osteocytes change significantly with age, we examined the ability of undifferentiated MSCs, adipogenically differentiated MSCs (ADI-MSCs) and osteogenically differentiated MSCs (OST-MSCs) to support HSCs. The proliferation and stemness of HSCs derived from cord blood and mobilized peripheral blood were investigated after seven days of co-culture with those three types of feeder cells.

Taking an unbiased approach, we investigated the epigenetic changes upon aging using ATAC-seq in MSCs. To this end, chromatin accessibility profiles were generated from a cohort of 16 healthy individuals between ages 21 and 59. Chromatin openness variations depending on age were analyzed and preliminary findings were discussed.

3. Materials and Methods

3.1 Materials

3.1.1 Primary human samples

Hematopoietic stem cells (HSC) were separated from cord blood and bone marrow of healthy individuals. Mesenchymal stromal cells (MSC) were expanded *in vitro* from the bone marrow of healthy human subjects. Lymphocytes and restricted precursors (LYM), monocytes, macrophages and restricted precursors (MON), granulocytic precursors (GRA), and erythroid precursors (ERP) were isolated from bone marrow of healthy individuals. Ethic approvals from the local ethics committee were available for the samples used in this project.

3.1.1.1 Cord blood

Cord blood was provided by Heidelberg University Women's Hospital, Klink Sankt Elisabeth Heidelberg and University Hospital Mannheim. The sample was collected directly after the delivery of healthy newborns by the responsible delivery nurses. Cord blood was transferred by compression of the umbilical vein towards the cord cut into a 50 ml Falcon tube provided with 10 ml PBS containing 10% Heparin/Sodium2500 as anti-coagulant. The samples were temporally stored at 4-8 °C for subsequent procedures.

3.1.1.2 Bone marrow

Bone marrow of healthy donors was taken by puncture of the iliac crest. The cortical bone was drilled under local anesthesia and the bone marrow was sampled by continuous aspiration using 20 ml syringes provided with 10.000 units of heparin. The bone marrow was subsequently mixed thoroughly with anticoagulant and immediately further processed.

3.1.1.3 Cell lines

The GM12878 cell line derived from human lymphoblastoid cells was received as courtesy of Eleni Kafkia, Patil group, EMBL.

3.1.2 Instruments

Table 1 A summary of instruments used in the project.

Name	Supplier
2100 Bioanalyzer	Agilent Technologies
AutoMACS separation columns	Miltenyi Biotech
AutoMACSTM Separator	Miltenyi Biotech
B5050 Laboratory Incubator	Heraeus
BD FACSAria III cell sorter	BD
BD FACScan™ Flow Cytometer	BD
BD LSRFortessa cell analyzer	BD
BD Vantage SE cell sorter	BD
Blue light transilluminator, ECX-F20	VWR
Centrifuges 5810, 5810R, 5415D, 5424	eppendorf
Colorview-12 camera	Olympus
Coulter MD II Series Analyzer	BD
Gel chamber	Febrikon Feinmechanik
Gel electrophoresis chamber Mini-Cell GT Systems	Bio-Rad
Gel electrophoresis chamber Wide Mini-Sub Cell GT Systems	Bio-Rad
HiSeq 2000 Sequencing System	Illumina
HiSeq 2500 Sequencing System	Illumina
Incubator ‘Hera cell’ 150	Kendro Laboratory Products
Innova 2000 shaker	New Brunswick
Mr. Frosty	Thermo Fisher Scientific
Multifuge 3S-R	Heraeus Instruments GmbH
Nano Drop ND-1000	PeqLab Biotechnologie
Nexterion B Microscope Slide	Schott
Olympus IX70	Olympus
Qubit Fluorometer	invitrogen
Sigma 1-15PK microcentrifuge	Sigma Laborzentrifugen
StepOnePlus Real-Time PCR Systems	Applied Biosystems
Sterile bench HERAsafe	Heraeus Instruments GmbH
TC20 Automated Cell Counter	BioRad
TE-2000	Nikon GmbH
ThermoCell Mixing Block MB-102	Alpha Laboratories
Transwell (6.5 mm diameter, 0.4 µm pore size)	Corning Holding GmbH

3.1.3 Chemicals

Table 2 A summary of chemicals used in the project.

Name	Supplier
1 kb DNA Ladder	New England Biolabs
100 bp DNA Ladder	New England Biolabs
100 bp plus DNA Ladder	Thermo Scientific
2-Propanol	Merck Millipore
6x DNA Loading Dye	Fermentas
Accutase	Sigma-Aldrich
Agarose	Sigma-Aldrich
Agarose Ultra-Quality	Carl Roth
BD FACSClean	BD
BD FACSFlow	BD
BD FACSRinse	BD
Bovine serum albumin	Stemcell Technologies
Calcium chloride	Sigma-Aldrich
Carboxyfluorescein diacetate N-succinimidyl ester	Sigma-Aldrich
Chloroform	Fluka Chemie
DAPI	Roche
Digitonin	Sigma-Aldrich
DMSO	Sigma-Aldrich
D-PBS	PAA Laboratories
EDTA	AppliChem
Ethanol	Merck Millipore
Ethidium bromide	Carl Roth
FICOLL Separation Solution	Biochrom
Formaldehyde Solution 37%	Merck Millipore
GelGreen Nucleic Acid Gel Stain 10,000x in water	Biotium
Glycerol	Merck Millipore
Heparin/Sodium2500	Ratiopharm
HEPES	Sigma-Aldrich
Hoechst 33342	Roche Diagnostics
IGEPAL CA-630 (NP40)	Sigma-Aldrich
Methanol	Merck Millipore
Nuclease-Free Water	B. Braun
Propidiumiodid	BD
Sodium chloride	Sigma-Aldrich
Sodium dodecyl sulfate, SDS	Sigma-Aldrich
Sodium hydroxide	Sigma-Aldrich
Streptomycin	Gibco
SYBR Green PCR Master Mix	Applied Biosystems
Triton-X-100	Sigma-Aldrich
TRIzol LS Reagent	Life Technologies
Trypsin-EDTA	Gibco
Trypan Blue 0.4%	Thermo Scientific

3.1.4 Miscellaneous materials

Table 3 A summary of miscellaneous materials used in the project.

Name	Supplier
12-well culture plates	Corning
24-well culture plates	Corning
Agencourt AMPure XP beads / SPRI	Beckman Coulter
Agilent High Sensitivity DNA Kit	Agilent Technologies
BD Falcon Tubes for Flow Cytometer	BD
Cover slips	Thermo Fisher Scientific
Cryo-vial, 2 ml	Nunc
DNA LoBind Tube 0.5 ml	Eppendorf
DNA LoBind Tube 1.5 ml	Eppendorf
Falcon 15 ml Polystyrene Conical Centrifuge Tubes	Thermo Fisher Scientific
Falcon 50 ml Polystyrene Conical Centrifuge Tubes	Thermo Fisher Scientific
MinElute Gel Extraction Kit	Qiagen
Neubauer cell counting chamber	Brand, Wertheim
Nextera DNA Sample Preparation Kit	Illumina
Nextera Index Kit	Illumina
PARTEC CellTrics Filter	Sysmex
QIAQuick Gel Extraction Kit	Qiagen
QIAQuick PCR Purification Kit	Qiagen
Qubit dsDNA HS Assay Kit	Thermo Fisher Scientific
Safe-Lock Tubes 1.5 ml	Eppendorf
Safe-Lock Tubes 2.0 ml	Eppendorf
Scapel Blades	Roth
Stericup® and Steritop™ Vacuum Driven Sterile Filters 0.22 µm	Merck Millipore
T25 culture flasks	Greiner
T75 culture flasks	Greiner

3.1.5 Oligonucleotides

Table 4 A summary of oligonucleotides used in the project.

Name	Sequence 5' -> 3'	Purpose
N701	TCGCCTTATAAGGCGA	Forward barcode primers for ATAC-seq library amplification and sequencing
N702	CTAGTACGCGTACTAG	
N703	TTCTGCCTAGGCAGAA	
N704	GCTCAGGATCCTGAGC	
N705	AGGAGTCCGGACTCCT	
N706	CATGCCTATAGGCATG	
N707	GTAGAGAGCTCTCTAC	
N708	CCTCTCTGCAGAGAGG	

N709	AGCGTAGCGCTACGCT	
N710	CAGCCTCGCGAGGCTG	
N711	TGCCTCTTAAGAGGCA	
N712	TCCTCTACGTAGAGGA	
N501	TAGATCGCGCGATCTA	Reverse barcode primers for ATAC-seq library amplification and sequencing
N502	CTCTCTATATAGAGAG	
N503	TATCCTCTAGAGGATA	
N504	AGAGTAGATCTACTCT	
N505	GTAAGGAGCTCCTTAC	
N506	ACTGCATATATGCAGT	
N507	AAGGAGTATACTCCTT	
N508	CTAAGCCTAGGCTTAG	
N517	GCGTAAGATCTTACGC	

3.1.6 Culture media

3.1.6.1 Medium for lymphoblastoid cell line

Table 5 Composition of culture medium for GM12878 cell line.

Component	Concentration	Supplier
RPMI 1640, GlutaMAX supplement	75%	Invitrogen
FBS	25%	Invitrogen

3.1.6.2 HSC-medium

Long-term bone marrow culture medium (LTBMC) was used to culture human HSCs.

Table 6 Composition of long-term bone marrow culture medium (LTBMC medium).

Component	Concentration	Supplier
IMDM	75%	PAA Laboratories
FCS	12.5%	Stemcell Technologies
Horse Serum	12.5%	Stemcell Technologies
Penicillin/Streptomycin	1%	PAA Laboratories
Hydrocortison 100	0.05%	Rotexmedica
L-Glutamine	1%	PAA Laboratories
Flt-3L	10 ng/ml	R&D Systems
TPO	10 ng/ml	R&D Systems

3.1.6.3 MSC-media

3.1.6.3.1 MSC maintenance medium

The maintenance culture medium for MSCs (7th medium) was prepared according to Zhao *et al.* (Zhao *et al.*, 2002).

Table 7 Composition of MSC maintenance medium.

Component	Concentration	Supplier
DMEM Low Glucose	60%	PAA Laboratories
MCDB-201 base medium	38%	Sigma-Aldrich
FCS	2%	Stemcell Technologies
L-Glutamine 200 mM	2 mM	PAA Laboratories
Penicillin 10.000 U/ml + Streptomycin 10.000 U/ml	100 U/ml	PAA Laboratories
Insulin 1.0 mg/ml + Transferrin 0.55 mg/ml + Selene 0.5 µg/ml Liquid Media Supplement	1%	Sigma-Aldrich
Linoleic acid	1%	Sigma-Aldrich
L-Ascorbic acid	0.1 mM	Sigma-Aldrich
Dexamethasone	20 nM	Sigma-Aldrich

3.1.6.3.2 Adipogenic differentiation medium

The adipogenic differentiation medium for MSCs was used to induce adipogenic differentiation of MSCs previously maintained in 7th medium.

Table 8 Composition of MSC adipogenic differentiation medium.

Component	Concentration	Supplier
DMEM High Glucose	90%	PAA Laboratories
FCS	10%	Stemcell Technologies
L-Glutamine 200 mM	2 mM	PAA Laboratories
Penicillin 10.000 U/ml + Streptomycin 10.000 U/ml	100 U/ml	PAA Laboratories
Insulin 1.0 mg/ml + Transferrin 0.55 mg/ml + Selene 0.5 µg/ml Liquid Media Supplement	1%	Sigma-Aldrich
1-methyl-3-isobutylxanthin (IBMX)	0.5 mM	Sigma-Aldrich
Dexamethasone	1 nM	Sigma-Aldrich

3.1.6.3.3 Osteogenic differentiation medium

The osteogenic differentiation medium for MSCs was used to induce osteogenic differentiation of MSCs previously maintained in 7th medium.

Table 9 Composition of MSC osteogenic differentiation medium.

Component	Concentration	Supplier
DMEM Low Glucose	90%	PAA Laboratories
FCS	10%	Stemcell Technologies
L-Glutamine 200 mM	2 mM	PAA Laboratories
Penicillin 10.000 U/ml + Streptomycin 10.000 U/ml	100 U/ml	PAA Laboratories
L-Ascorbic acid	0.2 mM	Sigma-Aldrich
beta-Glycerophosphate	10 mM	Sigma-Aldrich
Dexamethasone	100 nM	Sigma-Aldrich

3.1.6.3.4. R10 medium

Table 10 Composition of R10 medium.

Component	Concentration	Supplier
RPMI medium 1640	90%	PAA Laboratories
FCS	10%	Stemcell Technologies
L-Glutamine 200 mM	2 mM	PAA Laboratories
Penicillin 10.000 U/ml + Streptomycin 10.000 U/ml	100 U/ml	PAA Laboratories
HEPES	20 mM	Sigma-Aldrich

3.1.7 Buffers

Table 11 Composition of all buffers used in the project.

Name	Composition/Source
MACS Buffer	1 % FCS, 2 mM EDTA in PBS
TAE Buffer (50x)	20 M Tris/glacial acetic acid, 5 mM EDTA in H_2O
TE Buffer	10 mM Tris-HCl, 1 mM EDTA in H_2O

3.1.8 Antibodies

Table 12 List of antibodies used in the project.

Antibody	Conjugate	Concentration	Supplier
CD34 Mouse IgG1κ	APC	100 µg/ml	Becton Dickinson
CD38 Mouse IgG1κ	PE	50 µg/ml	Becton Dickinson
CD45 Mouse IgG1κ	FITC	50 µg/ml	Becton Dickinson
CD14 Mouse IgG2b	PE	50 µg/ml	Becton Dickinson

3.2 Methods

3.2.1 Isolation of bone marrow constituents

The isolation of bone marrow derived HSC, MON, GRA, ERP and LYM was carried out by FICOLL density gradient centrifugation followed by FACS sorting according to differential expressions of cell surface antigen markers CD34, CD45, CD14.

3.2.1.1 Density gradient centrifugation

The mononuclear cells from cord blood and bone marrow were isolated by FICOLL density gradient centrifugation. This method is based on the principle that the density of FICOLL (1.077 g/ml) is higher than the mononuclear cells but lower than erythrocytes and granulocytes. Using this method, different components of blood and bone marrow can be separated and isolated according to their density (Jaatinen *et al.*, 2007).

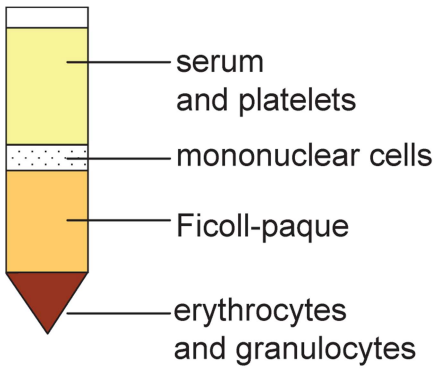

Figure 7 Phase separation of human bone marrow after density gradient centrifugation. The density of FICOLL is higher than the mononuclear cells but lower than erythrocytes and granulocytes. Using this method, different cellular components of the bone marrow can be separated according to their density.

There are four separated phases after a FICOLL centrifugation from top to the bottom: the blood serum and platelets phase, the mononuclear cell phase, the FICOLL paque phase and the bottom phase consisting of erythrocytes and granulocytes. Up to 30 ml cord blood or bone marrow diluted with PBS (ratio 1:1) was transferred into a 50 ml Falcon tube provided with 14 ml FICOLL separation solution. The two-phase suspension was centrifuged at 12,000 x g and room temperature for 25 min without brake. The interphase containing mononuclear cells was subsequently transferred by a 15 ml plastic pipette into a new tube containing 50 ml PBS. From this suspension, 20 µl were used for automatic determination of cell amount by Coulter MD II Series Analyzer (Beckman Coulter GmbH, Krefeld). The remaining suspension was washed again with 30 ml PBS at 400 g for 7 min.

3.2.1.2 Immunomagnetic isolation of cord blood HSCs

Cord bloods HSCs were isolated from the mononuclear cell fraction by immunomagnetic separation using CD34 MicroBeads (Miltenyi BiotecGmbH, Bergisch Gladbach). This method is based on the principle that CD34 antigen expressing cells are bound to the CD34 antibody coated on the surface of the magnetic MACS Microbeads allowing a column separation (Miltenyi *et al.*, 1990). As a first step, the mononuclear cell suspension was run through a separation column in a magnetic field. The magnetic Microbeads with $CD34^+$ cells on the surface were trapped in the column while the unbound $CD34^-$ fraction was discarded as flow through. As a second step, the $CD34^+$ cells were washed out from the column in the absence of the magnetic field. For each 10^8 mononuclear cells suspended in 300 µl MACS buffer, 100 µl of FcR blocking reagent was added and mixed with 100 µl magnetic CD34 Microbeads. The suspension was incubated for 30 min at 4 °C, diluted by MACS buffer to 30 ml and centrifuged at 400 g for 10 min. The cell pellet was resuspended in MACS buffer at a ratio of 10^8 cells per 500 µl MACS buffer. Using the AutoMACS system the LS separation column was rinsed once with 3 ml MACS buffer. Subsequently the cell-bead suspension was loaded on the column and washed three times with MACS buffer. To elute the $CD34^+$ cells out of the column 5 ml MACS buffer was used in absence of the magnetic field. The isolated cells were loaded on the separation column again to increase the purity of $CD34^+$ fraction. The isolated $CD34^+$ cells were counted by Neubauer chamber.

3.2.1.3 Flow cytometric isolation of bone marrow cells

The fluorescence-activated cell sorting (FACS) is a method to sort and analyze a heterogeneous population of cells based on scattered light and fluorescent properties of each single cell. It enables the measurement of the relative cell size, granularity and multiple fluorescent dyes simultaneously for more than thousands of cells within seconds (Bonner, 1972). Cell probes stained with fluorescent dyes pass through a monochromatic laser beam lined-up single-file based on the principle of hydrodynamic focusing (Shuler *et al.*, 1972). At the measurement point, scattered light and fluorescent signals of the single-cell were registered by optical sensors and converted into electronic signals. The scattered light signal of the cell striking the photo-detector placed directly in front of the laser beam (at 0° angle) is called “forward scatter” which is often taken as a measure for the relative size of a cell (Givan, 2004). The scattered light signal of the cell striking the photo-detector placed in 90° position to the laser beam is called “side scatter” which is often a measure for the irregularities or granularity on the surface or in the cytoplasm of the cell (Givan, 2004) (Figure 8). The detected fluorescent signals are quantitative measures for the relative expression levels of cell surface antigens given the fact that the emitted fluorescent signal is proportional to the amount of antibody bound to the cell surface.
At the analysis point of a flow cytometer with the laser beam, the sheath stream and the lenses for collection of forward scatter, side scatter and fluorescent signals are all at orthogonal angles to each other.

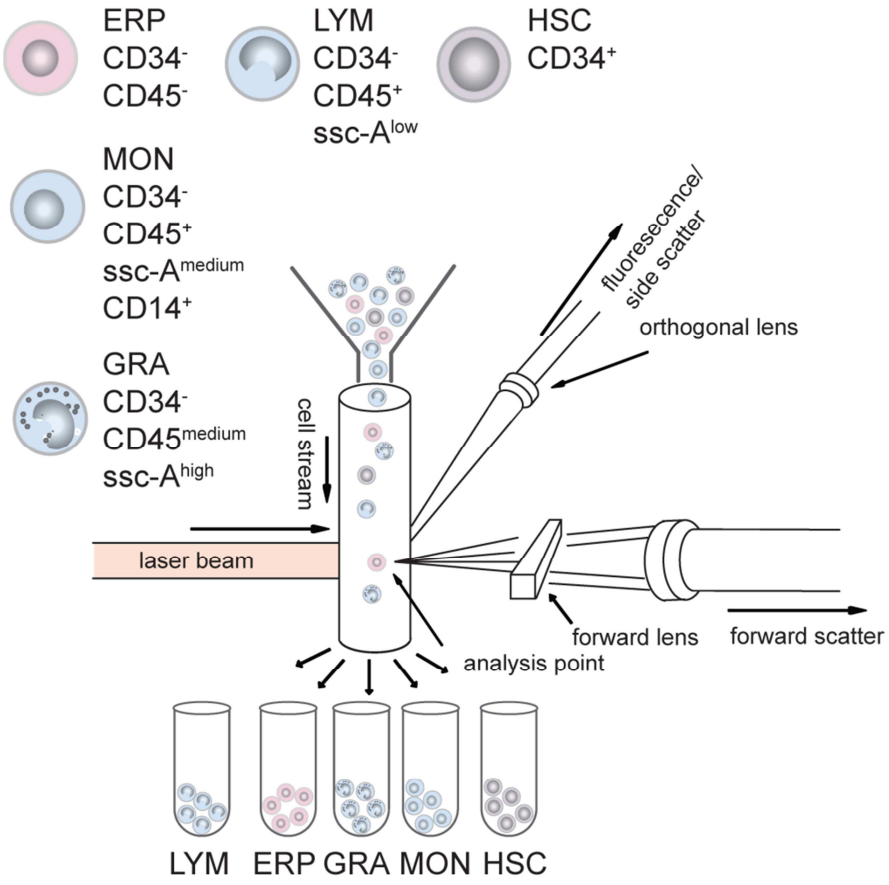

Figure 8 Principle of fluorescence-activated cell sorting. Bone marrow mononuclear cells were sorted into different populations based on forward scatter, side scatter and fluorescence carried by conjugated antibodies. At the analysis point, the laser beam, detectors of forward and reverse scatter are all at orthogonal angles to the flow direction of the cells. ERP, erythroid precursors; MON, monocytes, macrophages and restricted precursors; GRA, granulocytic precursors; LYM, lymphocytes and restricted precursors; SSC-A, side scatter area. Picture created based on Givan (Givan, 2011).

The FACS sorting was carried out using a BD FACS-Aria III cell sorter with BD FACS-Diva operation interface. The data analysis was performed using BD FACS-Diva software and FlowJo 7.6 Flow Cytometry software. The mononuclear cells were resuspended in 1 ml PBS for cell sorting. Four cell aliquots diluted in 100 µl PBS were used as autofluorescent and compensation controls. One aliquot was kept unstained as autofluorescent control. The other three cell aliquots were stained with 1 µl CD34 antibody, 1 µl CD45 antibody and 1 µl CD14 antibody, respectively. For every 10^7 mononuclear cells, the suspension was stained with 4 µl CD34, 4 µl CD45 and 4 µl CD14 antibody at 4 °C for 30 min. The cells were subsequently washed in MACS buffer at 400 x g for 6 min. The main sample was resuspended in 1-2 ml MACS buffer and filtered through a red PARTEC CellTrics 20 µm filter in a 15 ml tube. For cell sorting, 15 FACS tubes provided with 750 µl MACS buffer were prepared.

Right before cell sorting, 1 µl propidium iodide was added to each sample to exclude apoptotic and necrotic cells. After sorting, a small aliquot of sorted sample was re-measured on the FACS machine to determine the technical sorting purity. The sorted samples were washed once with 50 ml PBS at 400 x g for 7 min and cell pellets were frozen in Eppendorf tubes for subsequent procedures.

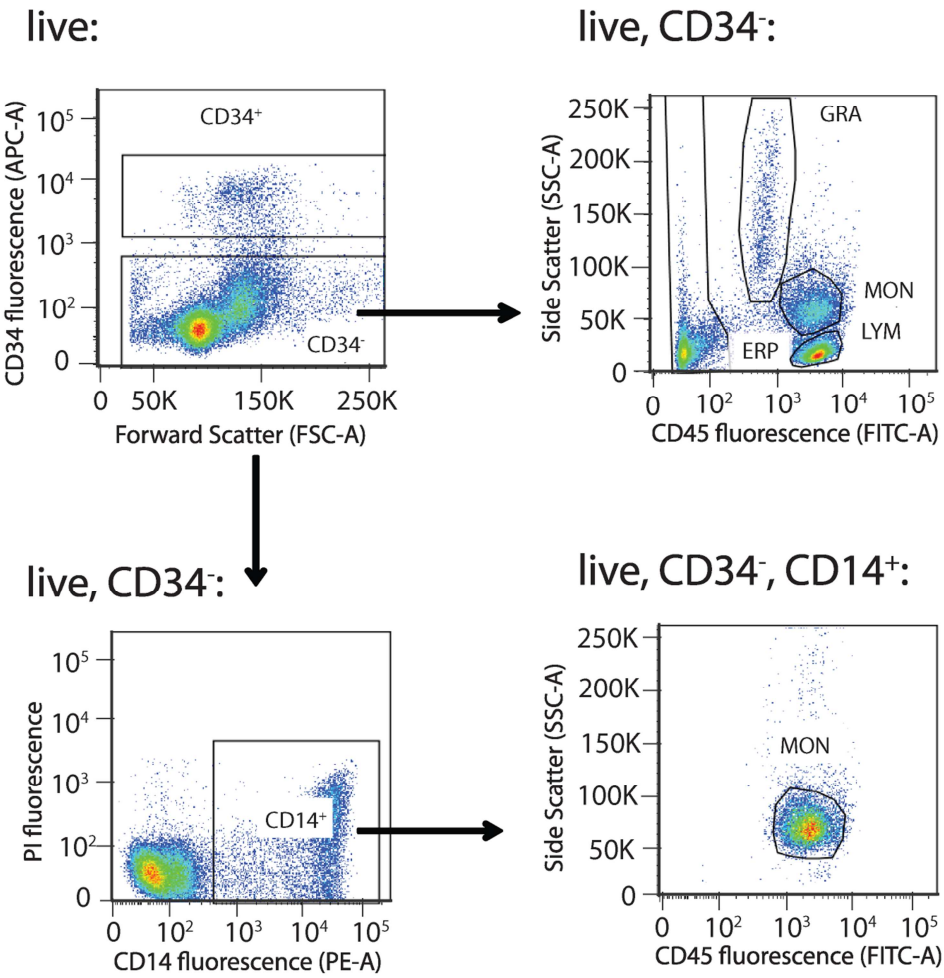

Figure 9 The mononuclear cell population was separated by hierarchical gating. Mononuclear cells were divided into HSCs and non-HSCs by the expression level of CD34 (CD34-APC). The $CD34^-$ population was further divided into lymphocytes and precursors (LYM), erythroid precursors (ERP), and granulocytic precursors (GRA) by their different side scatter properties (granularity) and the expression levels of CD45 (CD45-FITC). The monocytes, macrophages and precursors (MON) were additionally constrained by the expression level of CD14 (CD14-PE).

3.2.2 Isolation of MSCs

The mononuclear cells isolated from human bone marrow were seeded in 10 ml 7^{th} medium in a T75 or T25 culture flask at a density of $1x10^6$ cells per cm^2. With an optimal cell amount of $2.5x10^7$ cells, the initial medium containing non-adherent cells and debris was changed 72 h after seeding. Depending on the adherent growth of the MSCs, initial colonies were formed after 10-14 days of culture. MSCs were expanded and stored at early passage number (passage <4) in liquid nitrogen. Alternatively the MSCs were isolated from filter sets of bone marrow aspiration bags used for bone marrow transplantations. Those filter sets contained residual amounts of MSCs which were washed out with PBS and cultured in 7^{th} medium.

3.2.3 Culture of MSCs

The culture of MSC was set in 7^{th} medium at an initial density of $1x10^4$ cells/cm^2. The cells were passaged at 80-95% confluence after 3-7 days depending on the growth rate. The cells were passaged by removing the old medium, washing the cells once with PBS and adding 1.5 ml of 0.25% Trypsin-EDTA. After incubation at 37 °C for 3-5 min, the MSCs were fully dissolved from the cell surface and the proteolytic trypsin cleavage was stopped by adding 2 ml of R10 medium. The cell suspension was centrifuged at 400 x g for 7 min, the cell pellet was dissolved in 1 ml 7^{th} medium and the cell number was determined by Neubauer chamber. Subsequently the cells were seeded into a new culture flask provided with fresh 7^{th} medium at 1 x 10^4 cells/cm^2.

3.2.4 Culture of HSCs

The $CD34^+$ cells from cord blood and mobilized peripheral blood were grown in long-term bone marrow culture medium (LTBMC medium). The LTBMC medium was sterile filtered and stored at -20 °C. The medium was centrifuged once at 1600 g for 10 min at room temperature before usage. The supernatant was used for the HSC culture. The culture was set in 12- and 24-well format at 37 °C and 5% CO_2.

3.2.5 Culture of lymphoblastoid cell line

The GM12878 cells derived from human lymphoblastoids were grown in RPMI1640 medium provided with 25% FBS, as previously indicated. The cells were seeded at a concentration > 200,000 cells/ml. The culture was set in T25 flaks at 37 °C and 5% CO_2. Cells were passaged at a density of 200,000 – 500,000 cells/ml.

3.2.6 Carboxyfluorescein succinimidyl ester staining

To investigate the proliferation behavior of HSCs after seven days of *in vitro* co-culture with MSCs. The HSCs were stained with a fluorescent dye prior to the co-culture. The compound carboxyfluorescein diacetate succinimidyl ester (CFDA-SE) diffuses through the cell membrane and is subsequently cleaved by the intracellular esterases into the fluorescent carboxyfluorescein succinimidyl ester (CFSE). The CFSE molecules bind irreversibly to the amines of the free lysine chains which get divided homogeneously into two daughter cells after each cell division resulting in a decrease of the fluorescent signal by 50%.

Cord blood HSCs were washed once in MACS buffer (580 x g, 7 min, room temperature) and resuspended in 750 µl PBS with 0.1% FCS. An aliquot of 250 µl 10 µM CFDA-SE was added to the cells and incubated at 37 °C for 10 min. To stop the reaction, 7 ml ice cold RPMI 1640 provided with 10% FCS was added to the cells and incubated on ice for 5 min. Subsequently, the cells were washed twice in MACS buffer (580 x g, 7 min, RT), resuspended in long-term bone marrow culture medium (LTBMC) and cultured for up to seven days. An aliquot of the cells remained unstained and was kept separately in LTBMC. This was used as auto-fluorescent control of the flow cytometry analysis.

3.2.7 Propidium iodide staining

Cells measured by flow cytometry were stained with propidium iodide to evaluate cell viability. Propidium iodide is a membrane impermeant compound which is generally excluded from viable cells. In apoptotic and necrotic cells with permeant and impaired membranes, the fluorescent dye binds to DNA by intercalating between base pairs. Samples resuspended in MACS buffer were incubated with 1-2 µl propidium iodide at room temperature for 15 min prior to flow cytometry measurement.

3.2.8 Cryo-preservation of the cells

MSCs and cell lines were stored in -80 °C freezer and subsequently in liquid nitrogen. Each aliquot of $1x10^6$ MSCs was resuspended in 500 µl 7^{th} culture medium, 400 µl FCS and 100 µl DMSO in a cryovial. The vials were transferred to a Mr. Frosty freezing container provided with isopropanol and stored at -80 °C for 24 h. Frozen cells were maintained in liquid nitrogen for long-term storages.

3.2.9 Antibody staining of HSCs

The cells were counted by Neubauer chamber and washed in MACS buffer. Subsequently the cells were transferred into FACS tubes and washed again in MACS buffer (580 x g, 6 min, room temperature). The supernatant was discarded and a residual volume of 100 µl remained for antibody staining. For every fluorochrome, an unstained control to determine the autofluorescence of the cells was prepared. If multiple antibodies were used in parallel, fluorescent compensation controls were prepared for each fluorochrome by staining the cells using the corresponding antibody. The probes were stained at concentrations recommended by the manufacturer at 4 °C for 30 min. The cells were washed once in MACS buffer at 580 x g for 6 min. The remaining cell pellet was resuspended in 200 µl MACS-buffer. Prior to flow cytometry measurement, an aliquot of 1 µl propidium iodide was added to stain the apoptotic and necrotic cells.

3.2.10 Co-culture of HSCs and MSCs

A co-culture of HSCs and MSCs were used as a model to study interactions between the stem cell niche and HSCs *in vitro*. HSCs were cultured on a monolayer of MSCs for seven days.

3.2.10.1 Preparation of MSC feeder layer

An initial amount of $3x10^4$ MSCs per 24-well or $5x10^4$ MSCs per 12-well were seeded in 500 µl or 1 ml 7^{th} maintenance medium. After overnight incubation at 37 °C, the cells became adherent to the plastic well surface. The monolayer of cells were either kept in the maintenance medium or differentiated into adipogenic and osteogenic differentiated MSCs for 21 days obtaining undifferentiated MSCs, adipgenically differentiated MSCs (ADI-MSCs) and osteogenically differentiated MSCs (OST-MSCs), respectively.

3.2.10.2 Initiation and termination of the co-culture

To initiate the HSC-MSC co-culture, the MSC media were removed and the MSC, ADI-MSC and OST-MSC monolayers were washed twice with 1 ml PBS for each well. To each 24-well of confluent feeder cell layer, 1-2.5x10^5 $CD34^+$ cells resuspended in 500 µl long-term bone marrow culture medium (LTBMC) were added and co-cultured for seven days at 37 °C, 5% CO_2. To analyze the HSCs after seven days co-culture, the HSCs were separated physically from the MSCs by repeated pipetting of the culture medium. The HSCs were subsequently stained with fluorescent antibodies ready for flow cytometric analysis. To investigate the effects of indirect contact between HSCs and MSCs, co-culture experiments in a transwell setup were carried out. For each transwell insert containing a polycarbonate membrane with a pore size of 0.4 µm, HSCs were cultured in 100 µl LTBMC. The monolayers of MSCs, ADI-MSCs and OST-MSCs were cultured in 400 µl LTBMC per 24-well.

3.2.11 Differentiation of MSCs

Osteogenic and adipogenic differentiation protocols of MSCs were adapted from Pittenger *et al.* (Pittenger *et al.*, 1999). An initial amount of 30,000 MSCs in 0.5 ml 7^{th} medium were seeded to each 24-well until 60% confluence was obtained. Subsequently, the 7^{th} maintenance medium was substituted by adipogenic or osteogenic differentiation medium to induce the respective differentiation of the MSCs. The cells were cultured in differentiation medium for 21 days with medium changes every three days.

3.2.12 Staining of triglycerides in adipoblasts

The lipophilic dye BODIPY at a concentration of 10 µg/ml was added to adipogenically differentiated MSCs previously fixed with 4% paraformaldehyde (PFA) in a 24-well plate. After 20 min incubation at room temperature in absence of light, the cells were washed once by PBS. The stained cells were investigated by fluorescent microscopy in combination with DAPI nuclear staining.

3.2.13 Staining of hydroxyapatite in osteoblasts

Osteogenically differentiated MSCs form bone-like inorganic hydroxyapatite which was stained with antibody-based OsteoImage Assay. An aliquot of 0.5 ml diluted staining antibody from OsteoImage Assay Kit (Lonza) was added to osteogenically differentiated MSCs previously fixed with 4% PFA in a 24-well plate. After 30 min incubation at room temperature in absence of light, the cells were washed three times with the washing buffer provided by the OsteoImage Assay Kit. The stained cells were subsequently investigated by fluorescent microscopy in combination with DAPI nuclear staining.

3.2.14 ATAC-sequencing

3.2.14.1 Preparation of lymphoblastoid cells

The workflow for ATAC-seq library preparation was established using the human lymphoid cell line GM12878 in order to compare our sequencing results with the reference dataset published by Buenrostro *et al.* (Buenrostro *et al.*, 2013). The GM12878 cells were cultured as previously described. For our library preparation, an aliquot of 50,000 viable cells in exponential growth phase was harvested and quality checked by FACS sorting using propidium iodide life and death staining.

3.2.14.2 Preparation of MSCs

Primary mesenchymal stromal cells derived from healthy individuals of different ages were expanded in 7th culture medium. The cells were seeded into two 12-well plates at passage four. One plate was used for subsequent ATAC-seq workflow and the other plate for fluorescent microscopy imaging. The cell number in each well was determined by DAPI nuclear staining of the imaging plate. For each strain, three wells were imaged to determine the cell number using automatized cell counting (ImageJ). The adherent cells were harvested using 400 µl accutase, later neutralized using 600 µl R10 medium. From the suspension, 50,000 cells were taken for ATAC-seq library preparation.

3.2.14.3 Tagmentation

An aliquot of 50,000 cells in single-cell suspension was washed once with 200 µl ice-cold PBS at 500 x g, 4 °C for 5 min. The cell pellet was subsequently resuspended in 50 µl tagmentation mix containing 2.5 µl TDE, 25 µl 2x TD Buffer (both from Nextera kit), 22 µl nuclease-free H_2O and 0.5 µl 1% digitonin. The suspension was incubated at 37 °C for 30 min. The reaction mixture was purified using Qiagen PCR purification kit. The MinElute column was eluted with 12 µl elution buffer. The DNA concentration was measured by the Qubit system.

3.2.14.4 PCR-amplification of the library

The DNA mixture from the previous tagmentation step was mixed with 10 µl nuclease-free H_2O, 2.5 µl of 25 µM Nextera Indexing Primer i7, 2.5 µl of 25 µM Nextera Indexing Primer i5 and 25 µl of NEBNext High-Fidelity 2x PCR master mix. The PCR was run using the following program: 72 °C, 5 min; 98 °C, 30 sec; cycle start: 98 °C, 10 sec; 63 °C, 30 sec; 72 °C, 1 min, cycle close (run 5 cycles). To reduce GC and size bias in PCR, the remaining number of PCR cycles (N) was determined using a real-time PCR side reaction, allowing a termination of amplification prior to saturation. The additional cycles of PCR was run using the following program: 98 °C, 30 sec; cycle start: 98 °C, 10 sec; 63 °C, 30 sec; 72 °C, 1 min, cycle close (run N cycles).

3.2.14.5 Real-time PCR

The appropriate degree of PCR amplification was determined using real-time PCR which prevents the prepared ATAC-seq DNA library from containing too many multiplicated fragments. An over-amplification of the tagmented library would also lead to GC and fragment size bias caused by PCR. Using real-time PCR, the detection of the PCR amplification products in real time after every cycle is based on the fluorescent signal of the SYBR Green Dye I which intercalates into the double-stranded DNA. The SYBR Green Dye I is a cyanine dye which forms a complex with DNA and is excited by a laser beam at 522 nm. The measured fluorescence increases proportionally with the amplified products. After the amplification, an analysis of the real-time PCR amplification plot was performed.

For each sample, a real-time PCR master mix was prepared by adding 0.9 µl of 10x SYBR Green I Fluorescent Dye to 5 µl of NEBNext High Fidelity 2x PCR master mix and 3.6 µl of nuclease-free H_2O. An aliquot of 9.5 µl master mix was added to 5 µl of the previously amplified DNA library together with each 0.25 µl of the Nextera indexing forward and reverse primers used in previous steps. The real-time PCR was run using the following program: 98 °C, 30 sec; cycle start: 98 °C, 10 sec; 63 °C, 30 sec; 72 °C, 1 min, cycle close (run 25 cycles). As described by Buenrostro *et al.*, the additional number of cycles N was determined as the cycle number that corresponds to one-third of the maximum fluorescent intensity on the linear Rn versus cycle plot (Buenrostro *et al.*, 2013).

3.2.14.6 Agarose gel electrophoresis

For each gel, 1.08 g agarose in 100 ml 1 x TBE-Puffer was melted and poured into a BioRad gel chamber. To stain the gel, 4 µl of fluorescent nucleic acid gel dye were added. The 45 µl PCR product was mixed with 9 µl of 6 x loading dye and run at a constant voltage of 120 V for one hour. An aliquot of 8 µl 100 bp DNA plus ladder was run on the side of the samples. Gel pieces from right above the primer dimer band (ca. 100 bp) to 1 kb was cut and isolated with a scalpel on a blue light transilluminator at 470 nm. DNA was extracted using Qiagen gel extraction kit. The agarose gel slice of every sample was divided equally into two pieces and eluted with two MinElute columns. The concentration of the libraries was measured by Qubit system and the quality of the libraries was assessed by BioAnalyzer.

3.2.14.7 Assessment of ATAC-seq library quality

The quality of the prepared ATAC-seq DNA libraries was assessed using BioAnalyzer 2100 High Sensitivity DNA Assay according to descriptions of the manufacturer. This analysis method to test the quality and quantity of DNA libraries on a chip is based on the principle of capillary electrophoresis. DNA fragments of different lengths are separated according to their sizes along an electrical field in micro-capillary channels. The DNA fragments of different lengths are detected by a fluorescent sensor. For each prepared ATAC-seq library, an aliquot of 1 µl (up to 50 ng) was loaded on to the BioAnalyzer chip. A BioAnalyzer profile representing the

fragment size distribution of the loaded ATAC-seq library was acquired using the Agilent 2100 BioAnalyzer Software.

3.2.14.8 Measurement of DNA concentration

The concentrations of the ATAC-seq libraries were determined on a Qubit fluorometer. The Qubit system is based on the principle that a fluorescent dye has very low fluorescence until it binds to DNA. Upon intercalation between DNA bases, it becomes intensely fluorescent enabling the measurement of the sample DNA concentration on a fluorometer (Schweitzer *et al.*, 2003). For each sample, 1 µl was added to the buffer and dye provided by the Qubit DNA HS Assay kit according to descriptions of the supplier.

3.2.14.9 Deep sequencing of ATAC-seq library samples

The next-generation sequencing of the ATAC-seq libraries was carried out at the Genome Core Facility of EMBL Heidelberg. Up to eight samples were multiplexed in equal molarity and run on Illumina NextSeq 500 Platform to obtain 75 bp paired-end sequencing reads (ca. 120-150 million reads per sequencing lane). The first sample batch was sequenced on a Illumina HiSeq2000 machine with 50 bp single-end read lengths and 50 million reads per replicate.

3.2.14.10 Alignment and peak calling

Before alignment to the human reference genome the ATAC-seq sequences were quality-checked using FastQC focusing on criteria such as total number of reads, sequencing length distribution, sequence quality per base and duplication level. Subsequently, adaptor sequences were trimmed off the 75 bp paired-end reads using the software tool Trimmomatic. The sequencing reads were mapped to the hg19 reference human genome using Bowtie2. PCR duplicates were removed using Picard tools. For the mapped reads, a mapping score MAPQ was assigned. A cutoff (MAPQ<10) was taken to filter out reads with low mapping quality. Reads mapping to the mitochondrial genome as well as those reads having insertions or deletions were removed. The ATAC-seq peaks were subsequently called using the software

package MACS2 (Model-based Analysis of ChIP-Seq) with parameters "–nomodel –q 0.001".

After peak calling, the quality of the sequenced libraries was further checked using the transcription start site (TSS) enrichment score (Figure 10). This is defined as the ratio between ATAC-seq signal proximal to TSS (+/- 2kb window) and ATAC-seq signal distal to TSS (1kb window). A TSS enrichment score of 7 was used as an empirical threshold for signal-to-noise ratio. The Bioconductor package DiffBind was used to extract the read counts falling in a consensus set of peaks, which was defined as those peaks having signal for at least two different individuals per samples. To detect significant changes upon aging across sequencing samples, a differential peak analysis was carried out using DESeq2 with linear regression (Anders *et al.*, 2012). The size factors were calculated using "median ratio method". We tested the null hypothesis that the signal remains unchanged with age using the model "enzyme_batch_and_sex + donor age". The term "enzyme_batch_and_sex" accounts for batch and gender effects in ATAC-seq profiles. Statistical significance was tested according to a Wald test and p-values corrected for multiple testing with Benjamini-Hochberg. We took adjusted p-value <=0.05 as significant for all of the subsequent analyses.

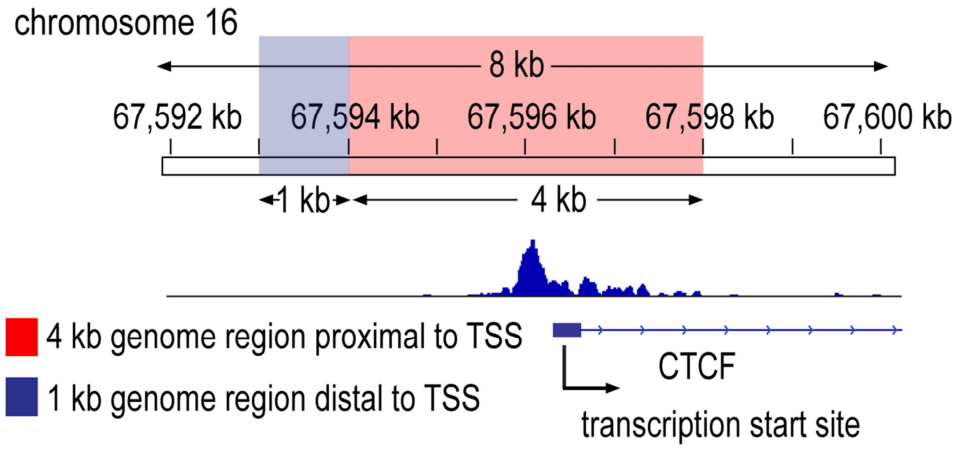

Figure 10 An average enrichment score was calculated based on annotated transcription start sites. The enrichment score is the ratio of 4 kb window around transcription start sites and ATAC-seq signal distal to transcription start sites of protein coding genes (1 kb window). Empirically, a threshold enrichment score of 7 is used for quality checks of the dataset. The open chromatin profile at locus of transcriptional repressor CTCF (CCCTC-binding factor) was shown.

4. Results

4.1 Immnunophenotypic characterization of the human bone marrow

4.1.1 Separation of bone marrow mononuclear cells into six cell types

Within the overarching goal of the collaborative working group in elucidating the molecular mechanisms of aging in human bone marrow, this project focuses on the age-associated alterations in human bone marrow microenvironment, *i.e.* the hematopoietic stem cell niche. Although the role of the marrow niche in maintaining the stemness of HSCs has been recognized, a molecular understanding of the interactions between stem cells and the marrow niche during the aging process remains elusive so far (Köhler *et al.*, 2009; Florian *et al.*, 2012).

As part of the large-scale SystemAge project, bone marrow samples from 59 healthy human individuals between ages of 20 and 60 were collected. The age-associated changes were investigated on transcriptome and proteome levels using shotgun mass spectrometry proteomics and RNA sequencing. The project has been approved by the Research Ethics Board of the University of Heidelberg and written informed consent was obtained from every human subject.

As described in the method section 3.1.1.2, bone marrow aspirates were taken by puncture of the iliac crest. The mononuclear cell fraction was subsequently isolated by FICOLL density gradient centrifugation. From each sample, the $CD34^+$ cells were isolated as the population with enriched hematopoietic stem cells (HSCs). CD34 is a common marker for hematopoietic stem cells. It is a glycoprotein which functions as a cell adhesion factor mediating the attachment of stem cells to the bone marrow extracellular matrix (Sidney *et al.*, 2014). Out of the $CD34^-$ cell population, granulocytic precursors (GRA) were defined by the medium expression of CD45 and high granularity reflected in the high expression of the side scatter (SSC-A). Erythroid precursors (ERP) was the $CD45^-$ population. Lymphocytes and precursors (LYM), monocytes, macrophages and precursors (MON) showed high expression levels of CD45; CD45 is a common leukocyte antigen that belongs to the protein tyrosine phosphatase (PTP) family. PTPs regulate various cellular processes including cell

growth and differentiation (Tonks, 2006). The MON population was further defined by the monocyte-specific cell surface marker CD14 (Figure 11). CD14 is a specific marker for monocytes, macrophages and precursors (MON). The cell type MSC was isolated *in vitro* by plastic adherent growth in the maintenance culture medium from the mononuclear cell fraction. The isolated cell types were subjected to further downstream shotgun proteomics and RNA sequencing analysis.

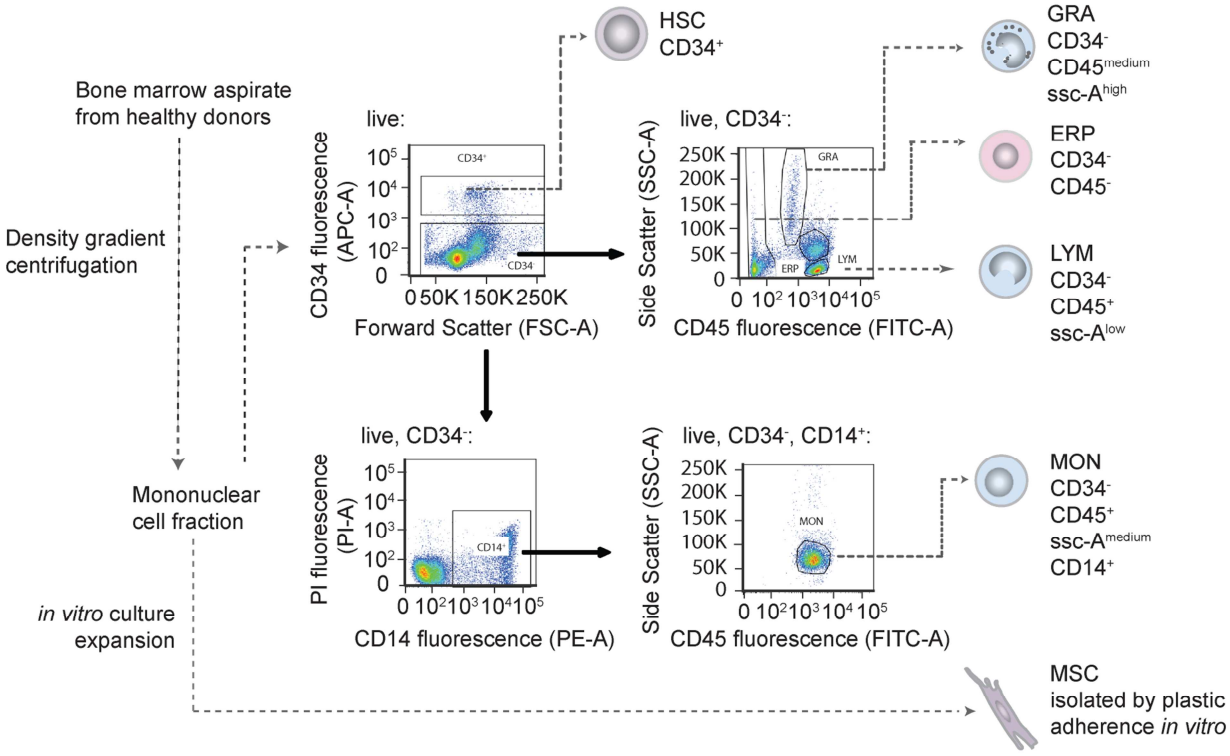

Figure 11 Overview of the experimental workflow and cell types used in the study. Bone marrow aspirates from healthy human individuals were separated by FICOLL gradient centrifugation into mononuclear cell fraction. Hematopoietic stem cells (HSC), lymphocytes and restricted precursors (LYM), monocytes, macrophages and restricted precursors (MON), granulocytic precursors (GRA) and erythroid precursors (ERP) were isolated by fluorescence-activated cell sorting (FACS). The live cell population was first separated into HSCs and non-HSCs by the expression level of CD34. The non-HSC population was subsequently sorted into LYM, MON, GRA and ERP by side scatter and expression levels of CD45. The MON population was additionally constrained by the expression of CD14. MSCs were isolated and expanded by plastic adherent growth *in vitro*.

The bone marrow donors were recruited over a time period of three years. Out of the total evaluable 59 donors, 24 were between ages 20 and 30; 13 were between 31 and 40; 12 were in the age group between 41 and 50 and 10 between ages 51 and 60. The stronger concentration of donors in the younger age groups is due to the fact that younger individuals were more willing to donate their bone marrow samples (Figure 12A).

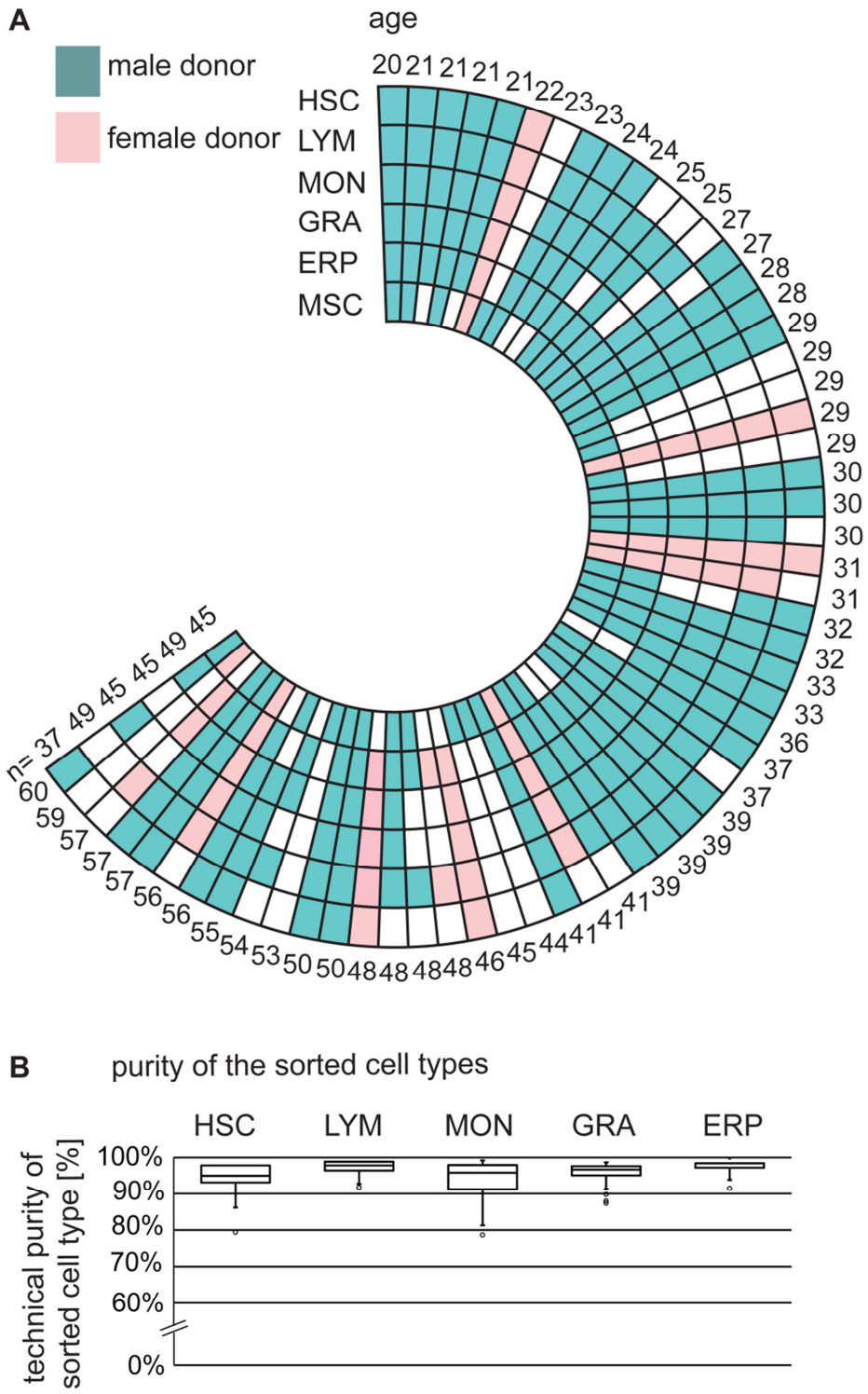

Figure 12 A general overview on the age distribution and the quality of isolated bone marrow samples. (A) The age and gender distribution of hematopoietic stem cells (HSC), lymphocytes and restricted precursors (LYM), monocytes, macrophages and restricted precursors (MON), granulocytic precursors (GRA), erythroid precursors (ERP) and mesenchymal stromal cells (MSC) derived from 59 human individuals are shown. Each section represents one cell type as indicated at the beginning of the circle. The age of the donors is indicated at the periphery of the circle. The gender of the donor is shown in green (male) and red (female). **(B)** The technical sorting purity of FACS-isolated bone marrow cells is shown by box plots.

4.1.2 Technical purity of sorted cell samples

For the intepretation of our downstream proteomics and transcriptomics results, it is essential to achieve a high degree of purity of the sorted cell types. Each time after FACS sorting, the purity of the separated cell populations was determined by remeasuring a small aliquot of sorted cells on the FACS machine using the same detection conditions. The purity of the sorted probe was calculated by the analysis of the post-sorted FACS data. The majority of the sorted samples have a purity above 90% as shown in figure 12B. For most of the sorted cell types, a major source of impurities was found to be erythroid progenitors and erythrocytes (ERP) (Figure 13). Due to their relatively small size, these cells tend to adhere on the surface of larger cells in the mononuclear cell fraction. Apart from ERP, cells of the mononuclear cell population outside of the sorting gates were another major source of impurity (Figure 13). The high sorting purity of the the isolated cell populations was confirmed by the subsequent proteomic measurements. In the proteomics dataset, all established cell type-specific markers could be identified in the corresponding cell type sorted by FACS.

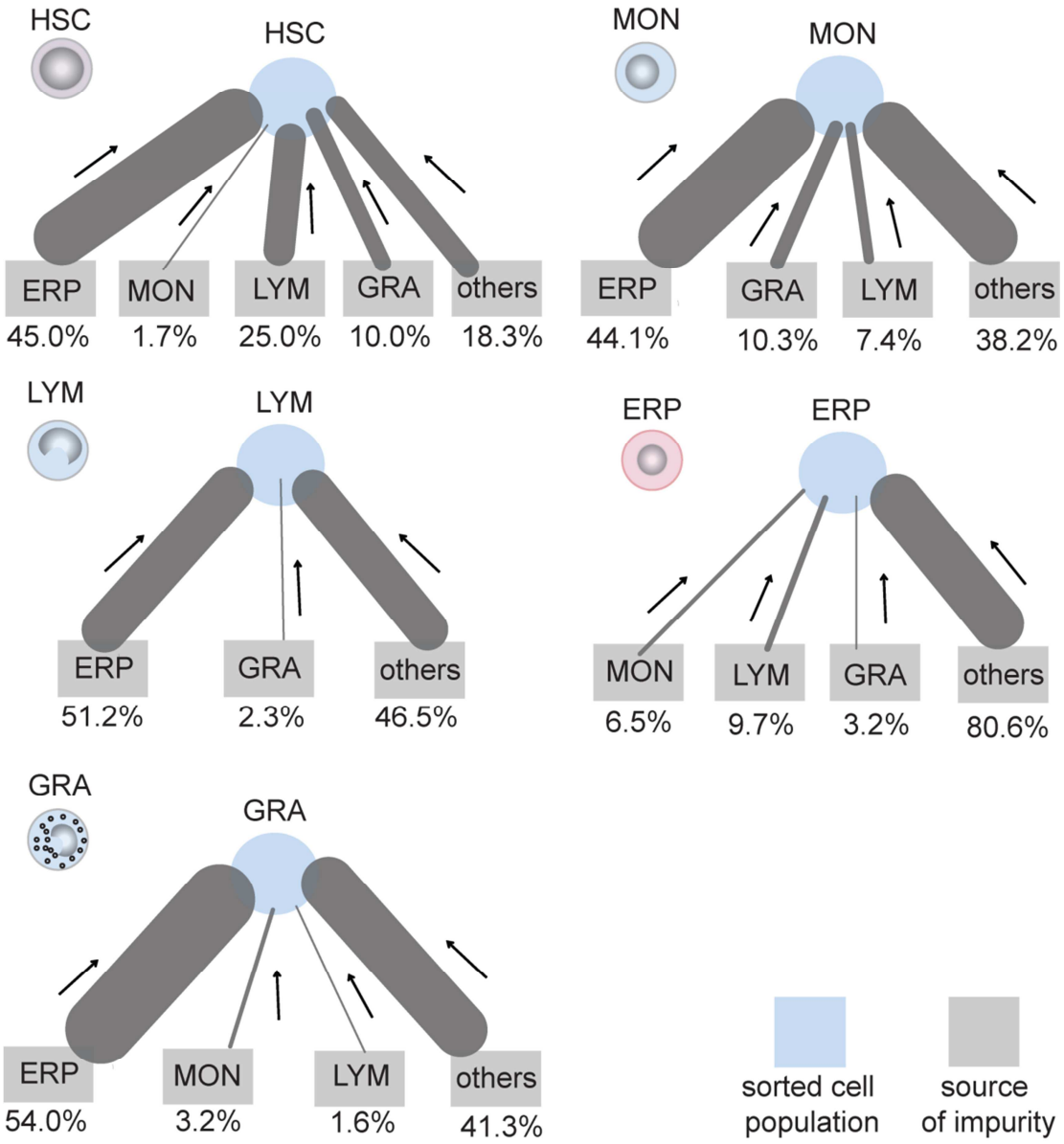

Figure 13 Sources of contamination in the FACS-sorted cell types. The contaminations for the FACS-sorted cell types hematopoietic stem cells (HSC), lymphocytes and restricted precursors (LYM), monocytes, macrophages and restricted precursors (MON), granulocytic precursors (GRA) and erythroid precursors (ERP) were determined. The sorted cell populations were shown in blue whereas sources of impurities were shown in grey. The box “others” indicated mononuclear cells apart from the gated cell types. The thickness of the edges between sorted cell population and source of impurities indicated the relative contribution of each source to the total impurity.

4.1.3 Individual variability in relative percentages of the major bone marrow constituents

To verify whether there might be alterations in the cellular composition of human bone marrow upon aging, we studied changes in the bone marrow constituent cells with respect to age.

The flow cytometry data generated during FACS isolation of the five cell types HSC, LYM, MON, GRA and ERP were analyzed to determine the relative percentage of each cell type in the mononuclear cell fraction. As shown in figure 14A, 31.1% of the bone marrow mononuclear cells were ERP, which was the largest population. However, broad variations in the relative percentages (5.6% to 69.1%) were observed among individual donors. Another 29.2% of the mononuclear cells consisted of LYM. The median relative percentage of MON in the mononuclear cell population was at 9.9% and the median relative percentage of GRA was 14.8%. The smallest fraction in the mononuclear cell fraction was HSC, which was at 2.0% (Figure 14A). Taking the median percentages of the cell types together, the five cell types sorted by FACS constituted about 87% of the mononuclear cell fraction in the bone marrow niche. In conclusion, variations were observed among the relative percentages of each cell type in the mononuclear cell population.

As a second step, we determined if the observed variations are associated with the biological age of the donors. For all five cell types measured by flow cytometry, a linear correlation was tested. As shown by the coefficients of determination (R^2), a linear correlation between the relative percentages in the mononuclear cell population with age was not observed (Figure 14A). In addition, a spearman test indicated that for each sorted cell type, the relative percentage does not correlate with the donor age (Supplementary Material, Table 2).

Overall, the variability in relative percentages observed among individual samples might be of technical or biological origins. Depending on the location of the puncture and volume of the bone marrow aspirate, the cellular composition of the mononuclear cell fraction might vary between samples. To further investigate the biological variability among individuals, a larger cohort with more samples from elderly donors would be required for statistical correlation tests with age.

4.1.4 Individual variability in relative cell size and granularity of the major bone marrow constituents

To investigate if the relative size and granularity of the samples vary between individual donors, the forward and side scatter properties of the FACS-sorted cells were studied. As described in the method section, the forward scatter is a measure for the relative size of a cell, whereas the granularity of the cell is reflected by the side scatter in flow cytometry (Givan, 2004). The knowledge about sample variability in cell size is *e.g*. useful for later normalization efforts of the downstream proteomics dataset. Fold changes in protein abundance can be *e.g.* put in relationship with the relative changes of the cell size to better interpret the experimental data.

Since the cohort of samples was acquired over a period of three years, the LYM population was used as an internal standard due to its dense cell population in order to compare between flow cytometry measurements. Changes in forward and side scatters of HSC, GRA, MON and ERP were investigated in relationship to the LYM population. As indicated in figure 14B and C, variations in cell size as well as cell granularity were observed for all four cell types. To investigate if the sample variations were correlated with the age of the donors, a linear correlation was tested. As shown by the coefficients of determination (R^2) in figure 14B and 14C, a linear correlation between the relative cell size and granularity with age was not observed (Figure 14B, 14C). In addition, a spearman test was carried out to study if the size and granularity of the sorted cell types are correlated with donor age. For all sorted cell types, there was no correlation between the relative cell size and granularity with age (Supplementary Material, Table 2).

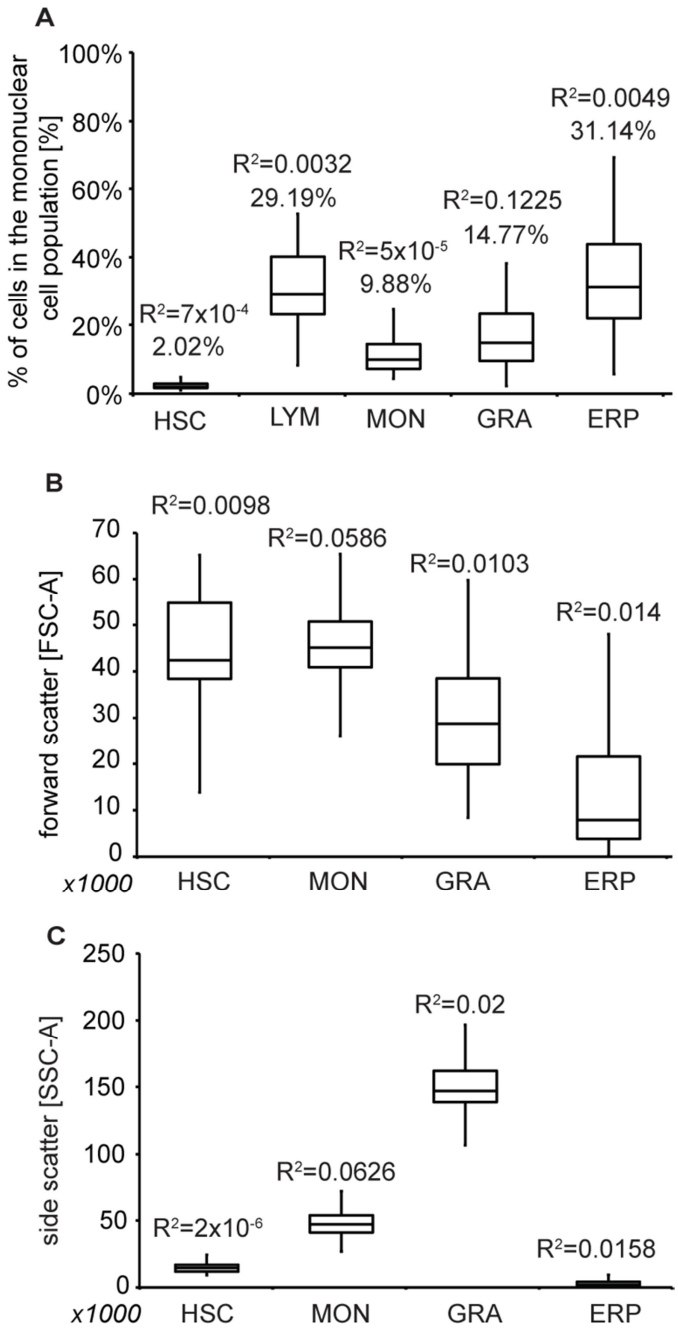

Figure 14 Relative percentages, cell size and granularity of major bone marrow constituents are not correlated with age. (A) The relative percentages of cell types HSC, LYM, MON, GRA and ERP in the mononuclear cell population were determined based on the flow cytometry data generated during the sorting process. The distribution of the relative percentages in each cell type is shown. The numbers of the analyzed samples are n=35 for HSC, n=45 for LYM, n=40 for MON, n=44 for GRA and n=45 for ERP. **(B)** The relative cell sizes reflected by the forward scatter of the flow cytometry data were determined for HSC, MON, GRA and ERP while using the LYM population as a standard. The numbers of samples analyzed are n=33 for HSC, n=40 for MON, n=44 for GRA and n=43 for ERP. **(C)** In analogy, the relative cell granularity reflected by the side scatter was determined based on the flow cytometry data. The numbers of samples analyzed are n=33 for HSC, n=40 for MON, n=44 for GRA and n=43 for ERP. R^2, coefficient of determination between donor age and relative percentage, cell size and cell granularity, respectively.

One phenotype generally observed in aged HSCs is the skewed differentiation potential towards myeloid lineage. Aged HSCs tend to differentiate more into cells of myeloid lineage, whereas the output of lymphoid-lineaged cells is decreased (Beerman *et al.*, 2017). The lymphoid to myeloid lineage skewing might be caused by changes in HSC differentiation or by altered proliferation of myeloid and lymphoid precursors (Geiger *et al.*, 2013; Beerman *et al.*, 2017). Following this hypothesis, changes in the relative percentages of myeloid (MON, GRA, ERP) and lymphoid cells (LYM) were investigated in relation to each other. As indicated by figure 15A, no correlation was observed between the myeloid to lymphoid ratio with the age of the sample donors. The myeloid-to-lymphoid ratios normalized by the concentration of mononuclear cells were plotted against donor age in figure 15B, no correlation between the normalized myeloid-to-lymphoid ratios with age was observed as well (Figure 15B). Additionally, Spearman tests indicated that there is no correlation between the myeloid-to-lymphoid ratios and donor age (Supplementary Material, Table 1).

Overall, no correlation with age was observed for the relative percentages, cell size and granularity of the bone marrow constituent cells. The variations among the samples might be of technical or biological origins. A larger cohort with more samples would be required for further statistical correlation tests with age.

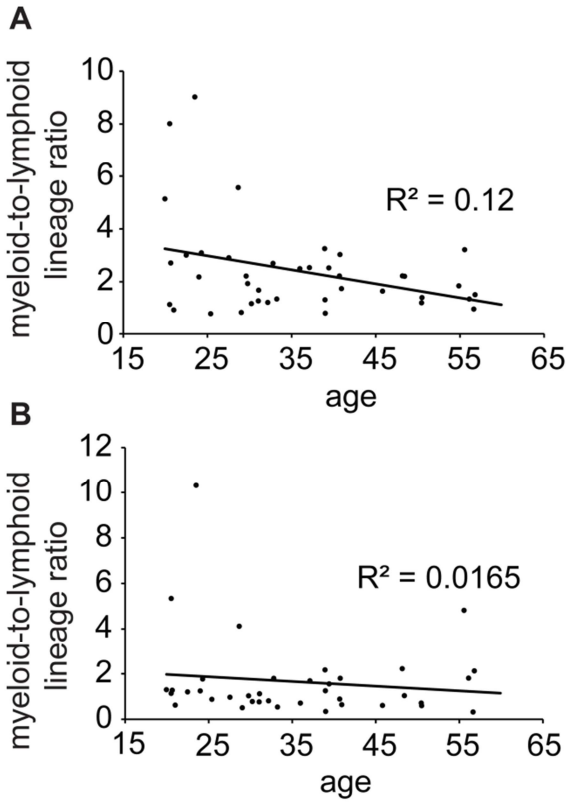

Figure 15 Ratios between relative percentages of myeloid and lymphoid cells in the mononuclear fraction are not correlated with the biological age of the donors. (A) The myeloid-to-lymphoid ratios (ERP, GRA and MON versus LYM) were determined based on the flow cytometry data generated during the sorting process. No correlation between the myeloid-to-lymphoid ratios with age was observed. **(B)** The myeloid-to-lymphoid ratios normalized by the concentration of mononuclear cells were plotted in relationship with age. No correlation between the normalized myeloid-to-lymphoid ratio with age was not observed. R^2, coefficient of determination between donor age and myeloid-to-lymphoid lineage ratios.

4.2 Differential HSC-supportive potential of MSCs, adipogenically differentiated MSCs and osteogenically differentiated MSCs

Among the six cellular components of the bone marrow characterized in this study, the cell type MSC interacts via cell surface receptors such as integrin beta 1 with the HSCs (Walenda *et al.*, 2010). MSCs have been reported to promote cell proliferation as well as maintenance of HSC stemness *ex vivo*. Based on this property, the interactions between the hematopoietic stem cells (HSCs) and the niche were studied *in vitro* using a co-culture system of $CD34^+$ HSCs and MSCs. It was shown by previous studies that aging MSCs *in vivo* possess increased potential towards adipogenic differentiation which might be responsible for the reduced potency of the MSCs to support hematopoiesis with age. We have therefore examined the supportive potentials of adipogenically differentiated MSCs (ADI-MSCs) which might

be responsible for the reduced potency of the MSCs to support hematopoiesis with age (Lee *et al.*, 2014; Marie, 2014). In this section, the *in vitro* supportive niche functions of undifferentiated MSCs, adipogenically differentiated MSCs (ADI-MSC) and osteogenically differentiated MSCs (OST-MSC) were studied.

4.2.1 Morphological characterization of MSCs

The MSCs in early passages (e.g. passage 0) showed a homogeneous, fibroblast-like morphology, whereas MSCs at higher passages (e.g. passage 7) became more heterogeneous, and ultimately stopped proliferation (Figure 16A). The adipocytes derived from MSCs exposed for 21 days *in vitro* to differentiation medium contained extensive intracellular lipid vesicles which were stained by the fluorescent dye BODIPY. The fluorescent microscopy image of the BODIPY-stained adipocytes was shown in figure 16B. In analogy, the osteoblasts were derived from MSCs exposed to differentiation medium at high calcium concentration. The OST-MSCs secret inorganic hydroxyapatite which forms precipitates on plastic surface. The hydroxyapatite of OST-MSCs was stained by an antibody-based assay OsteoImage. The fluorescent microscopy image of the OsteoImage stained OST-MSCs was shown in contrast to ADI-MSCs and MSCs in figure 16B.

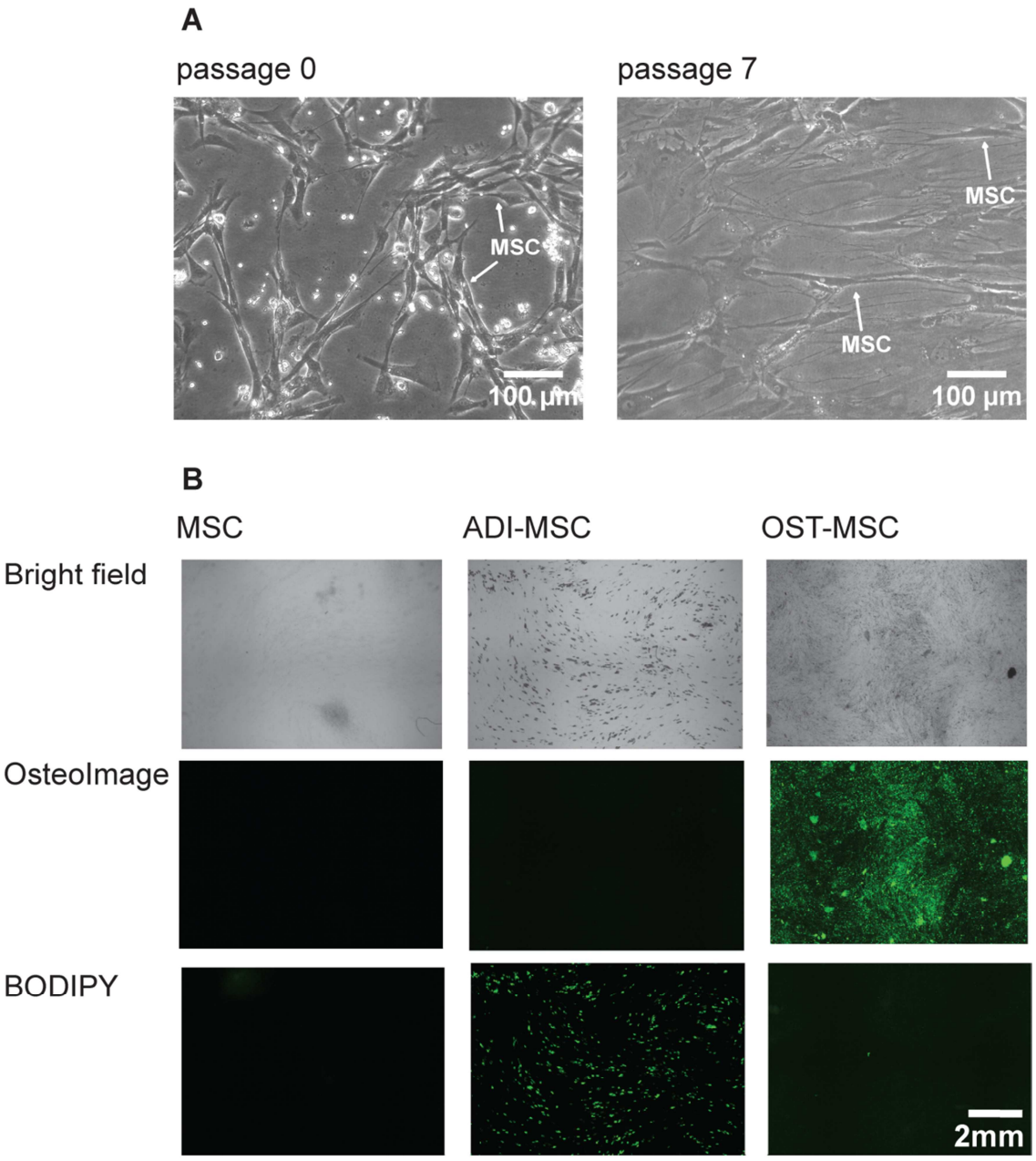

Figure 16 Morphological characterization of MSC. (A) MSCs at higher passages are more heterogeneous and ultimately stop proliferation. Representative light microscopy images of MSCs at early (passage 0) and late passage (passage 7) were shown. **(B)** Under high glucose adipogenic differentiation conditions, the MSCs showed characteristics of adipocytes after 21 days of *in vitro* culture. Under high calcium osteogenic differentiation conditions, the MSCs showed characteristics of osteoblasts after 21 days of *in vitro* culture. The triglycerides in adipogenically differentiated MSCs (ADI-MSCs) were characterized by BODIBY staining imaged by fluorescent microscopy. The secreted inorganic hydroxyapatites by osteogenically differentiated MSCs (OST-MSCs) were stained with antibody-based OsteoImage Assay.

4.2.2 Morphological characterization of HSCs

The morphology of $CD34^+$ HSC population was characterized by phase contrast and fluorescent microscopy. Freshly isolated HSCs were of a round shape and around 10 µm diameter in size (Figure 17A). The CD34 marker is a trans-membrane glycoprotein on the cell surface (Figure 17B). As indicated by the antibody-based fluorescent staining, the distribution of the CD34 antigen on the cell membrane was uneven (Figure 17B). Upon *in vitro* culture with MSCs, the cell morphology of HSCs became heterogeneous and showed both around and an elongated shape (Figure 17C) (Giebel *et al.*, 2004; Freund *et al.*, 2006). The co-culture with MSCs promotes proliferation and maintenance of the $CD34^+$ population, whereas without feeder cells the $CD34^+$ population decreases rapidly (Walenda *et al.*, 2010). The *in vitro* co-culture system serves as a surrogate model to study the cross-talks between HSCs and the bone marrow niche (Walenda *et al.*, 2010).

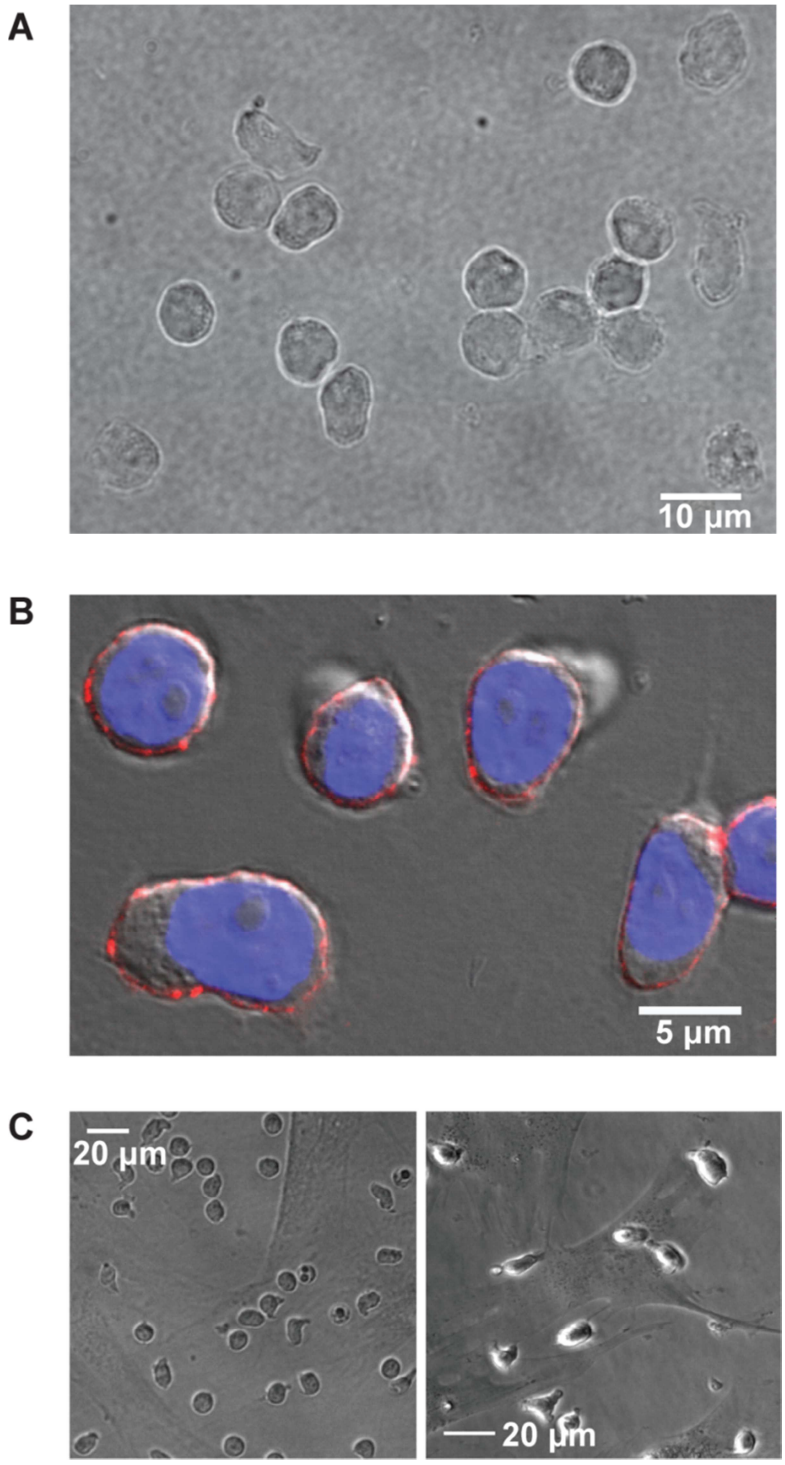

Figure 17 Microscopy images of CD34$^+$ HSCs. (A) Phase-contrast microscopy image of cord blood HSCs. The cells showed a round and oval shape. **(B)** Fluorescent microscopic images of CD34. The nuclei of the HSCs were stained by DAPI (blue). The CD34 antigen on the cell surface was stained by fluorescent antibody (red). **(C)** Microscopic images of HSC-MSC co-culture. HSCs isolated from mobilized peripheral blood (left) and cord blood HSCs (right) reside on the surface of adherent MSCs. Microscopy images taken by R. Saffrich, University Hospital Heidelberg.

4.2.3 Co-culture of $CD34^+$ HSCs with MSCs, adipogenically differentiated MSCs and osteogenically differentiated MSCs

Previous studies suggested that the increase in adipose tissue might be due to enhanced adipogenic differentiation of MSCs with age (Tuljapurkar *et al.*, 2011; Marie, 2014). The goal of this experiment is to study the impact of differentiation on the supportive potentials of MSCs for the proliferation and stemness of HSCs.

The MSCs were therefore differentiated into adipogenically differentiated MSCs (ADI-MSCs) and osteogenically differentiated MSCs (OST-MSCs) during 21 days *in vitro* culture in the respective adipogenic and osteogenic differentiation medium (Figure 18). HSCs derived from human cord blood were subsequently co-cultured either without MSCs, with MSCs, ADI-MSCs or OST-MSCs (Figure 18). The distribution of proliferated HSCs after seven days of co-culture was tracked by carboxyfluorescein succinimidyl ester (CFSE) staining (Figure 18). CFSE is a fluorescent dye whose signal decreases by 50% after each cell division. By analyzing the HSCs on a flow cytometer after seven days co-culture, the division history of the HSC population was determined (Figure 18).

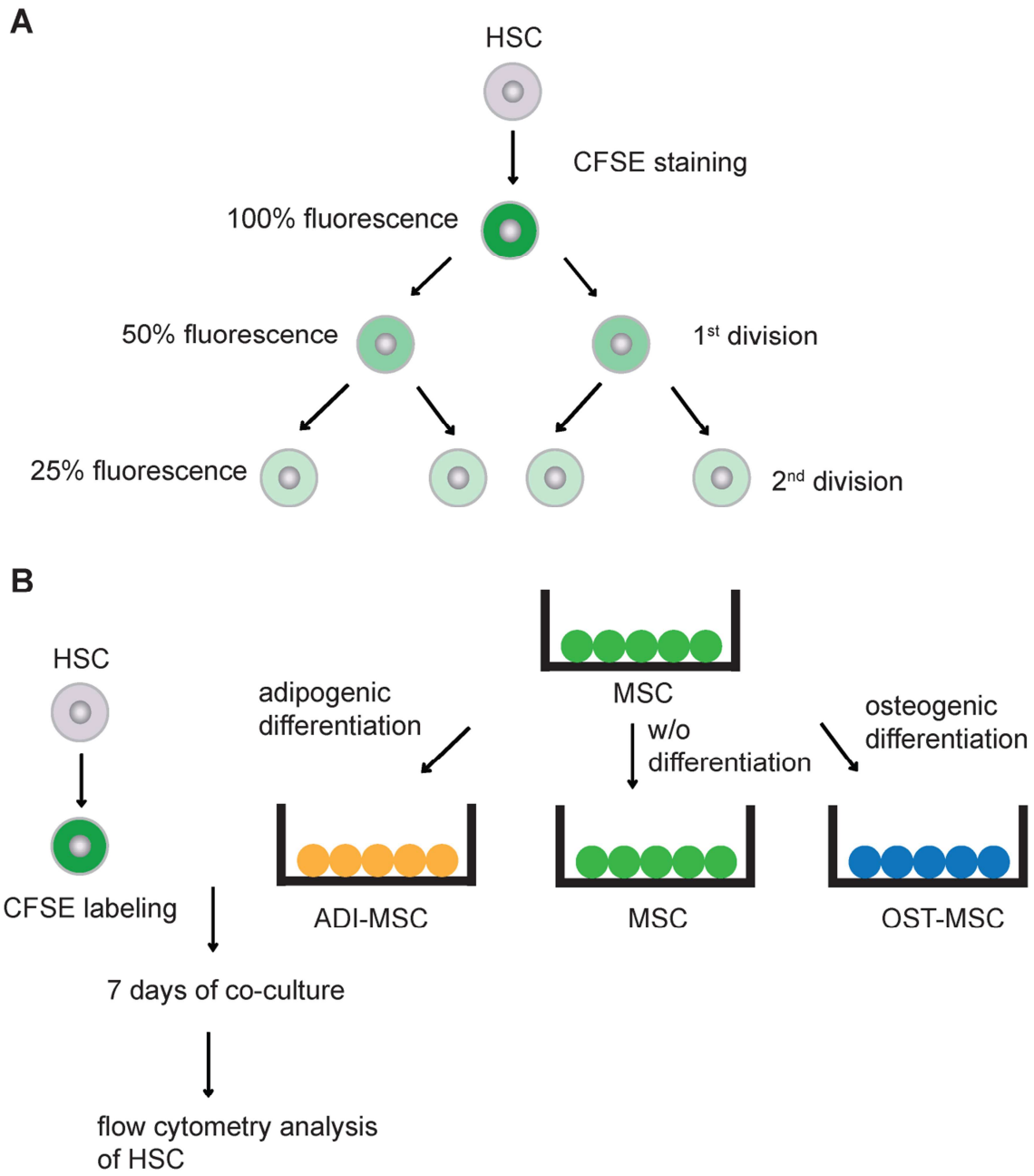

Figure 18 Experimental setup of the HSC-MSC co-culture system. (A) HSCs were stained with the cytoplasmic dye CFSE prior to seven days co-culture. The CFSE fluorescent signal decreases by 50% after each cell division. **(B)** The MSCs were first differentiated into ADI-MSCs and OST-MSCs or maintained undifferentiated. CFSE-labeled HSCs were subsequently co-cultured with ADI-MSCs, OST-MSCs or MSCs for seven days. The proliferation and stemness of co-cultured HSCs were measured by flow cytometry.

The percentages of cord blood HSCs that have undergone one, two, three, four, five and above five divisions after seven days of co-culture with MSCs, ADI-MSCs, OST-MSCs or without feeder cells are shown in figure 19A. We found that in total 74.7% of HSCs grown without feeder cells were at cell division steps above three (four, five and above five) (Figure 19A). Compared to HSCs grown on feeder cells, in total 99% of the HSCs grown on ADI-MSCs were at division steps above three, whereas in the cases of MSCs and OST-MSCs, those HSCs that had divided more than three times made up to 96.4% and 90.4% of the total HSC population, respectively. Based on the distribution of proliferated cells, one could confirm that MSCs as well as differentiated MSCs support the proliferation of HSCs in a co-culture setup. To further investigate the effects of differentiated MSCs on HSCs, the co-culture experiment was repeated using $CD34^+$ HSCs from human mobilized peripheral blood. In line with our previous observations made on cord blood HSCs, the distribution of proliferated peripheral blood HSCs grown on MSCs and OST-MSCs were similar whereas HSCs grown on ADI-MSCs showed higher proliferation (Figure 19B). Interestingly, for HSCs grown on MSCs and OST-MSCs, there were more cells at division step four (23.4% on MSCs, 22.5% on OST-MSCs) than at division step five (18.3% on MSCs, 16.6% on OST-MSCs) after seven days co-culture, which differs from our previous findings using cord blood HSCs. Further experiments using mobilized peripheral blood HSCs are required to follow up on this observation. In conclusion, the stronger proliferation-promoting effects of ADI-MSCs on HSCs were observed in cells both of cord blood and mobilized peripheral blood origin (Figure 19).

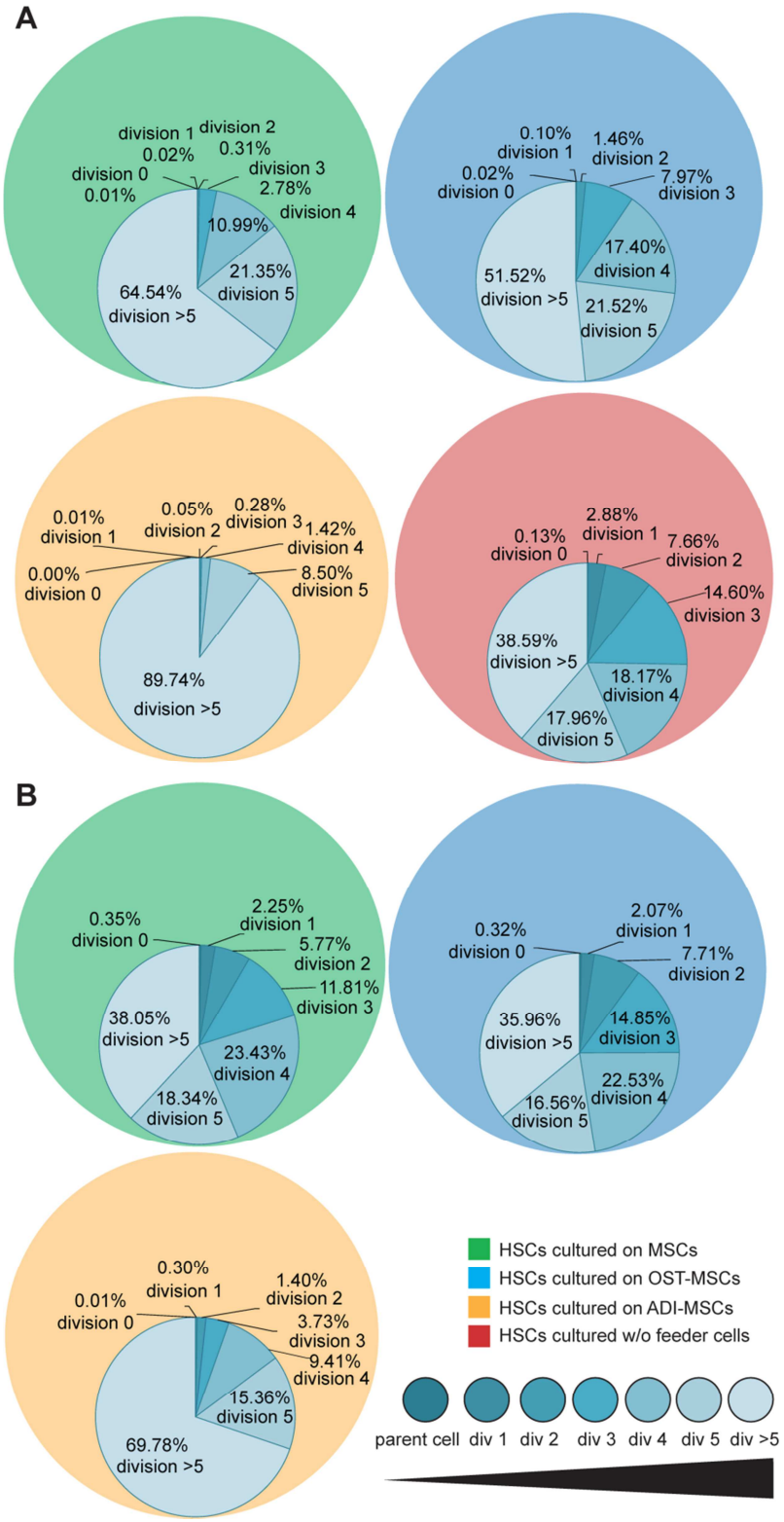

Figure 19 Distribution of proliferated cord and peripheral blood HSCs grown on MSCs, ADI-MSCs, OST-MSCs and without MSCs after seven days co-culture. (A) Cord blood HSC proliferation increased upon co-culture with MSC, ADI-MSC and OST-MSC as compared to HSCs without feeder cells. HSCs grown on ADI-MSCs showed stronger proliferation compared to cells grown on MSCs and OST-MSCs. HSCs having undergone more than five divisions could not be distinguished from each other, as the CFSE intensity dropped to auto-fluorescence after five divisions. HSCs at division steps higher than five are thus indicated as “division >5”. **(B)** Peripheral blood HSCs grown on ADI-MSCs showed stronger proliferation compared to cells grown on MSCs and OST-MSCs.

In order to see to what extent the feeder cells MSCs, ADI-MSCs and OST-MSCs exert their functions to maintain HSCs in a quiescent state through direct cell-cell contact, we used trans-well filters to physically separate the HSCs from feeder cells only allowing free diffusion of cytokines. With this setup, the effects of direct cell-cell interactions and signaling through secreted cytokines on the physiology of HSCs were studied and compared. In accordance with our previous observations using the direct cell-cell contact setup, the majority of the HSCs had undergone more than three division steps. In total 99% of the HSC population grown on ADI-MSCs were at cell division steps above three. For HSCs grown on MSC and OST-MSCs, those that had divided more than three-times made up to 97% of the total cell population (Figure 20). Comparing to our previous co-culture experiments with direct cell-cell contacts, HSCs grown in supernatants of MSCs and OST-MSCs showed stronger proliferation after seven days co-culture (Figure 20). This finding leads to the hypothesis that direct cell-cell contacts are required for MSCs and OST-MSCs to retain HSCs at lower proliferation. For ADI-MSCs, however, the lack of direct cell contact seems not to affect the proliferation of the HSCs suggesting that the supportive function of ADI-MSCs for HSCs is exerted through secreted cytokines.

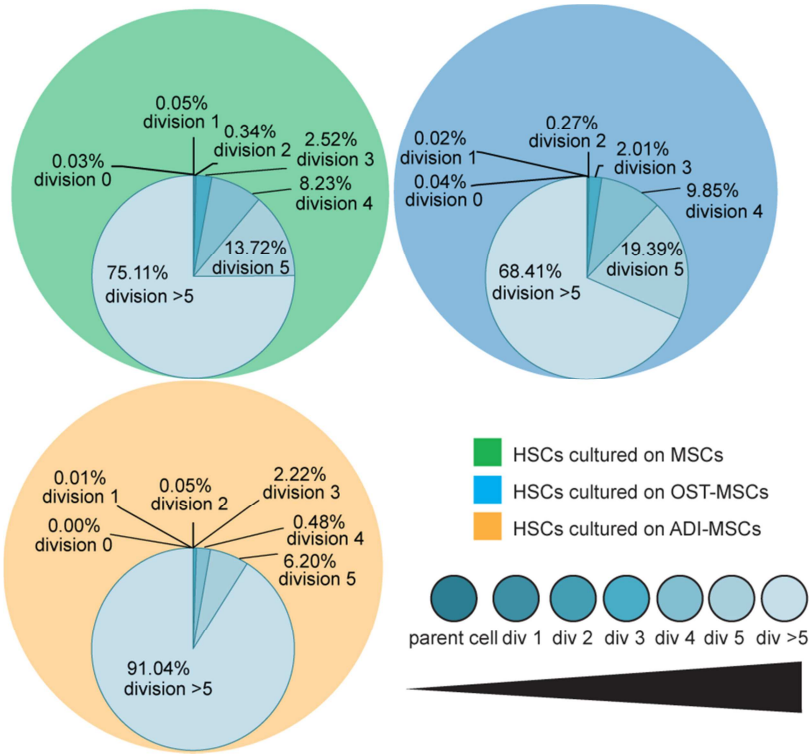

Figure 20 Distribution of proliferated cord blood HSCs grown in supernatants of MSCs, ADI-MSCs and OST-MSCs without direct cell-cell contacts after seven days co-culture. The majority of the HSCs had undergone more than three division steps. In total 99% of the HSC population grown on ADI-MSCs were at cell division steps above three. For HSCs grown on MSCs and OST-MSCs, those that had divided more than three-times made up to 97% of the total cell population.

4.2.4 Stemness of proliferated HSCs upon co-culture with MSCs, adipogenically differentiated MSCs and osteogenically differentiated MSCs

To determine the maintenance potential of the different preparations of MSCs, we measured the CD34 expression level in cord blood HSCs after seven days co-culture either without MSCs, with MSCs, ADI-MSCs and OST-MSCs (Figure 21A). Compared to HSCs grown without feeder cells, the CD34 expression levels of co-cultured HSCs were higher at division steps four, five and above five. The low CD34 expression levels of HSCs grown without feeder cells after the fourth division suggested a loss of stemness (Figure 21A). Based on this result one could confirm that MSCs as well as differentiated MSCs are required for the maintenance of HSCs. The CD34 expression level of HSCs grown under all conditions decreased with increasing number of divisions. This finding suggests that despite the protective environment provided by the MSCs, the *in vitro* proliferation of HSCs is accompanied by the decrease of stemness. At division step four, HSCs grown on MSCs showed higher expression level of CD34 compared to cells grown on OST-MSCs. The CD34 expression level of HSCs grown on ADI-MSCs was not indicated due to low percentage cells at this division step. At division step five, HSCs grown on MSCs, ADI-MSCs and OST-MSCs showed similar levels of CD34 expression. At division steps above five, despite the standard errors, the CD34 expression level of HSCs grown on ADI-MSCs was higher than the ones grown on other feeder cell types (Figure 21A). Similar results were obtained using HSCs derived from peripheral blood. At division step four, HSCs grown on MSCs and OST-MSCs showed similar levels of CD34 expression (Figure 21B). At division step five, the CD34 expression levels of HSCs grown on OST-MSCs and MSCs remained low (Figure 21B). The CD34 expression level of HSCs grown on ADI-MSCs was higher which was not observed previously with HSCs from cord blood. At division steps above five, in line with our previous experiment using cord blood HSCs, peripheral blood HSCs grown on ADI-MSCs showed a higher level of CD34 expression compared to HSCs grown on MSCs and OST-MSCs (Figure 21B). However, due to the variability of the sample sources, further experiments need to be carried out to confirm our preliminary findings.

In conclusion, these results demonstrate that MSCs, ADI-MSCs and OST-MSCs not only support the proliferation of HSCs, but also maintain their primitive immunephenotype over a number of cell divisions compared to HSCs grown without feeder cells. At division steps above five, HSCs grown on ADI-MSCs showed a higher level of CD34 expression compared to HSCs grown on MSCs and OST-MSCs (Figure 21).

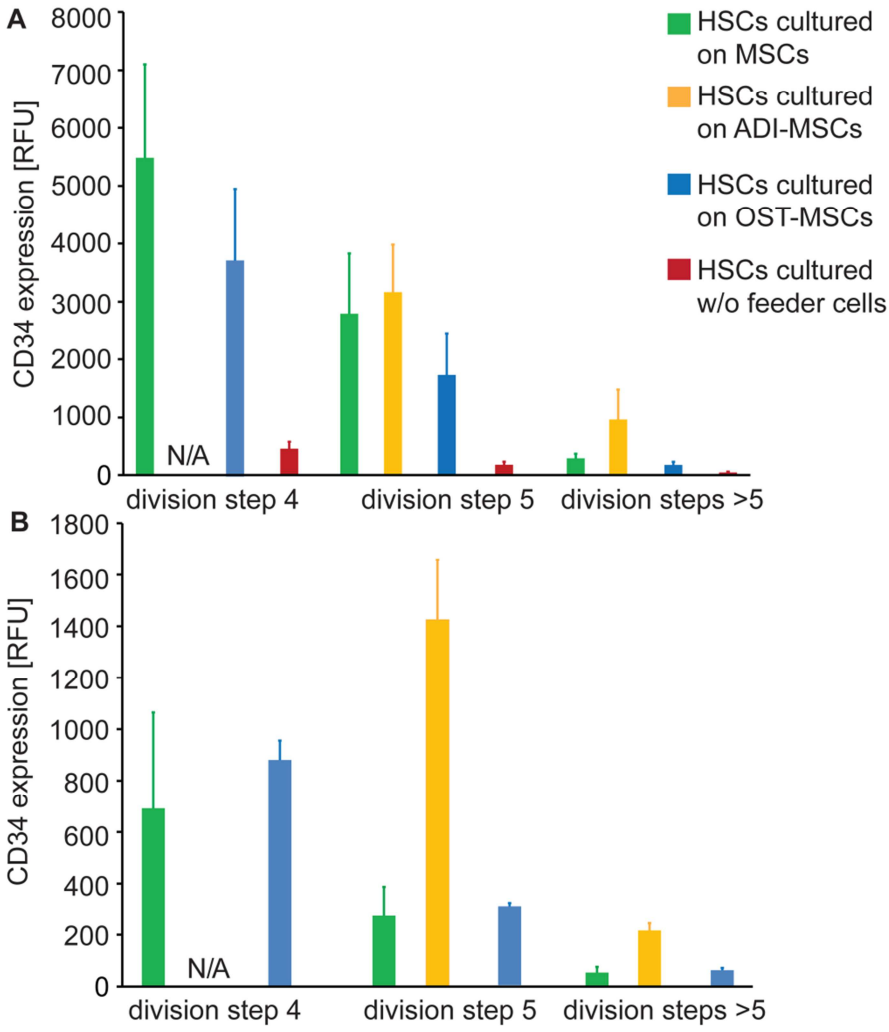

Figure 21 CD34 expression levels of cord and peripheral blood HSCs grown on MSCs, ADI-MSCs, OST-MSCs and without MSCs after seven days of co-culture. (A) CD34 expression levels of cord blood derived HSCs at division steps four, five and above five are shown. HSCs grown on MSCs, ADI-MSCs and OST-MSCs maintained their primitive immunophenotype over a number of cell divisions compared to HSCs grown without feeder cells. **(B)** CD34 expression levels of peripheral blood derived HSCs at division steps four, five and above five are shown. HSCs grown on ADI-MSCs showed higher CD34 expression levels than HSCs grown on OST-MSC and MSCs at division steps five and above five. Experiments were performed in biological triplicates; standard errors are indicated by the error bars.

Using trans-well filters to physically separate the HSCs from feeder cells only allowing free diffusion of cytokines, the CD34 expression levels of cord blood HSCs grown without direct cell-cell contacts in the supernatants of MSCs, ADI-MSCs and OST-MSCs were studied (Figure 22). At division steps five and above five, the CD34 expression level of HSCs grown on ADI-MSCs was higher than the ones grown on other feeder cell types. This finding leads to the hypothesis that ADI-MSCs are able to maintain the stemness of HSCs through secreted cytokines (Figure 22). Taking the results of proliferation into consideration, one can conclude that HSCs grown in the supernatant of ADI-MSCs possess a high rate of proliferation while still maintaining a high CD34 expression level.

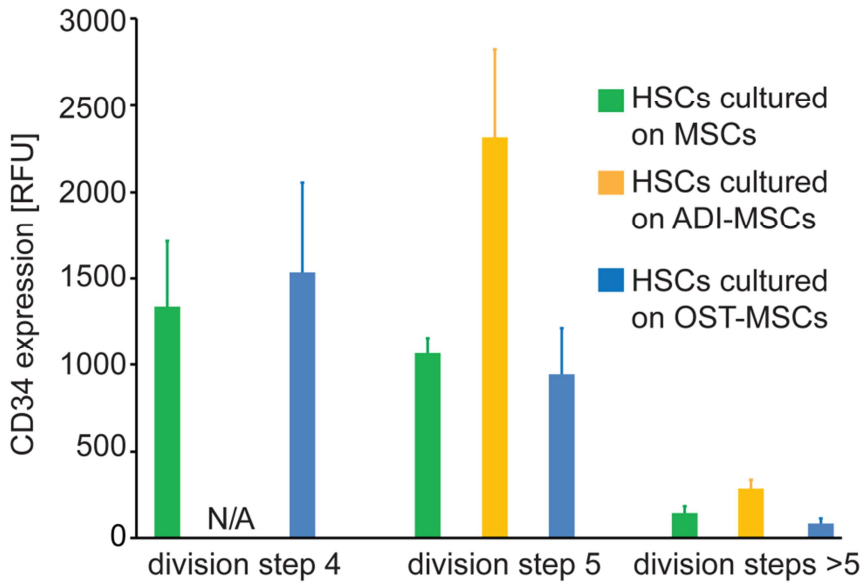

Figure 22 CD34 expression levels of cord blood HSCs grown in supernatants of MSCs, ADI-MSCs and OST-MSCs without direct cell-cell contacts after seven days co-culture. CD34 expression levels at division steps four, five and above five are shown. HSCs grown on ADI-MSCs showed higher level of CD34 expression than OST-MSC and MSCs at division steps five and above five. Experiments were performed in biological triplicates; standard errors are indicated by the error bars.

4.3 Chromatin accessibility landscape of aging MSCs

To study the age-associated changes on chromatin levels in the human hematopoietic stem cell niche, the genome-wide chromatin accessibility assay ATAC-seq was performed using MSCs from donors of different ages. In aging cellular systems, the general hypothesis is that the heterochromatin region of the genome loosens up while the euchromatin is hypermethylated at specific DNA loci (Booth *et al.*, 2016). In bone marrow derived MSCs, transcriptomic studies showed that the expression of many homeobox transcription factors including HOXA5, HOXB3 and HOXB7 are repressed upon aging. Moreover, the master regulator of adipogenesis PPARγ was repressed upon aging (Wagner *et al.*, 2009). These findings were confirmed by a DNA methylation study which demonstrated that differences upon aging were observed in homeobox genes and genes involved in cell differentiation (Bork *et al.*, 2010). However, the relationship between chromatin accessibility and aging in MSCs is not yet defined.

ATAC-seq profiles chromatin accessibility genome-wide. By overlaying ATAC-seq with ChIP-seq data, Lara-Astiaso *et al.* provided a comprehensive model of chromatin dynamics during 16 stages of murine hematopoietic differentiation (Lara-Astiaso *et al.*, 2014). Moreover, ATAC-seq dataset generated in the primary $CD4^+$ T cells revealed novel gender-specific elements that escape X chromosome inactivation (Qu *et al.*, 2015). The ATAC-seq method initially published by Buenrostro *et al.* was developed for the GM12828 human lymphoid cell line grown in suspension, as datasets on multiple molecular levels were available for this cell line (Buenrostro *et al.*, 2013).

4.3.1 Adaptation of the ATAC-seq protocol

In order to establish this method in our lab, preliminary experiments were performed using the same GM12828 cell line as described in the published protocol (Buenrostro *et al.*, 2013). During this process, different technical changes were made according to the local laboratory conditions. Subsequently, the workflow was applied to human primary MSCs. The ATAC-seq sample preparation consists of four major steps including cell culture, lysis and transposition, library amplification and purification, and deep sequencing (Figure 23).

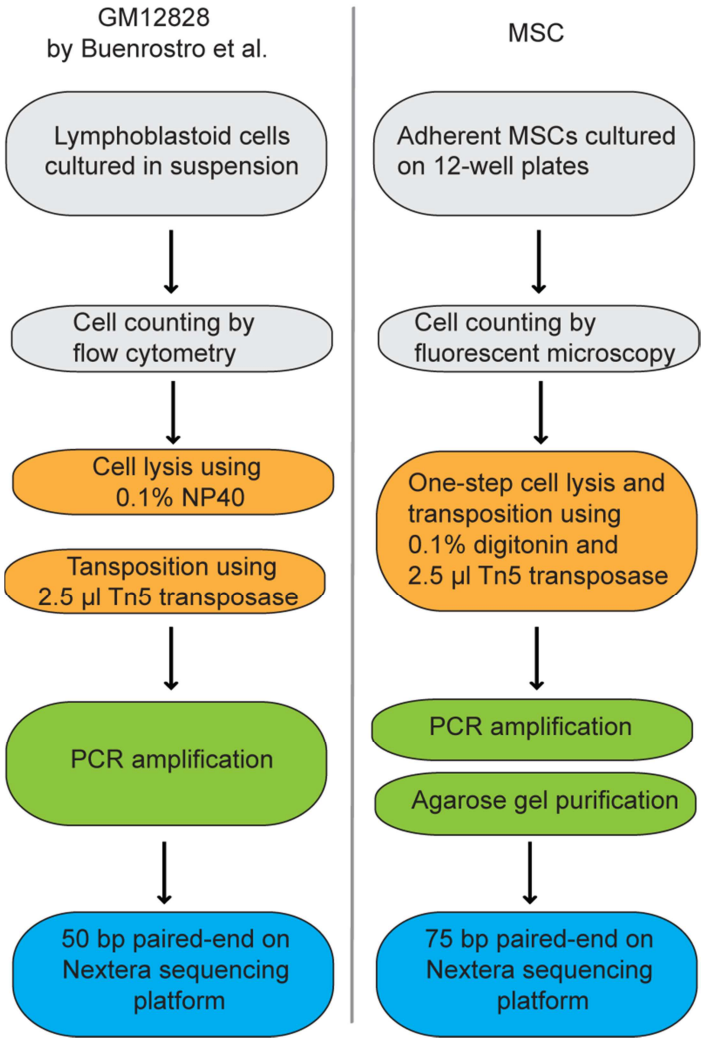

Figure 23 Workflow of ATAC-seq adapted to MSCs. The published protocol for the human lymphoblastoid cell line GM12828 was adapted to primary MSCs. The sample preparation pipeline consists of four major steps including cell culture (gray), lysis and transposition (orange), library amplification and purification (green), and deep sequencing (blue).

For each ATAC-seq sample, cells were harvested 24 h after the last passage. In the course of our test experiments, we found that the viability of the cells were crucial for the signal-to-noise ratio of the ATAC-seq dataset. A propidium iodide labeling ensured the cell viability to be higher than 95%. As the MSCs were grown on plastic surface, the adherent cells were counted by a DAPI nucleus staining followed by an automated cell counting (ImageJ) (Figure 23). For each library 50,000 cells were detached by the proteolytic enzyme accutase (Sigma-Aldrich). The cells were subsequently lysed by the non-ionic detergent digitonin. As digitonin can be used in combination with the Tn5 tagmentase, the one-step lysis and tagmentation was applied to the MSC samples. The nuclei were tagmented using 2.5 µl Tn5 transposase. The tagmentation step is based on the principle of Tn5 transposase to randomly insert sequencing primers into open chromatin regions of the genome (Buenrostro *et al.*, 2013). The ratio between the starting cell number and tagmentation enzyme affects the fragment size distribution of prepared libraries. In case of under-tagmentation, the majority of the tagmented DNA fragments are larger than 1,500 bp in size. This leads to lower coverage of the library as fragments larger than 1.2 kb do not cluster on the flow cell of the sequencer. The information encoded by the larger fragments is therefore lost by low sequencing yields. The tagmented DNA library was subsequently amplified by PCR. The number of amplification cycles N was determined by real-time PCR assay with the aim to avoid over-amplification resulting in large proportions of duplicated fragments in the library. To ensure proper quality of the ATAC-seq libraries prior to sequencing, the fragment size distribution of ATAC-seq libraries was routinely examined on BioAnalyzer. For the MSC samples, libraries were sequenced on an Illumina NextSeq500, with around 50 million reads per replicate. The libraries were sequenced 75 bp paired-end. The sequencing depth covers the human genome at about 2.3-fold.

The fragment size distribution of the library shows that the majority of the DNA fragments consisted of short fragments less than 200 base pairs (Figure 24). These were mostly fragments from nucleosome depleted regions (NDR), where most regulatory elements reside. Similar to published data, we also observed a periodicity of nearly every 200 bp for the insert size distribution, suggesting that fragments were protected by different integer numbers of nucleosomes (Figure 24). The sequenced ATAC-seq DNA fragments also showed a periodicity of around 10 bp throughout the fragment size distribution. This periodicity is due to the so-called helical pitch of DNA.

Once a transposase inserts an adaptor into the open region of the chromatin, the regions 10 bp apart from the insertion site are protected from subsequent transposase attacks due to steric hindrance (Adey *et al.*, 2010) (Figure 24).

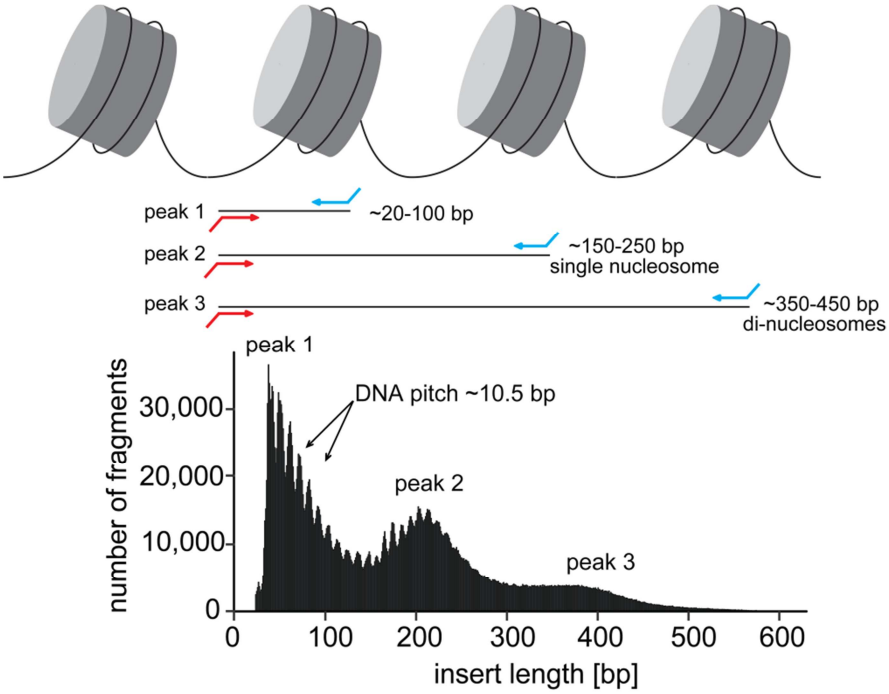

Figure 24 Insert size distribution of sequenced ATAC-seq library. Fragment size distribution of sequenced library showed nucleosome periodicity of approximately 200 bp indicating that the chromosomal DNA was protected by an integer number of nucleosomes. The periodicity of approximately 10.5 bp generated by the DNA helical pitch was due to steric hindrance of the inserted Tn5 transposase primers.

4.3.2 Changes of chromatin accessibility in aging MSCs

4.3.2.1 Overview of MSC samples

ATAC-seq libraries were prepared from MSC samples derived from 16 individuals (12 male and 4 female subjects). The age of the healthy donors ranged from 21 to 59 years (Figure 26). By correlating the ATAC-seq profiles of the samples with donor age, alterations in chromatin accessibility upon aging were studied.

4.3.2.2 Quality checks of the dataset

Prior to sequencing, the fragment size distribution of the ATAC-seq libraries was assessed using BioAnalyzer (Figure 25). The pattern of the nucleosome periodicity served as a major quality check for ATAC-seq libraries. An example of qualitatively good library was shown in contrast to a library which was excluded from sequencing. Both samples were prepared from the same MSC donor (Figure 25). A bird eye view on the fragment size distribution of all sequenced samples was shown in figure 26. The presence of the three major peaks in the ATAC-seq library was a requirement for further downstream processing of the sample.

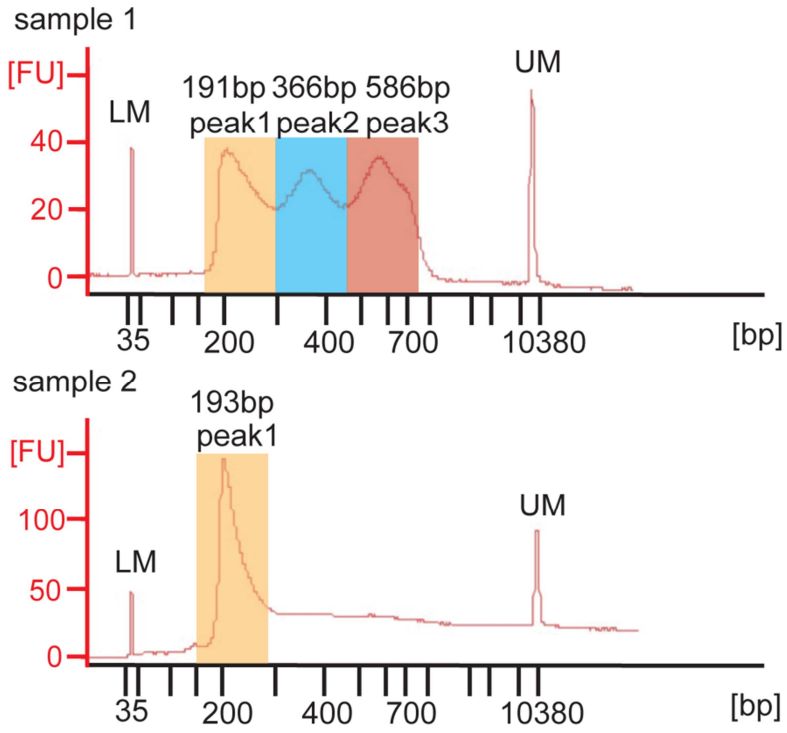

Figure 25 The library fragment size distribution serves as quality check prior to sequencing. An example of qualitatively good library (sample 1) is shown in contrast to a library which was excluded from sequencing (sample 2). Both replicates were prepared from the MSC donor #409 (age 30, male). Sample 2 showed no nucleosome periodicity suggesting an unsuccessful tagmentation of the cells. The two peaks at 35 and 10,380 bp on the BioAnalyzer profiles are DNA markers (LM: lower marker; UM: upper marker).

After sequencing, an effective measure to assess the signal-to-noise ratio of our sequencing dataset is the transcriptional start site (TSS) enrichment score which was described in the human ENCODE project (Bernstein *et al.*, 2012). After alignment of the sequencing reads to the genome, the number of reads mapped proximal to a reference set of TSS (in a +/- 2kb window) is divided by the number of reads mapped distal to the TSS (in a 1 kb window). A random mapping of the reads to the genome would therefore result in a TSS enrichment score of four (4 kb window proximal to TSS divided by 1 kb window distal to TSS). Using our test sequencing datasets, we found that an enrichment score higher than seven would allow us to identify enough ATAC-seq peaks to profile the open chromatin accessibility of the sample. A bird eye view for all samples is represented in figure 26. As indicated in figure 26, all sequenced samples showed an enrichment score higher than seven. The quality checks applied prior- and post-sequencing indicated that the current ATAC-seq dataset was reliable and of good quality to address questions on age-associated differences in chromatin accessibility.

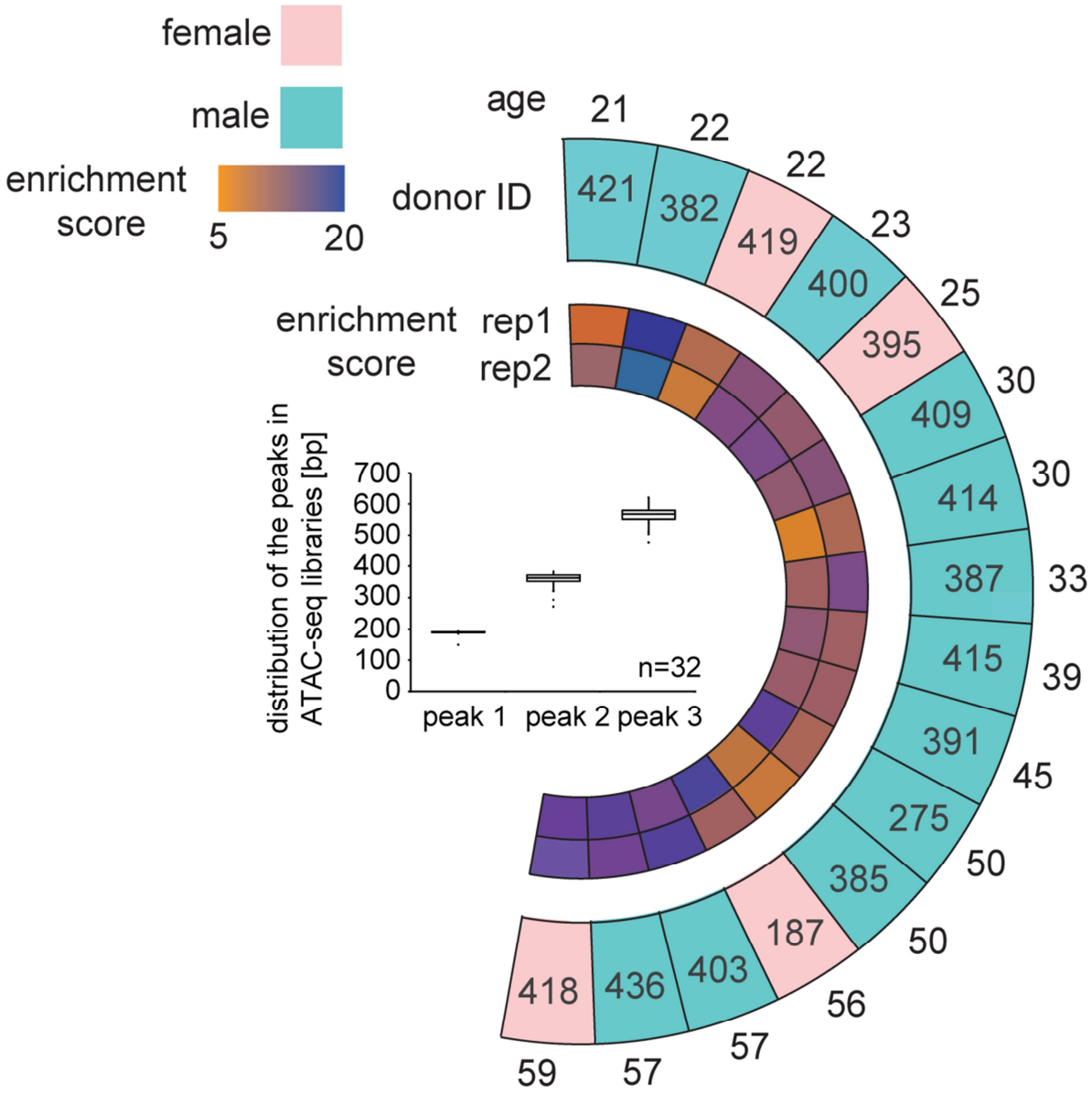

Figure 26 Overview on the age and gender distribution as well as the quality of prepared ATAC-seq libraries. ATAC-seq libraries were prepared from a cohort of 16 individuals. The gender of the donor was visualized by red (female) and green (male). The age of the donors was indicated at the periphery of the circle. The transcription start site enrichment scores of the samples were visualized by a color gradient ranging from 5 (brown) to 20 (blue) in the inner circle. For each MSC donor, two biological replicates were sequenced (rep1 & rep2). A bird eye view on the fragment size distribution of the sequenced libraries was shown by the box plot indicating the distribution of the three major peaks in ATAC-seq library.

4.3.2.3 Individual variations of mitochondrial DNA content

As mitochondrial DNA is not associated with nucleosomes and hence gives rise to short fragments upon Tn5 transposition, ATAC-seq libraries may contain 10–90% of mitochondrial reads (Buenrostro *et al.*, 2013; Qu *et al.*, 2015; Montefiori *et al.*, 2016). We therefore assessed the content of mitochondrial DNA in our samples derived from primary MSCs. The variations between individual donors ranged from 6.0 to 49.1% (Figure 27A). As indicated in figure 27B, the content of mitochondrial DNA between replicates from the same donor was similar. For each donor, the average percentage of mitochondrial DNA in the library was plotted against the age of the donor. As shown by the coefficients of determination (R^2) in figure 27C, there is no linear correlation between the percentages of mitochondrial DNA reads in the ATAC-seq library and donor age (Figure 27C). Thus our dataset indicated that the percentages of the mitochondrial reads in the ATAC-seq library vary between donors. There was, however, no correlation with donor age. We cannot exclude the possibility that under the same *in vitro* culture conditions, MSCs derived from different donors might produce different copy numbers of mitochondria. Follow-up experiments are required to further prove this hypothesis.

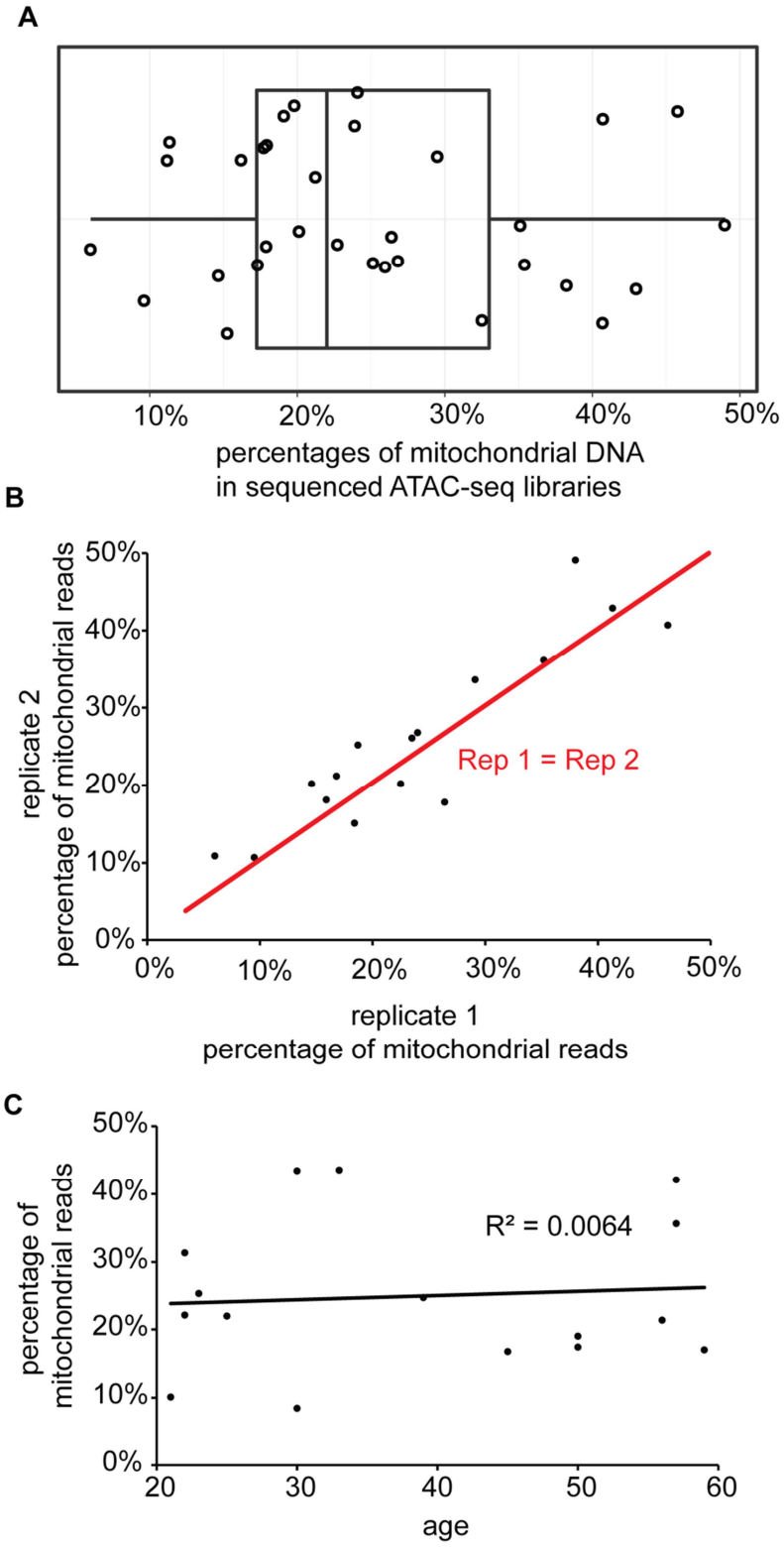

Figure 27 Percentages of mitochondrial reads in sequenced libraries. (A) The percentages of mitochondrial reads in ATAC-seq libraries ranged from 6.0% to 49.1%. **(B)** The percentages of mitochondrial reads between replicates derived from the same donor were similar. **(C)** The average percentages of mitochondrial reads are not correlated with the biological age of the donors. R^2, coefficient of determination between donor age and percentage of mitochondrial reads.

4.3.2.4 Open chromatin profiles of MSC-specific marker regions

MSCs are characterized by a combination of cell surface markers (Wagner *et al.*, 2006). To determine if there are ATAC-seq peak signals at the transcriptional sites of these markers, we examined the genome regions encoding these protein markers in our ATAC-seq dataset. The transcription start site regions of the positive markers were observed in contrast to those of the negative markers which characterize the MSCs through their absence (Dominici *et al.*, 2006).

Commonly used positive markers to identify MSCs are CD73 (NT5E), CD90 (THY1) and CD105 (ENG). The negative markers are CD45 (PTPRC) and CD34 (CD34). As illustrated by the open chromatin profile of one donor (age 21, male), strong ATAC seq signals were observed in the transcription start site regions of CD73 and CD90 suggesting a transcriptional expression of these two genes (Figure 28). For the marker CD105, however, a strong signal at the transcription start site was not found. The open chromatin profile of the negative marker CD45 showed no peak signal in the transcriptional start site region. However, a slightly strong ATAC-seq signal at the transcriptional start site region of CD34 was observed (Figure 28).

In conclusion, for the common positive markers of MSCs, peaks at transcriptional start sites of CD73 and CD90 were observed. Among the common negative markers of MSCs, no ATAC-seq signal was found for the genomic region of CD45. Since ATAC-seq only profiles the open chromatin regions of the genome, conclusions on gene expression can be only drawn together with information on transcriptomic level (*e.g*. RNA-seq data). Our present dataset defines the open chromatin landscape of MSCs. In combination with other phenotypic markers, the open chromatin profiles of these marker regions may provide a unique fingerprint for the identification of MSCs on chromatin level.

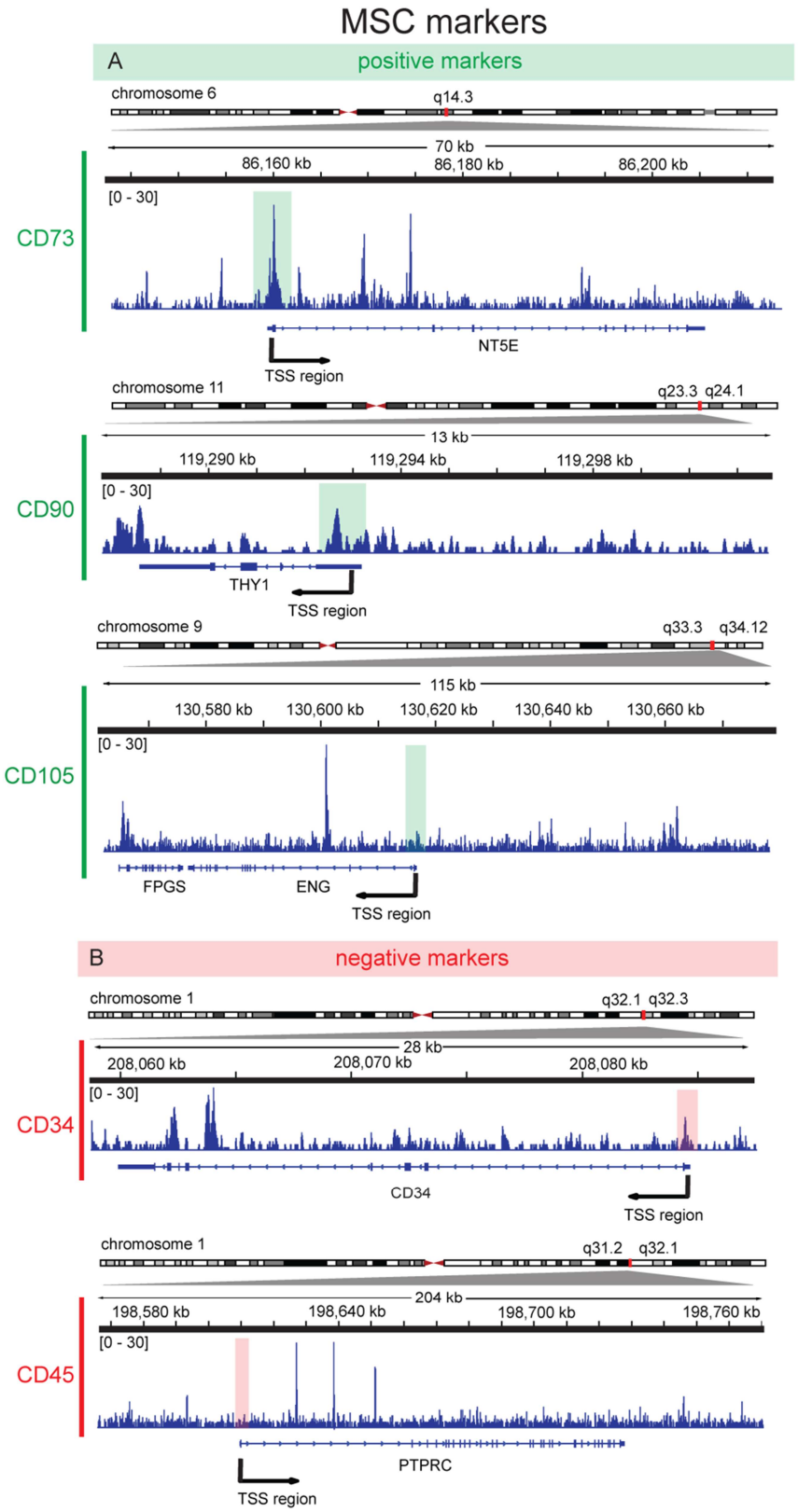

Figure 28 ATAC-seq reads mapped to MSC-specific marker gene regions CD73, CD90, CD105 (positive markers) and CD45, CD34 (negative markers). ATAC-seq data of donor #421 (age 21, male) is shown at the corresponding loci on the genome. **(A)** For the positive markers, peaks at transcriptional start sites (TSS) of CD73 and CD90 were observed. No signal was observed at TSS of CD105. **(B)** For the negative markers, no ATAC-seq peak was found at TSS of CD45. A slightly strong signal was observed at TSS of CD34.

4.3.2.5 Association of age with alterations in chromatin accessibility

The ATAC-seq peaks were determined using the software package MACS2 (Model-based Analysis of ChIP-seq) with the parameters "-nomodel –q 0.001" (Zhang *et al.*, 2008). In total 122,884 peaks were identified in the ATAC-seq dataset generated from 16 healthy donors (Figure 29).

To detect significant changes upon aging across sequencing samples, a differential peak analysis was carried out using the software package DESeq2 with linear regression (Differential Expression Analysis for Sequence Count Data) (Anders *et al.*, 2012). The null hypothesis that the signal remains unchanged with age was tested. Statistical significance was tested according to a Wald test and p-values were corrected for multiple testing with Benjamini-Hochberg. At a false discovery rate of 5%, we could identify 4,579 peaks that changed significantly upon aging (Figure 29). Out of this group, 3,050 ATAC-seq peaks decreased with age whereas 1,529 peaks increased with age (Figure 29).

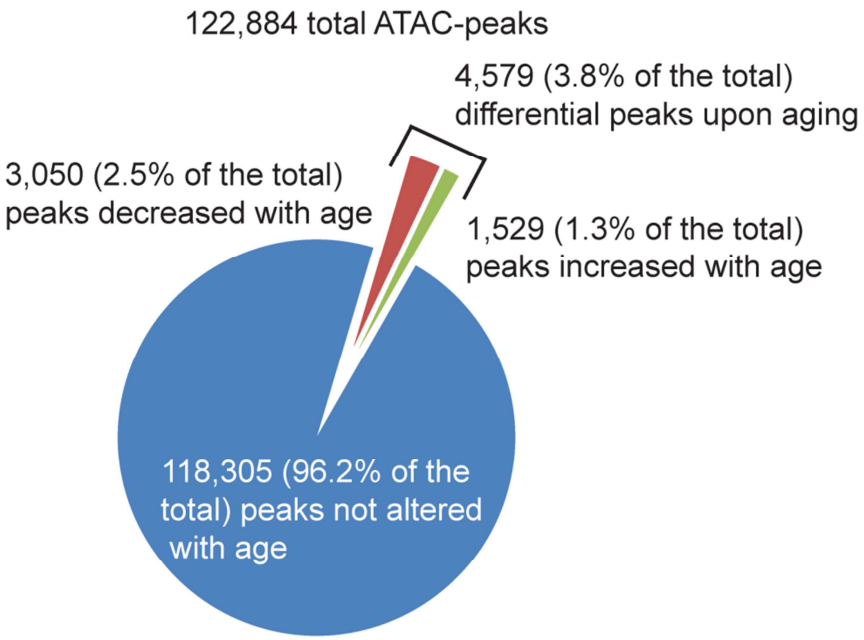

Figure 29 A set of 4,579 differential ATAC-seq peaks were identified at a false discovery rate of 5%. Out of 122,884 ATAC-seq peaks identified in the entire MSC dataset, 4,579 peaks (3.8%) changed with age of the donors. Out of this group, 3,050 ATAC-seq peaks (2.5%) decreased with age while 1,529 ATAC-seq peaks (1.3%) increased with age.

A genomic segmentation of the ATAC-seq peaks totally identified showed that the majority of the peaks were found in the intergenic and intron regions (Figure 30A). The segmentation of the differential ATAC-seq peaks showed that the majority of the peaks were found in the intergenic and intron regions as well (Figure 30B). Using a binomial test we found that peaks annotated to promoter-transcription start site (TSS) regions were significantly over-represented in the set of differential peaks compared to the set of consensus peaks (Figure 30).

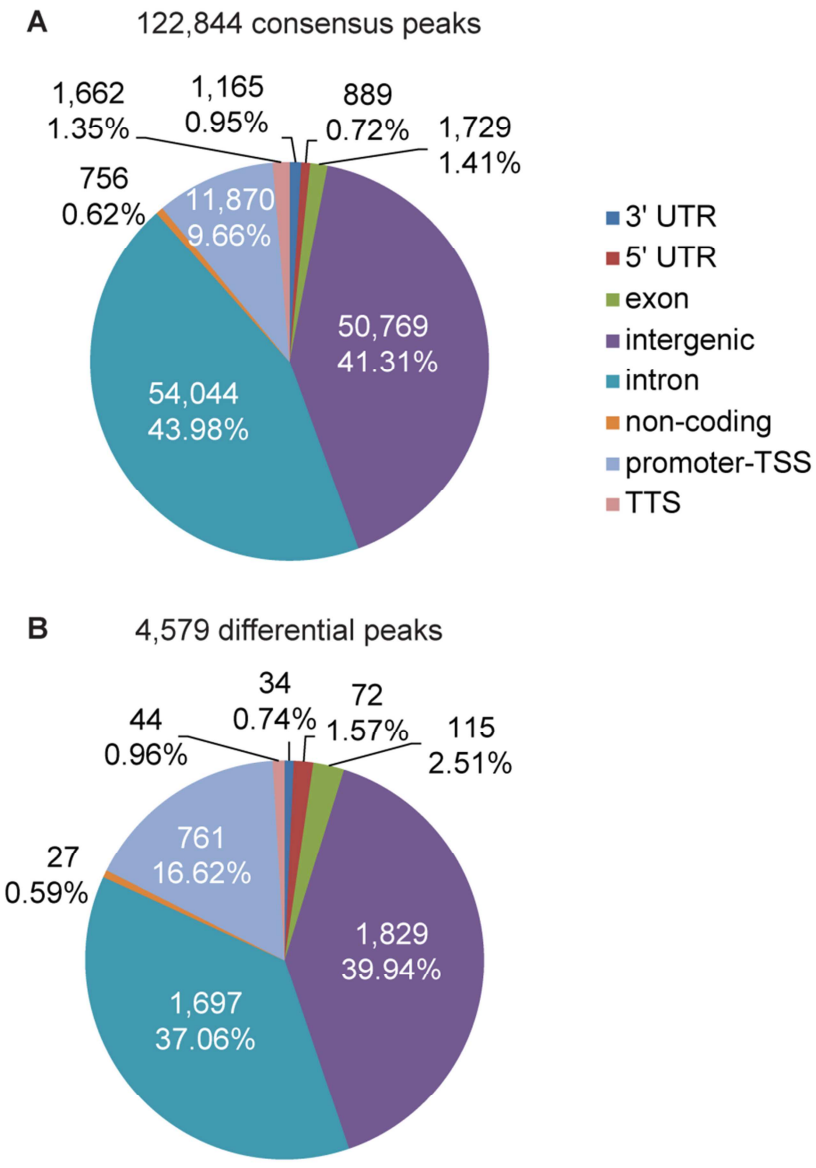

Figure 30 Genomic annotation of the consensus and differential ATAC peaks. The majority of the ATAC-seq peaks are annotated to the intergenic and intron regions in both **(A)** consensus and **(B)** differential ATAC-seq peaks. A comparison between consensus and differential peaks showed that peaks annotated to promoter-TSS regions are over-represented in the set of differential peaks. Abbreviations: 3' UTR (3' untranslated region); 5' UTR (5' untranslated region); promoter-TSS (promoter-transcription start site); TTS (transcription termination site).

To determine the relationship between alterations in chromatin accessibility and age, we performed a principle component analysis (PCA) on the 500 top variable peaks. After corrections for batch effects of the tagmentation enzymes and gender effects of the donor, we found that age is associated with the alterations observed in the ATAC-seq dataset. The first component (PC1) explains 39.1% of the variation between samples and separates the youngest (*i.e.* < age 30) from the elderly donors (age 56, 57, 59). Under the second component, individuals of age group 30-40 are grouped closely to each other; with individuals of age 56 and 57 more distant from individuals of age 21 and 23 (Figure 31).

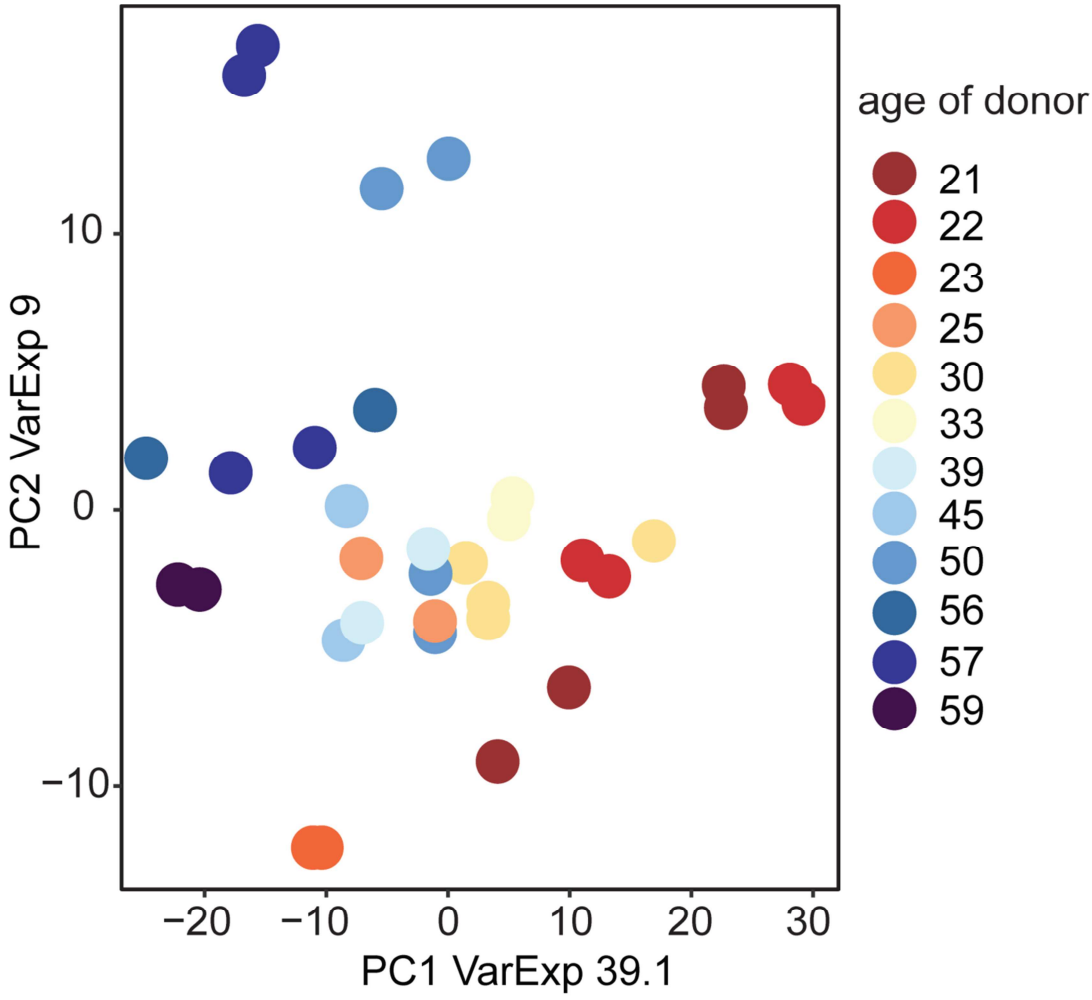

Figure 31 Age is associated with the differential peaks in ATAC-seq data. Age of the sample donors is indicated by the color code from dark red (21 years) to dark blue (59 years). The first component (PC1) explains 39.1% of the variation. The second component (PC2) explains 9% of the variation. Image generated by Mariana Ruiz, EMBL HD.

4.3.2.6 Functional analysis of differential ATAC-seq peaks upon aging

To investigate which category of genes is most likely to change their chromatin state upon aging in MSCs, a gene ontology (GO) enrichment analysis was performed on the set of 4,579 differential ATAC-seq peaks upon aging. Each peak was assigned to the nearest gene on the genome. These peaks on the genome were assigned to 3,580 genes, with multiple ATAC-seq peaks annotated to the same gene. Additionally, an enrichment analysis was performed for pathways of the KEGG collection (Kyoto encyclopedia of genes and genomes) (Kanehisa *et al.*, 2000). The analysis was performed using the ClueGO plugin in the software Cytoscape, with total ATAC-seq peaks detected set as background (Bindea *et al.*, 2009).

As shown in figure 32, the significantly enriched gene ontology terms for biological processes are mostly cell developmental processes such as “nervous system development”, “structure morphogenesis” and “multicellular organismal development”. The process regulating cell differentiation was also enriched. The enriched terms for molecular functions indicated that genes involved in “regulating DNA binding”, “RNA polymerase II activity”, “transport across cell membranes” and “protein tyrosine kinase activity” are enriched upon aging, suggesting that these cellular processes might play critical roles in the natural aging process of MSCs. To determine whether the differential peaks upon aging are enriched in specific pathways, we performed an enrichment analysis in the pathways of the KEGG collection. The results indicated that aging-associated genes are especially enriched in “hippo signaling pathway”, “TGF-beta signaling pathways”, and pathways that are typical for cancer cells. The hippo signaling pathway and TGF-beta signaling pathway are pathways regulating cell proliferation and apoptosis suggesting that these functions might be altered with age. The pathway involved in cell-cell adhesion was also found to be altered upon aging as well (Figure 32C).

The results of the enrichment analysis are partially in line with the findings of previous studies on aging MSCs (Wagner *et al.*, 2009; Bork *et al.*, 2010). A gene ontology analysis on methylation changes upon aging indicated that GO terms “sequence-specific DNA binding” and “multicellular organismal development” were enriched in hypomethylated DNA sites upon aging which agrees with the findings in our ATAC-

seq data (Bork *et al.*, 2010). Gene expression data suggested that “transcription factor activity” and “mesoderm development” enriched in up-regulated genes with age (Wagner *et al.*, 2009). Furthermore, TGF-beta/BMP signaling pathways affected in aged MSCs (Wagner *et al.*, 2009). Our data on chromatin level suggested that pathways involved in cell adhesion, trans-membrane transport and tyrosine kinase activity are altered, which might affect the ability of MSCs to function as a stem cell niche. These novel findings may serve as a starting point for future follow-up validation experiments.

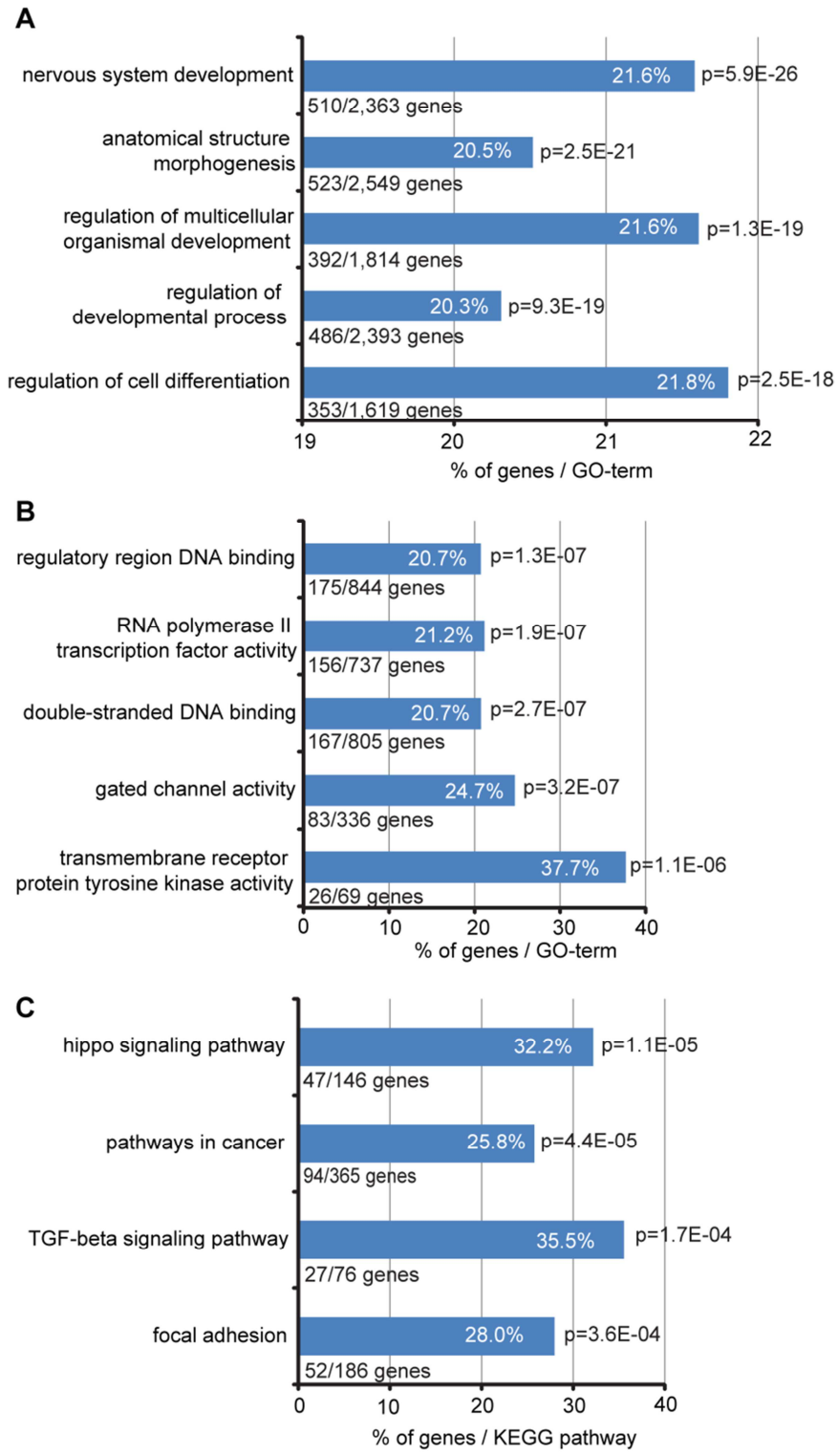

Figure 32 Gene ontology (GO) and KEGG enrichment analysis in MSCs. A functional analysis was carried out on genes annotated to differential ATAC-seq peaks upon aging. The number of genes enriched to each term is represented as percentage of the total number of genes in the term. **(A)** The top five enriched GO-terms of the category “biological processes”. **(B)** The top five enriched GO-terms of the category “molecular functions”. **(C)** The top five enriched pathways in the KEGG collection. p, p-value of the enrichment analysis.

4.3.2.7 Age-associated ATAC-seq peaks localized in promoter regions

To further study the differential ATAC-seq peaks upon aging, we focused on the peaks annotated to the promoter-transcription start site region as they are over-represented in the set of differential peaks. Out of the 4,579 differential ATAC-seq peaks, 761 peaks were localized to promoter regions. The most significant peak regions (*i.e.* peaks regions with the lowest p-values) were ranked by their median ATAC-seq signal intensity (Supplementary Material Table 4).

Remarkably, three out of the top four peaks annotated to promoter regions were either associated to stem cell proliferative disorders or key metabolic pathways (Figure 33). FGFR1 oncogene partner (FGFR1OP) was reported to be involved in several stem cell myeloproliferative disorders (Popovici *et al.*, 1999). TP53-inducible glycolysis and apoptosis regulator (TIGAR) is involved in glycolysis and apoptosis of the cells (Wanka *et al.*, 2012) and ceramide synthase 6 (CER6) regulates the metabolism of ceramides and sphinosines (Peters *et al.*, 2015). Only the biological function of tetratricopeptide repeat protein 21B (TTC21B) remains elusive so far. One mouse study suggested that TTC21B might contribute to the development of cellular cilia (Norris *et al.*, 2012). Figure 33 illustrates the changes of the ATAC-seq peaks in the promoter regions of these genes. The dataset shown here was normalized by DESeq2 (Differential gene expression analysis based on negative binomial distribution).

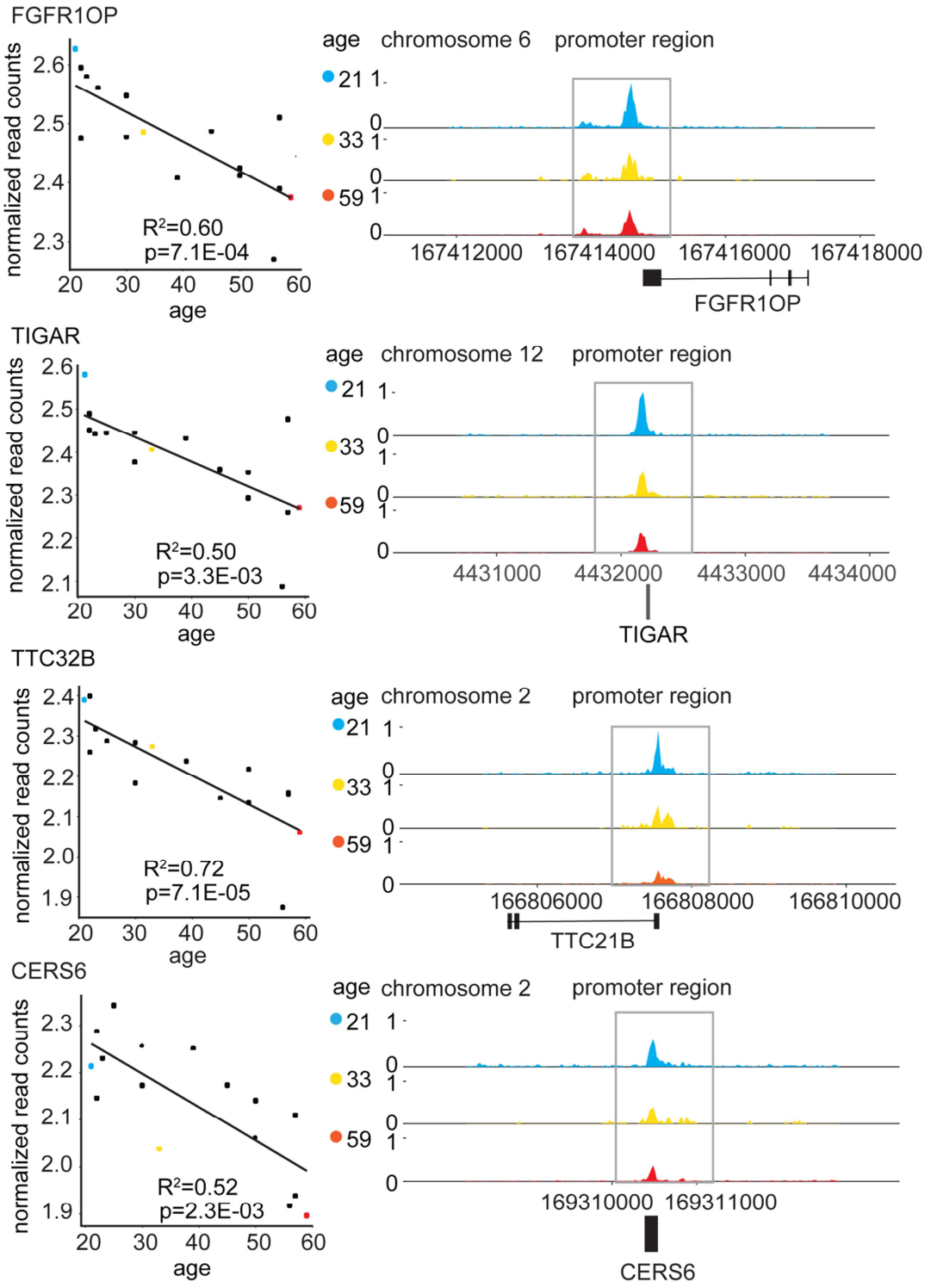

Figure 33 The ATAC-seq peaks localized in the promoter regions of the genes FGFR1OP, TIGAR, TTC32B and CERS6 decrease with age of the donor. The ATAC-seq peak signal intensity of all donors was plotted against the age of the donor (left). As an illustration, the ATAC-seq profiles of MSC samples derived from three individuals of age 21 (upper track), 33 (middle track) and 59 (lower track) were compared (right). The total library sizes were normalized. R^2, coefficient of determination between donor age and normalized read counts; p, p-value of the linear regression between donor age and normalized read counts.

The FGFR1OP gene can be fused by chromosomal translocation with fibroblast growth factor receptor (FGFR1, CD331) which is a receptor tyrosine kinase (Popovici *et al.*, 1999). It is a proto-oncogene involved in human cancers as a result of their duplication and fusion with other genes (Katoh *et al.*, 2014). In general, the family of fibroblast growth factors (FGF) was reported to be involved in the aging of MSCs (Wagner *et al.*, 2009). Moreover, it was shown by previous studies that fibroblast growth factors appear to promote self-renewal in MSCs while maintaining their stemness *in vitro* (Coutu *et al.*, 2011). As shown in figure 34, some of the direct interaction partners of FGFR1OP were also up- or down-regulated with age. Interestingly, the chromatin region of tyrosine kinase ABL1 involved in cell proliferation, differentiation and apoptosis was more open with age (Khorashad *et al.*, 2013), along with WRNIP1, the gene encoding the ATPase. WRNIP1 was reported to be involved in Werner's syndrome which is characterized by premature aging (Kawabe *et al.*, 2006). The gene encoding phosphofurin acidic cluster sorting protein 1 (PACS1) was up-regulated with age (Figure 34). Mutation of this gene was reported to be linked to a rare genetic syndrome characterized by developmental delay (Schuurs-Hoeijmakers *et al.*, 2016).

The gene TIGAR was reported to protect cells from starvation-induced apoptosis by up-regulating respiration (Wanka *et al.*, 2012). Furthermore, it was reported that the gene P53 induces the expression of a set of antioxidant genes such as TIGAR to lower cellular reactive oxygen species (ROS) levels (Feng *et al.*, 2011). Biochemically, TIGAR was reported to decrease cellular levels of fructose-2,6-bisphosphate which is an allosteric regulator of cellular glucose metabolic pathways (Bensaad *et al.*, 2006; Madan *et al.*, 2011). Three direct interaction partners of TIGAR were found in our mass spectrometry based shot-gun proteomics dataset (Figure 34). The tuberous sclerosis 2 gene (TSC2) is a tumor suppressor which is associated with the genetic disease tuberous sclerosis (Inoki *et al.*, 2002). The amyloid beta precursor protein (APP) is associated to Alzheimer disease. It was also reported to modulate neuronal synapse formation (Priller *et al.*, 2006). The ubiquitin-conjugating enzyme E2 L3 (UBE2L3) is associated with various autoimmune diseases as the gene product ubiquitinylates the NF-κB precursor (Lewis *et al.*, 2015).

For ceramide synthase 6 (CER6) it was reported that the gene regulates the metabolism of ceramides and sphinosines (Peters *et al.*, 2015). Proteins encoded by CER6 are integral membrane proteins of the ER that catalyze the synthesis of ceramides (Reynolds *et al.*, 2004). In aging MSCs, one previous study reported that the ceramide composition of cell membranes is altered upon aging in MSCs (Kilpinen *et al.*, 2013). One direct interaction partner of CER6, ATP synthase subunit b (ATP5F1), was found to be down-regulated in proteomics dataset (Figure 34). ATP5F1 encodes a subunit of mitochondrial ATP synthase (Vaca Jacome *et al.*, 2015). In conclusion, together with their direct interaction partners, these age-associated genes identified in our ATAC-seq dataset provide a candidate list for future follow-up studies.

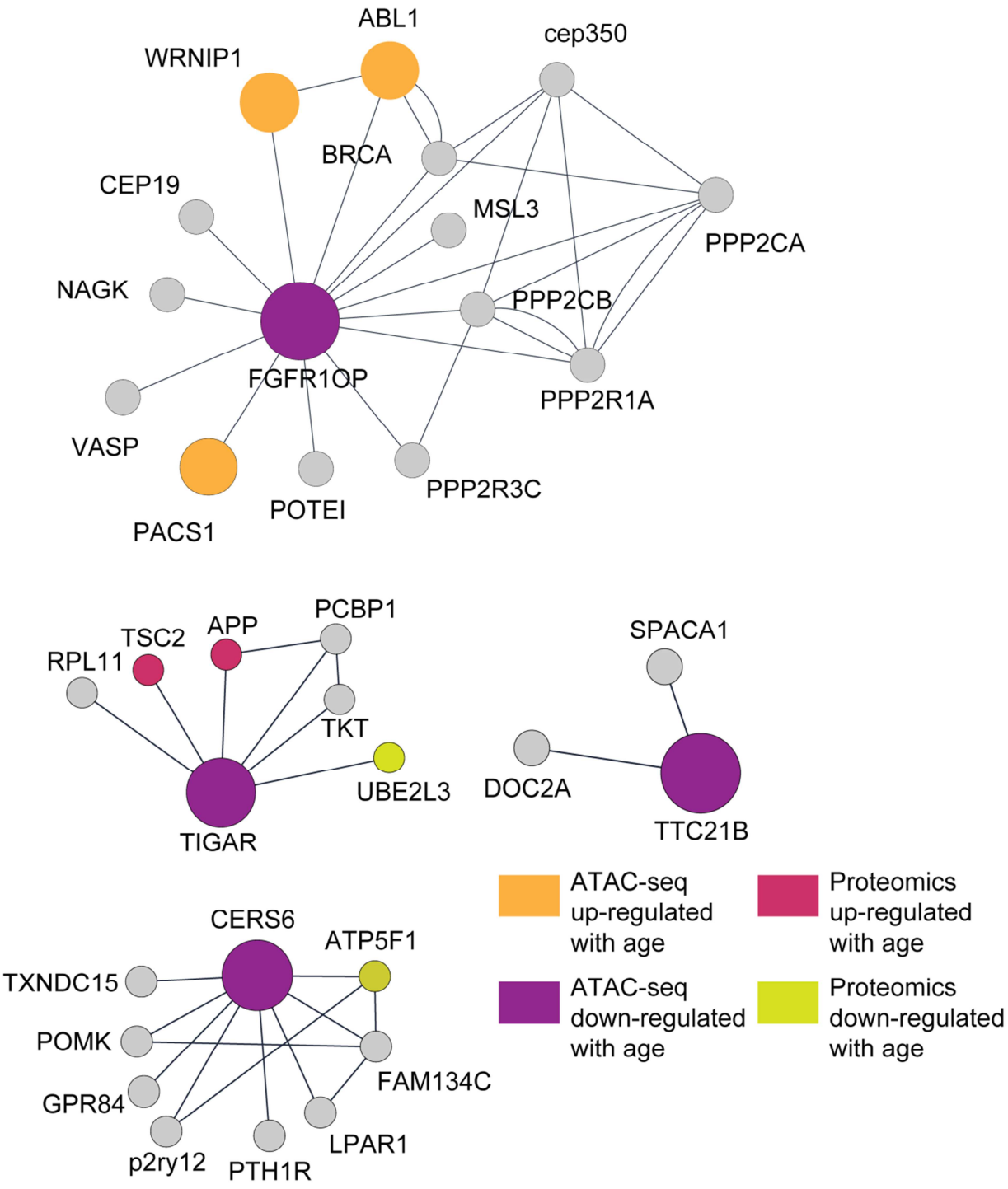

Figure 34 Network representations of the direct interaction partners of genes FGFR1OP, TIGAR, TTC32B and CERS6. Genes identified in the ATAC-seq dataset were shown in orange (up-regulated with age) or purple (down-regulated with age). Genes identified in the shotgun mass-spectrometry proteomics dataset were shown in pink (up-regulated with age) or green (down-regulated with age).

4.3.2.8 DNA motif enrichment analysis on differential ATAC-seq peaks localized in promoter regions

We focused on annotated promoter regions to further analyze which DNA binding motifs are differentially accessible between old and young individuals. Among the 761 peaks annotated to promoter regions, 664 peaks have a negative slope with age, suggesting that the promoter regions are more accessible in young individuals, whereas 97 peaks are more accessible in aged donors.

Using a web-based tool AME (analysis for motif enrichment), we wanted to know if there is any prevalence of a particular transcription factor binding site in differential peak regions compared to consensus peak regions. To this end, a motif enrichment analysis on the sequences in differential peaks annotated to promoter regions was carried out. The same number of non-differential promoter regions was used as control. Four motif databases (homoco v10, jasper 2013, swissregulon human and mouse, footprintDB v 1) were used to answer the question, whether there is an over-representation of the motif in the differential peaks as compared to the control. The top five significantly enriched motifs for regions more open in younger individuals are binding motifs of the transcription factor AP-2 gamma (TFAP2C), Krueppel-like factor 16 (KLF16), hypermethylated in cancer 1.p2 (HIC1.p2), Wilms-Tumor-Protein (WT1) and metal regulatory transcription factor 1.p2 (MTF1.p2) (Figure 35). TFAP2C is *e.g.* a sequence-specific DNA-binding transcription factor involved in the activation of several developmental genes. On the other hand, the motif enrichment in regions more open in elderly individuals indicated AT rich motifs that resemble TATA box motifs. These are binding motifs of the homeobox C11, A10, C10 and A13 (HOXC11, HOXA10, HOXC10 and HOXA13) as well as engrailed homeobox (EN). This finding suggests that as the individual ages, TATA box containing promoters are more likely to be present as open chromatin region (Figure 35).

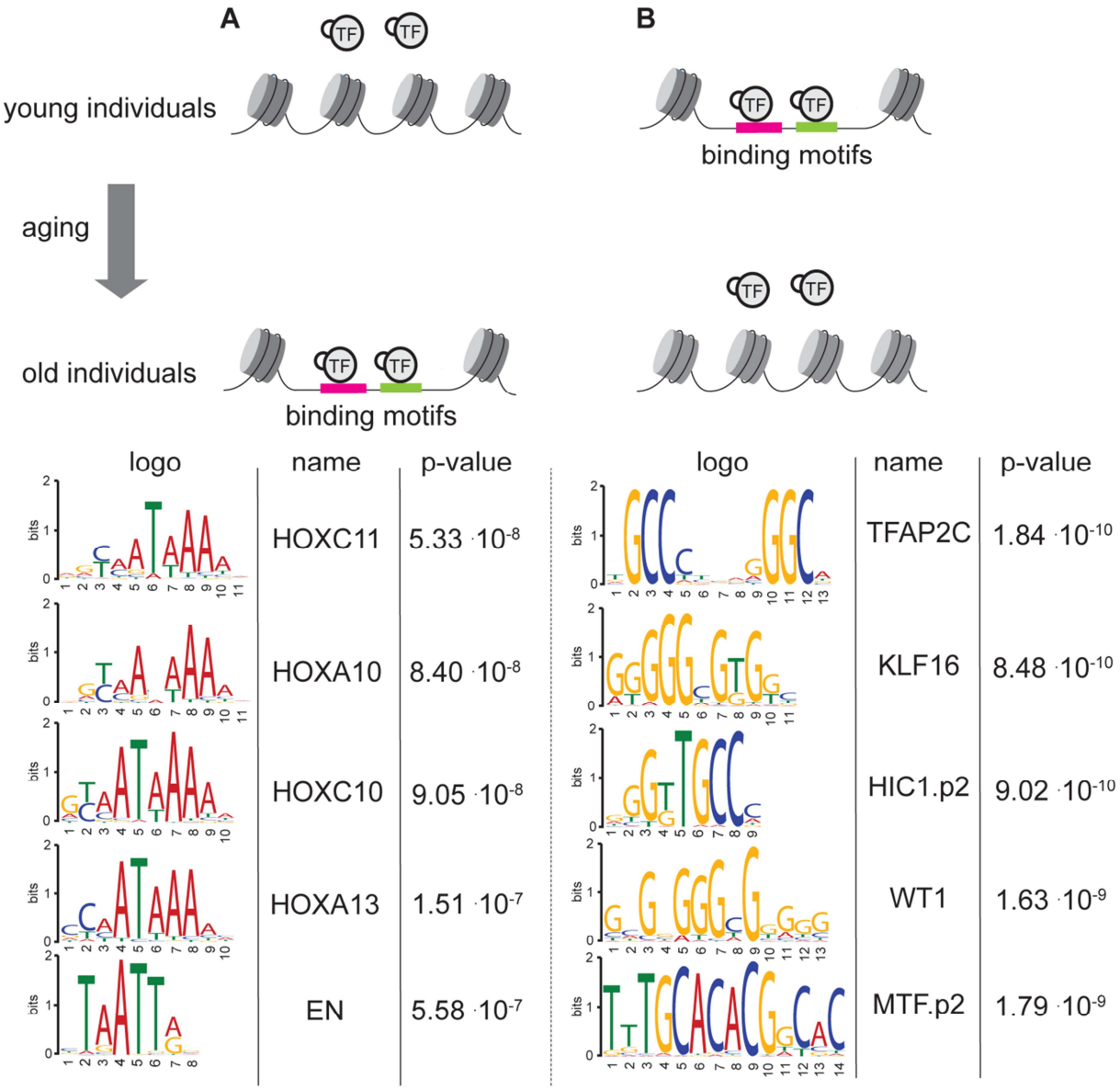

Figure 35 Ten transcription factor motifs that are enriched in differential promoter regions. (A) The top five significantly enriched motifs that are more accessible in old individuals are binding motifs of the homeobox C11, A10, C10 and A13 (HOXC11, HOXA10, HOXC10 and HOXA13) as well as engrailed homeobox (EN). **(B)** The top five enriched motifs that are more accessible in young individuals are binding motifs of transcription factor AP-2 gamma (TFAP2C), Krueppel-like factor 16 (KLF16), hypermethylated in cancer 1.p2 (HIC1.p2), Wilms-Tumor-Protein (WT1) and metal regulatory transcription factor 1.p2 (MTF1.p2).

Previous studies on transcriptomic and DNA methylation levels showed that the expression of many homeobox transcription factors (including HOXA5, HOXB3 and HOXB7) as well as genes involved in cell differentiation are changed upon aging (Wagner *et al.*, 2009; Bork *et al.*, 2010). Our findings based on ATAC-seq dataset confirmed the importance of homeobox transcription factors in aging MSCs. Among the transcriptional factors overrepresented in younger individuals, none of the

candidates was reported previously to be changing in aging MSCs. However, transcription factors such as KLF16 and WT1 are involved in cancer development (Yang *et al.*, 2007; Yang, 2009). Remarkably, the MTF1 transcription factor regulates the metal homeostasis and oxidative stress, which are important biological process in aging (Bahadorani *et al.*, 2010).

In conclusion, the DNA motif enrichment analysis may serve as a starting point for future multi-omics integration efforts. The downstream effects of the aging-associated transcription factors described here can be validated and further studied in future proteomics and transcriptomics datasets.

5. Discussion and Outlook

To study the effects of aging on human bone marrow niche and hematopoietic stem cells, 59 bone marrow aspirate samples derived from healthy individuals between ages 20 and 60 were collected and characterized by flow cytometry.

First, I investigated the age-related proportional and morphological changes of the major cellular components of the bone marrow comprising of hematopoietic stem cells (HSC), lymphocytes and restricted precursors (LYM), monocytes, macrophages and restricted precursors (MON), granulocytic precursors (GRA) and erythroid precursors (ERP) based on the flow cytometry data obtained during cell sorting.

The interactions between HSCs and the niche were studied *in vitro* using a co-culture system of HSCs and MSCs. In this set of experiments, the supportive potentials of undifferentiated MSCs, adipogenically differentiated MSCs (ADI-MSCs) and osteogenically differentiated MSCs (OST-MSCs) for HSCs were explored. The proliferation and stemness of $CD34^+$ HSCs were investigated after seven days of co-culture with these three types of feeder cells.

We investigated in MSCs the epigenetic changes upon aging using ATAC-sequencing (ATAC-seq). The ATAC-seq library preparation protocol was adapted for primary MSCs. Subsequently, sequencing data were generated from a cohort of 16 healthy individuals from ages 21 to 59. In this chapter, results obtained from these three parts of experiments are discussed. Future perspectives on possible follow-up studies are outlined.

5.1 Age correlation of changes in relative percentage, cell size and granularity of major bone marrow constituents

In our study on the major constituents of the bone marrow, changes observed in relative percentage, cell size and granularity are not correlated with the age of the donors (Figure 14). These findings are consistent with the previous observations made by Bain (Bain, 1996). In that study, bone marrow aspirates in healthy subjects were sampled from the iliac crest, 30 men and 20 women, between ages 21 and 56. From each individual, about 0.1-0.2 ml of the bone marrow was taken (Bain, 1996). The aspirates were subsequently profiled and characterized based on morphological traits under light microscope (Bain, 1996). Although using a different method of cell characterization, no age-associated correlations in cellular compositions and morphological changes were found. However, comparing their results with the present study, differences are found in the relative cellular compositions of the bone marrow. A summary of the findings published by Bain revealed that the relative percentages of ERP, GRA, MON and LYM are around 26%, 37%, 23% and 14%, respectively (Bain, 1996). The cell type nomenclature used by Bain was approximated to the definitions of the present study. The relative proportions obtained in our study showed that ERP constitute to 31.1% of the bone marrow cell fraction whereas the relative percentages of GRA, MON, and LYM are 14.8%, 9.9% and 29.2%, respectively (Figure 14A). One reason for this discrepancy could be due to the different experimental setups. A density gradient centrifugation of the bone marrow aspirate was *e.g.* not performed in the Bain study, which might result into a higher percentage of the polymorphonuclear GRA in the total population. In addition, the definition of bone marrow cell types solely by a set of morphologic straits also leads to differences compared to immunephenotypic identification of cell populations.

5.2 Effects of adipogenic differentiation on the supportive potential of MSCs

HSCs rely on a cellular microenvironment to maintain their stem cell function. As cross-talks with the niche contribute to the regulation of HSC proliferation and maintenance of stemness, an *in vitro* model was developed by co-culturing MSCs with $CD34^+$ HSCs. The MSCs serve as a substitution for the cellular environment of the niche with their stromal supportive ability.

We showed that undifferentiated MSCs, adipogenically differentiated MSCs (ADI-MSCs) and osteogenically differentiated MSCs (OST-MSCs) not only support the proliferation of HSCs, but also maintain the CD34 expression in HSCs at a high level over a number of population doublings. Remarkably, compared to MSCs and OST-MSCs, the co-culture with ADI-MSCs increased the proliferation of HSCs much stronger while maintaining the HSCs at higher CD34 expression level (Figure 19-21).

Based on the observations of the co-culture experiments, one can hypothesize that ADI-MSCs provide an even better niche for HSCs than undifferentiated MSCs. To further prove this hypothesis, however, the relationship between high CD34 expression and *in vivo* stemness of the HSCs needs to be investigated. As described in the introduction section 1.2.4, previous studies on aged hematopoietic compartment showed that despite high expression levels of CD34 in some HSC populations, these cells possessed lower *in vivo* stemness and differentiation potential (Geiger *et al.*, 2013). To follow-up on our co-culture experiments, one can perform a serial transplantation assay in mouse to functionally study the stemness and differentiation potentials of the $CD34^+$ HSCs either co-cultured with ADI-MSCs, undifferentiated MSCs or freshly isolated.

Another key issue on the supportive potential of ADI-MSCs is the quantification of the differentiation status of ADI-MSCs. On transcriptome level, the expression of several transcription regulators such as peroxisome proliferator-activated receptor gamma (PPARγ), CCAAT/enhancer binding protein (CEBPα) and fatty acid binding protein (FABP) are commonly used markers to characterize the adipogenic differentiation (Siersbaek *et al.*, 2010; Polini *et al.*, 2011). Together with BODIPY staining of the adipocytic triglycerides, the degree of MSC adipogenic differentiation can be further

characterized and related to the effects of ADI-MSCs on the proliferation and stemness of HSCs in future experiments.

5.3 Influences of the niche on the proliferation and stemness of HSCs

Our findings of the co-culture experiment using trans-wells physically separate the HSCs from MSCs suggested that direct cell-cell contacts might be required for MSCs and OST-MSCs to retain HSCs at a lower proliferation rate (Figure 20). Strikingly, we could observe that HSCs cultured in the supernatant of ADI-MSCs showed a similar proliferation profile after seven days compared to HSCs grown directly on ADI-MSCs (Figure 19, 20).

Using this experimental setup, the dynamics of the direct versus indirect interactions between HSCs and the niche can be investigated by series of time course experiments. The HSCs co-cultured on MSCs and differentiated MSCs with or without direct cell contacts can be *e.g.* studied after 12 hours, one day and three days. One can speculate here that different mechanisms of interactions come into effects at different time points, which might affect the proliferation as well as the stemness of HSCs.

In addition, one could further investigate the immunephenotype of co-cultured HSCs using additional stemness marker CD38. The $CD34^+/CD38^-$ cells represent a more primitive HSC subpopulation (Sutherland *et al.*, 1989; Weilbaecher *et al.*, 1991; Petzer *et al.*, 1996). By measuring the differentiation markers such as CD13 (myeloid differentiation marker), CD45 (general lymphoid marker) and CD56 (markers for natural killer cells), one could track the differentiation lineage of the proliferated HSCs in relationship with different numbers of cell divisions after seven days of co-culture.

To further investigate the intrinsic changes in HSCs upon co-culture with different feeder cells, gene expression can be profiled by RNA-seq. Chromatin accessibility profiles can be generated by ATAC-seq. A combined analysis will uncover changes on molecular levels underlying the observed differences in proliferation rate and CD34 expression. The findings from *in vitro* co-culture experiments can be related to

the *in vivo* observations in aged hematopoietic compartment with increased amount of adipose tissue (Sudo *et al.*, 2000; Marie, 2014). This will answer the question to what extent does the *in vitro* niche model using adipogenically differentiated MSCs reflect the actual aging fatty bone marrow *in vivo*.

5.4 Variations of HSCs derived from cord and peripheral blood in proliferation and stemness upon co-culture

In our experiments, we co-cultured HSCs derived from cord blood and mobilized peripheral blood either with MSCs, ADI-MSCs and OST-MSCs. The $CD34^+$ HSCs provide a commonly studied population of stem and progenitor cells which can be enriched in adequate amount by magnetic cell separation using Dynabeads (details in section 3.2.1.2). A comparison between the distributions of proliferated HSCs after seven days indicated that cells of both sources showed similar proliferation profiles (Figure 19). In both experiments at division steps five and above five, the CD34 expression level of HSCs co-cultured on ADI-MSCs was the highest (Figure 21). However, we found differences between cord and peripheral blood HSCs in relative CD34 expression across culture conditions (Figure 21). The observed variations can be due to cell-intrinsic properties of the cord and peripheral blood HSCs. It was previously shown that HSCs derived from mobilized peripheral blood are less adherent to the niche compared to cells derived from cord blood and bone marrow (Wagner *et al.*, 2007).

To further develop the co-culture system, different levels of niche adherence in cord and mobilized peripheral blood HSCs can be measured by microscopy-based adherence assays (Zepeda-Moreno *et al.*, 2011). This assay quantifies living HSCs that lose adhesion due to gravitational force from the MSC feeder cell layer. The HSCs are co-cultured with MSCs on a 24-well plate. After an incubation time period defined by the experimenter, the plate is turned upside down. HSCs not physically attached to the MSCs will fall down. The numbers of the adherent versus non-adherent HSCs can be determined by microscopy. Using this assay, the fractions of adherent and non-adherent HSCs from cord and peripheral blood can be separated from each other. The gene expression of these four HSC populations co-cultured with MSCs can be profiled to investigate if there are any factors contributing to stemness

and adherence. The differences in proliferation rate and stemness between cord and peripheral blood HSCs can be related to the variations in niche adherence.

5.5 Integration of different molecular levels to a comprehensive regulatory network in MSCs

Integration of chromatin accessibility data with gene expression and protein levels leads to deeper understanding of aging MSCs. Among the 16 samples sequenced with ATAC-seq, 13 MSC samples were measured by mass-spectrometry proteomics method as well (manuscript in preparation, Gavin and Ho lab). The 4,579 differential ATAC-seq peaks upon aging were assigned to the nearest 3,580 genes (Figure 36). There were 6,509 expressed genes detected on protein level using shotgun proteomics (manuscript in preparation, Gavin and Ho lab). A preliminary comparison of ATAC-seq and protein data revealed that 1,192 genes were commonly detected (Figure 36). To my best knowledge, no direct comparisons between ATAC-seq and proteomics data have been done to date. One study on aging $CD8^+$ T cells showed a positive correlation between age-related changes in gene expression and chromatin accessibility at promoter regions with a correlation coefficient of r=0.34 (Ucar *et al.*, 2017). One can speculate that the correlation between chromatin accessibility and gene expression is higher than the correlation between chromatin accessibility and protein level data as transcription is more directly affected by the status of chromatin accessibility.

To obtain a more holistic view on the transcription regulatory landscape in aging MSCs, the integration of gene expression data on transcriptome level (*e.g*. RNA-seq data) would be required (Ackermann *et al.*, 2016; Koh *et al.*, 2016). This will help us to better interpret our age-associated changes in chromatin accessibility and further test our hypotheses generated from our observations in the ATAC-seq dataset.

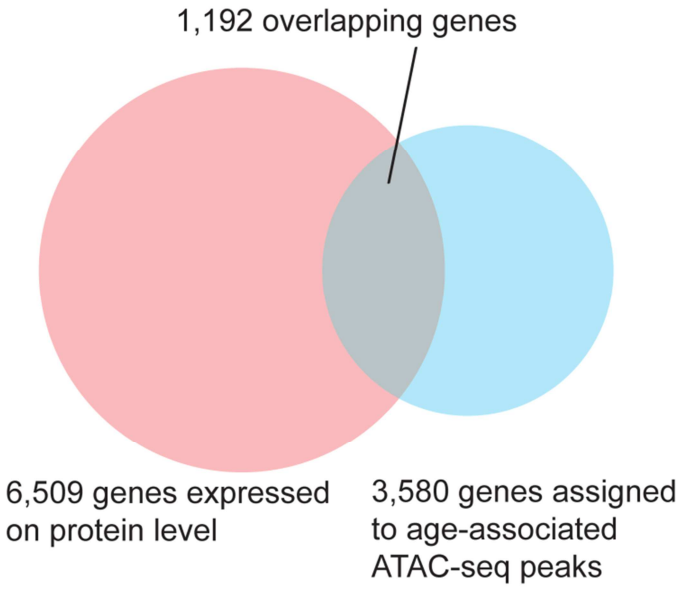

Figure 36 Overview of overlapping genes annotated to ATAC-seq peaks with the proteomics dataset. The 4,579 differential ATAC-seq peaks upon aging were annotated to the nearest 3,580 genes (blue). There were 6,509 genes expressed on protein level detected in the mass-spectrometry based shotgun proteomics dataset (red). A set of 1,192 genes was commonly detected in both experiments.

5.6 Future perspectives on age-related changes in chromatin accessibility of MSCs

The ATAC-seq data on MSCs generated in this study provides a solid foundation for future follow-up studies. Further analyses of the data will aim at describing a set of common aging features on chromatin level by comparing ATAC-seq profiles of MSCs from aged versus young donors. If possible, the number of samples derived from aged donors will be further increased to gain more prediction power to build our statistical model. The ATAC-seq samples derived from female donors will also be increased to obtain a more gender-balanced dataset.

One aspect worth exploring in future experiments is the commonly described lineage skewing of MSCs towards adipogenic differentiation upon aging (section 1.4.4) (Stenderup *et al.*, 2003). As chromatin structure undergoes major modifications during the differentiation process in stem cells, changes can be captured by chromatin accessibility profiling methods such as ATAC-seq (Ramirez *et al.*, 2017). By inducing adipogenic and osteogenic differentiation in young and aged MSCs during 21 days *in vitro* culture, the dynamics of chromatin accessibility can be

captured at different time points during the differentiation process. The intrinsic regulatory mechanisms of the biased differentiation potential towards adipocytes can be studied in a time course.

Focusing on aging, it is of interest to investigate changes in open chromatin profiles of the human sex chromosomes. Considering the gender differences in human average lifespan, one can speculate that women and men age differently (Austad *et al.*, 2016). By studying primary $CD4^+$ T cells isolated from healthy individuals, Qu *et al.* found novel elements that escape X chromosome inactivation and predicted gender-specific gene regulatory networks across autosomes (Qu *et al.*, 2015). Using our ATAC-seq dataset, gender-specific gene regulatory networks can be further investigated in the context of aging.

Our ATAC-seq data showed that the chromatin regions at certain promoters are open and accessible. One recent study identified that the chromatin accessibility profile is highly cell-type specific (Corces *et al.*, 2016). Moreover, the accessibility of distal elements, such as enhancers, was found to be more cell-type specific than those of promoters or patterns of gene expression (Corces *et al.*, 2016). This is probably due to the fact that different distal enhancers can regulate the same gene in different cell types (Corces *et al.*, 2016). In analogy to this study, one can ask the question if a certain group of chromatin region is more age-dependent apart from the promoter regions. Corces *et al.* created an enhancer cytometric atlas using ATAC-seq data previously generated from known cell types by a machine learning algorithm. This atlas was subsequently used to predict unknown cell types (Corces *et al.*, 2016). In analogy, one could try to create an atlas to predict the age of MSCs based on open chromatin profiles generated by ATAC-seq. This would serve as a very useful diagnostic tool to check the quality of MSCs prior to their clinical applications.

Due to the supportive function of MSCs for HSCs, one can investigate the changes in chromatin accessibility in aged HSCs together with MSCs. Previous studies suggested that the methylation pattern in HSCs changes dramatically upon aging (Beerman *et al.*, 2010; Bocker *et al.*, 2011). On the chromatin level, another aspect would be to study the age-associated changes on chromatin compactness in HSCs, as experimental findings suggested that aging leads to a general loss of heterochromatin (Booth *et al.*, 2016). This hypothesis can be tested in HSCs using ATAC-seq data together with *e.g*. RNA-seq and proteomics datasets. The MSC-HSC

co-culture system serves as an *in vitro* model to study the effects of the niche on stem cells on epigenetic level. Changes in chromatin structures can be captured by *e.g*. co-culturing aged HSCs with young MSCs and *vice versa*. Thereby it might be interesting to explore to what extent the ATAC-seq profile of aged HSCs can be "rejuvenated" upon co-culture with young MSCs. Subsequently, the question if age-associated changes of chromatin accessibility in the niche cells affect the chromatin accessibility profiles of HSCs can be addressed.

6. References

Ackermann, Wang, Schug, Naji and Kaestner (2016) 'Integration of ATAC-seq and RNA-seq identifies human alpha cell and beta cell signature genes', *Molecular Metabolism*, 5(3), pp. 233–244. doi: 10.1016/j.molmet.2016.01.002.

Adey, Morrison, Asan, Xun, Kitzman, Turner, Stackhouse, MacKenzie, Caruccio, Zhang, *et al.* (2010) 'Rapid, low-input, low-bias construction of shotgun fragment libraries by high-density in vitro transposition.', *Genome biology*, 11(12), p. R119. doi: 10.1186/gb-2010-11-12-r119.

Alberts, Johnson, Lewis, Raff and Roberts (2015) 'Molecular biology of the cell, 6th edition by B. Alberts, A. Johnson, J. Lewis, M. Raff, K. Roberts, and P. Walter', *Biochemistry and Molecular Biology Education*, 36, p. 171. doi: 10.1002/bmb.20192.

Anders and Huber (2012) 'Differential expression of RNA-Seq data at the gene level–the DESeq package', *EMBL, Heidelberg, Germany*, 11, p. R106. doi: 10.1186/gb-2010-11-10-r106.

Arai, Hirao, Ohmura, Sato, Matsuoka, Takubo, Ito, Koh and Suda (2004) 'Tie2 / Angiopoietin-1 Signaling Regulates Hematopoietic Stem Cell Quiescence in the Bone Marrow Niche', *Cell*, 118(2), pp. 149–161. doi: 10.1016/j.cell.2004.07.004.

Armstrong (2013) *Epigenetics*, *Garland Science*. doi: 10.1007/s00439-014-1442-4.

Austad and Fischer (2016) 'Sex Differences in Lifespan', *Cell Metabolism*, 23(6), pp. 1022–1033. doi: 10.1016/j.cmet.2016.05.019.

Bahadorani, Mukai, Egli and Hilliker (2010) 'Overexpression of metal-responsive transcription factor (MTF-1) in Drosophila melanogaster ameliorates life-span reductions associated with oxidative stress and metal toxicity', *Neurobiology of Aging*, 31(7), pp. 1215–1226. doi: 10.1016/j.neurobiolaging.2008.08.001.

Bain (1996) 'The bone marrow aspirate of healthy subjects.', *British journal of haematology*, 95(3), pp. 574–5. doi: 10.1046/j.1365-2141.1996.d01-1786.x.

Bain, Clark and Wilkins (2009) *Bone Marrow Pathology: FOURTH EDITION*, *Bone Marrow Pathology: FOURTH EDITION*. doi: 10.1002/9781444309782.

Beerman, Bock, Garrison, Smith, Gu, Meissner and Rossi (2013) 'Proliferation-dependent alterations of the DNA methylation landscape underlie hematopoietic stem cell aging', *Cell Stem Cell*, 12(4), pp. 413–425. doi: 10.1016/j.stem.2013.01.017.

Beerman, Luis, Singbrant, Lo Celso and Mendez-Ferrer (2017) 'The evolving view of the hematopoietic stem cell niche', *Experimental Hematology*. doi: 10.1016/j.exphem.2017.01.008.

Beerman, Maloney, Weissmann and Rossi (2010) 'Stem cells and the aging hematopoietic system', *Current Opinion in Immunology*, 22(4), pp. 500–506. doi: 10.1053/j.seminhematol.2008.07.010.

Bensaad, Tsuruta, Selak, Vidal, Nakano, Bartrons, Gottlieb and Vousden (2006) 'TIGAR, a p53-Inducible Regulator of Glycolysis and Apoptosis', *Cell*, 126(1), pp. 107–120. doi: 10.1016/j.cell.2006.05.036.

Benz, Copley, Kent, Wohrer, Cortes, Aghaeepour, Ma, Mader, Rowe, Day, *et al.* (2012) 'Hematopoietic stem cell subtypes expand differentially during development and display distinct lymphopoietic programs', *Cell Stem Cell*, 10(3), pp. 273–283. doi: 10.1016/j.stem.2012.02.007.

Bernstein, Birney, Dunham, Green, Gunter and Snyder (2012) 'An integrated encyclopedia of DNA elements in the human genome.', *Nature*, 489, pp. 57–74. doi: 10.1038/nature11247.

Bindea, Mlecnik, Hackl, Charoentong, Tosolini, Kirilovsky, Fridman, Pagès, Trajanoski and Galon (2009) 'ClueGO: A Cytoscape plug-in to decipher functionally grouped gene ontology and pathway annotation networks', *Bioinformatics*, 25(8), pp. 1091–1093. doi: 10.1093/bioinformatics/btp101.

Le Blanc and Mougiakakos (2012) 'Multipotent mesenchymal stromal cells and the innate immune system', *Nature Reviews Immunology*, 12(5), pp. 383–396. doi: 10.1038/nri3209.

Bocker, Hellwig, Breiling, Eckstein, Ho and Lyko (2011) 'Genome-wide promoter DNA methylation dynamics of human hematopoietic progenitor cells during differentiation and aging', *Blood*, 117(19), pp. e182-9. doi: 10.1182/blood-2011-01-331926.

Bonner (1972) 'Fluorescence Activated Cell Sorting', *Review of Scientific Instruments*, 43(3), p. 404. doi: 10.1063/1.1685647.

Booth and Brunet (2016) 'The Aging Epigenome', *Molecular Cell*, pp. 728–744. doi: 10.1016/j.molcel.2016.05.013.

Bork, Pfister, Witt, Horn, Korn, Ho and Wagner (2010) 'DNA methylation pattern changes upon long-term culture and aging of human mesenchymal stromal cells', *Aging Cell*, 9(1), pp. 54–63. doi: 10.1111/j.1474-9726.2009.00535.x.

Buenrostro, Giresi, Zaba, Chang and Greenleaf (2013) 'Transposition of native chromatin for fast and sensitive epigenomic profiling of open chromatin, DNA-binding proteins and nucleosome position.', *Nature methods*, 10(12), pp. 1213–8. doi: 10.1038/nmeth.2688.

Buenrostro, Wu, Litzenburger, Ruff, Gonzales, Snyder, Chang and Greenleaf (2015) 'Single-cell chromatin accessibility reveals principles of regulatory variation.', *Nature*, 523(7561), pp. 486–490. doi: 10.1038/nature14590.

Challen, Boles, Chambers and Goodell (2010) 'Distinct Hematopoietic Stem Cell Subtypes Are Differentially Regulated by TGF-β1', *Cell Stem Cell*, 6(3), pp. 265–278. doi: 10.1016/j.stem.2010.02.002.

Chambers and Goodell (2007) 'Hematopoietic stem cell aging: Wrinkles in stem cell potential', *Stem Cell Reviews*, 3(3), pp. 201–211. doi: 10.1007/s12015-007-0027-1.

Chambers, Shaw, Gatza, Fisk, Donehower and Goodell (2007) 'Aging hematopoietic stem cells decline in function and exhibit epigenetic dysregulation', *PLoS Biology*, 5(8), pp. 1750–1762. doi: 10.1371/journal.pbio.0050201.

Civin, Strauss, Brovall, Fackler, Schwartz and Shaper (1984) 'Antigenic analysis of hematopoiesis. III. A hematopoietic progenitor cell surface antigen defined by a monoclonal antibody raised against KG-1a cells.', *Journal of immunology*, 133(1), pp. 157–165.

De Clercq (2003) 'The bicyclam AMD3100 story.', *Nature reviews. Drug discovery*, 2(7), pp. 581–587. doi: 10.1038/nrd1134.

Corces, Buenrostro, Wu, Greenside, Chan, Koenig, Snyder, Pritchard, Kundaje, Greenleaf, *et al.* (2016) 'Lineage-specific and single-cell chromatin accessibility charts human hematopoiesis and leukemia evolution', *Nature Genetics*, 48(10), pp. 1193–1203. doi: 10.1038/ng.3646.

Coutu and Galipeau (2011) 'Roles of FGF signaling in stem cell self-renewal, senescence and aging', *Aging*, 3(10), pp. 920–933. doi: 10.18632/aging.100369.

Creyghton, Cheng, Welstead, Kooistra, Carey, Steine, Hanna, Lodato, Frampton, Sharp, *et al.* (2010) 'Histone H3K27ac separates active from poised enhancers and predicts developmental state', *Proceedings of the National Academy of Sciences*, 107(50), pp. 21931–21936. doi: 10.1073/pnas.1016071107.

Docheva, Popov, Mutschler and Schieker (2007) 'Human mesenchymal stem cells in contact with their environment: Surface characteristics and the integrin system', *Journal of Cellular and Molecular Medicine*, 11(1), pp. 21–38. doi: 10.1111/j.1582-4934.2007.00001.x.

Dominici, Le Blanc, Mueller, Slaper-Cortenbach, Marini, Krause, Deans, Keating, Prockop and Horwitz (2006) 'Minimal criteria for defining multipotent mesenchymal stromal cells. The International Society for Cellular Therapy position statement.', *Cytotherapy*, 8(4), pp. 315–7. doi: 10.1080/14653240600855905.

Dykstra, Olthof, Schreuder, Ritsema and de Haan (2011) 'Clonal analysis reveals multiple functional defects of aged murine hematopoietic stem cells', *The Journal of Experimental Medicine*, 208(13), pp. 2691–2703. doi: 10.1084/jem.20111490.

Feng, Lin and Wu (2011) 'The Regulation of Aging and Longevity: A New and Complex Role of p53.', *Genes & cancer*, 2(4), pp. 443–52. doi: 10.1177/1947601911410223.

Florian, Dörr, Niebel, Daria, Schrezenmeier, Rojewski, Filippi, Hasenberg, Gunzer, Scharffetter-Kochanek, *et al.* (2012) 'Cdc42 activity regulates hematopoietic stem cell aging and rejuvenation', *Cell Stem Cell*, 10(5), pp. 520–530. doi: 10.1016/j.stem.2012.04.007.

Frenette, Pinho, Lucas and Scheiermann (2013) *Mesenchymal Stem Cell: Keystone of the Hematopoietic Stem Cell Niche and a Stepping-Stone for Regenerative Medicine*, *Annual Review of Immunology*. doi: doi:10.1146/annurev-immunol-032712-095919.

Freund, Bauer, Boxberger, Feldmann, Streller, Ehninger, Werner, Bornhaeuser, Oswald and Corbeil (2006) 'Polarization of human hematopoietic progenitors during contact with multipotent mesenchymal stromal cells: effects on proliferation and clonogenicity.', *Stem cells and development*, 15(6), pp. 815–829. doi: 10.1089/scd.2006.15.815.

Friedenstein, Gorskaja and Kulagina (1976) 'Fibroblast precursors in normal and irradiated mouse hematopoietic organs.', *Experimental hematology*, 4(5), pp. 267–74.

Geiger, de Haan and Florian (2013) 'The ageing haematopoietic stem cell compartment', *Nature Reviews Immunology*, 13(5), pp. 376–389. doi: 10.1038/nri3433.

Giebel, Corbeil, Beckmann, Höhn, Freund, Giesen, Fischer, Kögler and Wernet (2004) 'Segregation of lipid raft markers including CD133 in polarized human hematopoietic stem and progenitor cells', *Blood*, 104(8), pp. 2332–2338. doi: 10.1182/blood-2004-02-0511.

Giebel and Punzel (2008) 'Lineage development of hematopoietic stem and progenitor cells', *Biological Chemistry*, pp. 813–824. doi: 10.1515/BC.2008.092.

Givan (2004) 'Flow cytometry', in *Methods in Molecular Biology: Flow cytometry protocols*, pp. 1–31. doi: 10.1385/1592597734.

Givan (2011) 'Flow Cytometry Protocols', *Platelets*, 699, pp. 1–29. doi: 10.1007/978-1-61737-950-5.

Hashimoto (1962) 'Pathology of bone marrow.', *Acta haematologica*, 27, pp. 193–216. doi: 10.1159/000206782.

Hayflick (1965) 'The limited in vitro lifetime of human diploid cell strains', *Experimental Cell Research*, 37(3), pp. 614–636. doi: 10.1016/0014-4827(65)90211-9.

Hayflick and Moorhead (1961) 'The serial cultivation of human diploid cell strains', *Experimental Cell Research*, 25(3), pp. 585–621. doi: 10.1016/0014-4827(61)90192-6.

Heintzman, Stuart, Hon, Fu, Ching, Hawkins, Barrera, Van Calcar, Qu, Ching, *et al.* (2007) 'Distinct and predictive chromatin signatures of transcriptional promoters and enhancers in the human genome', *Nature Genetics*, 39(3), pp. 311–318. doi: 10.1038/ng1966.

Ho, Haas and Champlin (2000) 'Hematopoietic Stem Cell Transplantation'. CRC Press, p. 624.

Ho and Wagner (2007) 'The beauty of asymmetry: asymmetric divisions and self-renewal in the haematopoietic system', *Current Opinion in Hematology*, 14(4), pp. 330–336. doi: 10.1097/MOH.0b013e3281900f12.

Ho, Wagner and Mahlknecht (2005) 'Stem cells and ageing. The potential of stem cells to overcome age-related deteriorations of the body in regenerative medicine.', *EMBO reports*, 6 Spec No, pp. S35-8. doi: 10.1038/sj.embor.7400436.

Hogart, Lichtenberg, Ajay, Anderson, Margulies and Bodine (2012) 'Genome-wide DNA methylation profiles in hematopoietic stem and progenitor cells reveal overrepresentation of ETS transcription

factor binding sites', *Genome Research*, 22(8), pp. 1407–1418. doi: 10.1101/gr.132878.111.

Horwitz, Le Blanc, Dominici, Mueller, Slaper-Cortenbach, Marini, Deans, Krause and Keating (2005) 'Clarification of the nomenclature for MSC: The International Society for Cellular Therapy position statement.', *Cytotherapy*, 7(5), pp. 393–5. doi: 10.1080/14653240500319234.

Huang, Law, Francis, Palsson and Ho (1999) 'Symmetry of initial cell divisions among primitive hematopoietic progenitors is independent of ontogenic age and regulatory molecules.', *Blood*, 94(8), pp. 2595–604.

Huang, Pan, Jia, Zheng, Xie, Gu, McNiece and Wang (2007) 'Ex vivo expansion and transplantation of hematopoietic stem/progenitor cells supported by mesenchymal stem cells from human umbilical cord blood', *Cell Transplant*, 16(6), pp. 579–585.

Inoki, Li, Zhu, Wu and Guan (2002) 'TSC2 is phosphorylated and inhibited by Akt and suppresses mTOR signalling', *Nature Cell Biology*, 4(9), pp. 648–657. doi: 10.1038/ncb839.

Ito, Hirao, Arai, Matsuoka, Takubo, Hamaguchi, Nomiyama, Hosokawa, Sakurada, Nakagata, *et al.* (2004) 'Regulation of oxidative stress by ATM is required for self-renewal of haematopoietic stem cells', *Nature*, 431(7011), pp. 997–1002. doi: 10.1038/nature02989.

Jaatinen and Laine (2007) 'Isolation of Mononuclear Cells from Human Cord Blood by Ficoll-Paque Density Gradient', in *Current Protocols in Stem Cell Biology*. doi: 10.1002/9780470151808.sc02a01s1.

Jansen, Hanks, Thompson, Dugan and Akard (2005) 'Transplantation of hematopoietic stem cells from the peripheral blood', *Journal of Cellular and Molecular Medicine*, 9(1), pp. 37–50. doi: 10.1111/j.1582-4934.2005.tb00335.x.

Kanehisa and Goto (2000) 'Kyoto Encyclopedia of Genes and Genomes', *Nucleic Acids Research*, 28, pp. 27–30. doi: 10.1093/nar/28.1.27.

Kaplan, Li, Sabo, Thomas, Stamatoyannopoulos, Biggin and Eisen (2011) 'Quantitative Models of the Mechanisms That Control Genome-Wide Patterns of Transcription Factor Binding during Early Drosophila Development', *PLoS Genet*, 7(2), p. e1001290. doi: 10.1371/journal.pgen.1001290.

Karimbocus (2016) *Opening up the primary human bone marrow niche to quantitative proteomics*. University of Heidelberg.

Katoh and Nakagama (2014) 'FGF Receptors: Cancer Biology and Therapeutics', *Medicinal Research Reviews*, 34(2), pp. 280–300. doi: 10.1002/med.21288.

Katz, Tindle, Sutherland and Greaves (1985) 'Identification of a membrane glycoprotein associated with haemopoietic progenitor cells', *Leukemia Research*, 9(2), pp. 191–198. doi: 10.1016/0145-2126(85)90082-7.

Kawabe, Seki, Yoshimura, Nishino, Hayashi, Takeuchi, Iguchi, Kusa, Ohtsuki, Tsuyama, *et al.* (2006) 'Analyses of the interaction of WRNIP1 with Werner syndrome protein (WRN) in vitro and in the cell', *DNA Repair*, 5(7), pp. 816–828. doi: 10.1016/j.dnarep.2006.04.006.

Kent, Copley, Benz, Dykstra, Bowie and Eaves (2008) 'Regulation of hematopoietic stem cells by the steel factor/KIT signaling pathway', *Clinical Cancer Research*, pp. 1926–1930. doi: 10.1158/1078-0432.CCR-07-5134.

Khorashad, Kelley, Szankasi, Mason, Soverini, Adrian, Eide, Zabriskie, Lange, Estrada, *et al.* (2013) 'BCR-ABL1 compound mutations in tyrosine kinase inhibitor-resistant CML: Frequency and clonal relationships', *Blood*, 121(3), pp. 489–498. doi: 10.1182/blood-2012-05-431379.

Kilpinen, Tigistu-Sahle, Oja, Greco, Parmar, Saavalainen, Nikkilä, Korhonen, Lehenkari, Käkelä, *et al.* (2013) 'Aging bone marrow mesenchymal stromal cells have altered membrane glycerophospholipid composition and functionality.', *Journal of lipid research*, 54(3), pp. 622–35. doi: 10.1194/jlr.M030650.

Klauke and De Haan (2011) 'Polycomb group proteins in hematopoietic stem cell aging and malignancies', in *International Journal of Hematology*, pp. 11–23. doi: 10.1007/s12185-011-0857-0.

Koh, Sinha, Barkal, Morganti, Chen, Weissman, Ang, Kundaje and Loh (2016) 'An atlas of transcriptional, chromatin accessibility, and surface marker changes in human mesoderm development', *Scientific Data*, 3, p. 160109. doi: 10.1038/sdata.2016.109.

Köhler, Schmithorst, Filippi, Ryan, Daria, Gunzer and Geiger (2009) 'Altered cellular dynamics and endosteal location of aged early hematopoietic progenitor cells revealed by time-lapse intravital imaging in long bones', *Blood*, 114(2), pp. 290–298. doi: 10.1182/blood-2008-12-195644.

Kopp, Avecilla, Hooper, Shmelkov, Ramos, Zhang and Rafii (2005) 'Tie2 activation contributes to hemangiogenic regeneration after myelosuppression', *Blood*, 106(2), pp. 505–513. doi: 10.1182/blood-2004-11-4269.

Kouzarides (2007) 'Chromatin Modifications and Their Function', *Cell*, pp. 693–705. doi: 10.1016/j.cell.2007.02.005.

Kubo, Li, Kurazumi, Takemoto, Ohshima, Murata, Katsura, Morikage, Furutani and Hamano (2012) 'Hypoxic Preconditioning Enhances Angiogenic Potential of Bone Marrow Cells With Aging-Related Functional Impairment', *Circulation Journal*, 76(4), pp. 986–994. doi: 10.1253/circj.CJ-11-0605.

Lapidot, Dar and Kollet (2005) 'How do stem cells find their way home?', *Blood*, 106(6), pp. 1901–1910. doi: 10.1182/blood-2005-04-1417.

Lara-Astiaso, Weiner, Lorenzo-Vivas, Zaretsky, Jaitin, David, Keren-Shaul, Mildner, Winter, Jung, *et al.* (2014) 'Chromatin state dynamics during blood formation.', *Science (New York, N.Y.)*, 55(August), pp. 1–10. doi: 10.1126/science.1256271.

Larsson and Karlsson (2005) 'The role of Smad signaling in hematopoiesis', *Oncogene*, 24(37), pp. 5676–5692. doi: 10.1038/sj.onc.1208920.

Lee, Shibata, Rao, Strahl and Lieb (2004) 'Evidence for nucleosome depletion at active regulatory regions genome-wide.', *Nature genetics*, 36(8), pp. 900–5. doi: 10.1038/ng1400.

Lee, Yi, Ahn, Lim, Hong, Cho, Lim, Song and Kwon (2014) 'Senescing human bone-marrow-derived clonal mesenchymal stem cells have altered lysophospholipid composition and functionality.', *Journal of proteome research*, 13(3), pp. 1438–49. doi: 10.1021/pr400990k.

Lewis, Vyse, Shields, Boeltz, Gordon, Spector, Lehner, Walczak and Vyse (2015) 'UBE2L3 polymorphism amplifies NF-κB activation and promotes plasma cell development, linking linear ubiquitination to multiple autoimmune diseases', *American Journal of Human Genetics*, 96(2), pp. 221–234. doi: 10.1016/j.ajhg.2014.12.024.

Li, Thomas, Sabo, Eisen, Stamatoyannopoulos and Biggin (2011) 'The role of chromatin accessibility in directing the widespread, overlapping patterns of Drosophila transcription factor binding.', *Genome Biology*, 12(4), p. R34. doi: 10.1186/gb-2011-12-4-r34.

Madan, Gogna, Bhatt, Pati, Kuppusamy and Mahdi (2011) 'Regulation of glucose metabolism by p53: emerging new roles for the tumor suppressor.', *Oncotarget*, 2(12), pp. 948–57. doi: 10.18632/oncotarget.389.

Mann (2006) 'Functional and quantitative proteomics using SILAC.', *Nature reviews. Molecular cell biology*, 7(12), pp. 952–8. doi: 10.1038/nrm2067.

Marie (2014) 'Bone cell senescence: Mechanisms and perspectives', *Journal of Bone and Mineral Research*, pp. 1311–1321. doi: 10.1002/jbmr.2190.

Méndez-Ferrer, Michurina, Ferraro, Mazloom, Macarthur, Lira, Scadden, Ma'ayan, Enikolopov and Frenette (2010) 'Mesenchymal and haematopoietic stem cells form a unique bone marrow niche.', *Nature*, 466(7308), pp. 829–34. doi: 10.1038/nature09262.

Miltenyi, Müller, Weichel and Radbruch (1990) 'High gradient magnetic cell separation with MACS.', *Cytometry*, 11(2), pp. 231–8. doi: 10.1002/cyto.990110203.

Moerman, Teng, Lipschitz and Lecka-Czernik (2004) 'Aging activates adipogenic and suppresses

osteogenic programs in mesenchymal marrow stroma/stem cells: The role of PPAR-??2 transcription factor and TGF-??/BMP signaling pathways', *Aging Cell*, 3(6), pp. 379–389. doi: 10.1111/j.1474-9728.2004.00127.x.

Montefiori, Hernandez, Zhang, Gilad, Ober, Crawford, Nobrega and Sakabe (2016) 'Reducing mitochondrial reads in ATAC-seq using CRISPR/Cas9', *bioRxiv*, (January), p. 87890. doi: 10.1101/087890.

Moore (2006) 'Stem Cells and Their Niches', *Science*, 311(5769), pp. 1880–1885. doi: 10.1126/science.1110542.

Muguruma, Yahata, Miyatake, Sato, Uno, Itoh, Kato, Ito, Hotta and Ando (2006) 'Reconstitution of the functional human hematopoietic microenvironment derived from human mesenchymal stem cells in the murine bone marrow compartment', *Blood*, 107(5), pp. 1878–1887. doi: 10.1182/blood-2005-06-2211.

Muller-Sieburg and Sieburg (2006) 'Clonal diversity of the stem cell compartment.', *Current Opinion in Hematology*, 13(4), pp. 243–248. doi: 10.1097/01.moh.0000231421.00407.65.

Nakamura-Ishizu and Suda (2013) 'Hematopoietic stem cell niche: An interplay among a repertoire of multiple functional niches', *Biochimica et Biophysica Acta - General Subjects*, pp. 2404–2409. doi: 10.1016/j.bbagen.2012.08.023.

Nakamura-Ishizu and Suda (2014) 'Aging of the hematopoietic stem cells niche', *International Journal of Hematology*, pp. 317–325. doi: 10.1007/s12185-014-1641-8.

Ni, Ebata, Alipanahiramandi and Lee (2012) 'Two SET domain containing genes link epigenetic changes and aging in Caenorhabditis elegans', *Aging Cell*, 11(2), pp. 315–325. doi: 10.1111/j.1474-9726.2011.00785.x.

Nilsson, Johnston, Whitty, Williams, Webb, Denhardt, Bertoncello, Bendall, Simmons and Haylock (2005) 'Osteopontin, a key component of the hematopoietic stem cell niche and regulator of primitive hematopoietic progenitor cells', *Blood*, 106(4), pp. 1232–1239. doi: 10.1182/blood-2004-11-4422.

Norris and Grimes (2012) 'Mouse models of ciliopathies: the state of the art', *Disease Models & Mechanisms*, 5(3), pp. 299–312. doi: 10.1242/dmm.009340.

Papayannopoulou, Craddock, Nakamoto, Priestley and Wolf (1995) 'The VLA4/VCAM-1 adhesion pathway defines contrasting mechanisms of lodgement of transplanted murine hemopoietic progenitors between bone marrow and spleen.', *Proceedings of the National Academy of Sciences of the United States of America*, 92(21), pp. 9647–9651. doi: 10.1073/pnas.92.21.9647.

Peters, Vorhagen, Brodesser, Jakobshagen, Brüning, Niessen and Krönke (2015) 'Ceramide synthase 4 regulates stem cell homeostasis and hair follicle cycling.', *The Journal of investigative dermatology*, 135(6), pp. 1501–9. doi: 10.1038/jid.2015.60.

Petzer, Hogge, Landsdorp, Reid and Eaves (1996) 'Self-renewal of primitive human hematopoietic cells (long-term-culture-initiating cells) in vitro and their expansion in defined medium.', *Proceedings of the National Academy of Sciences*, 93(4), pp. 1470–1474. doi: 10.1073/pnas.93.4.1470.

Pittenger (1999) 'Multilineage Potential of Adult Human Mesenchymal Stem Cells', *Science*, 284(5411), pp. 143–147. doi: 10.1126/science.284.5411.143.

Pittenger, Mackay, Beck, Jaiswal, Douglas, Mosca, Moorman, Simonetti, Craig and Marshak (1999) 'Multilineage potential of adult human mesenchymal stem cells', *Science*, 284(5411), pp. 143–147. doi: 10.1126/science.284.5411.143.

Polini, Pisignano, Parodi, Quarto and Scaglione (2011) 'Osteoinduction of human mesenchymal stem cells by bioactive composite scaffolds without supplemental osteogenic growth factors', *PLoS ONE*, 6(10). doi: 10.1371/journal.pone.0026211.

Pollina and Brunet (2011) 'Epigenetic regulation of aging stem cells', *Oncogene*, 30(28), pp. 3105–3126. doi: 10.1038/onc.2011.45.

Ponomaryov, Peled, Petit, Taichman, Habler, Sandbank, Arenzana-Seisdedos, Magerus, Caruz, Fujii, *et al.* (2000) 'Induction of the chemokine stromal-derived factor-1 following DNA damage improves human stem cell function', *Journal of Clinical Investigation*, 106(11), pp. 1331–1339. doi: 10.1172/JCI10329.

Popovici, Zhang, Grégoire, Jonveaux, Lafage-Pochitaloff, Birnbaum and Pébusque (1999) 'The t(6;8)(q27;p11) translocation in a stem cell myeloproliferative disorder fuses a novel gene, FOP, to fibroblast growth factor receptor 1.', *Blood*, 93(4), pp. 1381–9.

Priller, Bauer, Mitteregger, Krebs, Kretzschmar and Herms (2006) 'Synapse Formation and Function Is Modulated by the Amyloid Precursor Protein', *The Journal of Neuroscience*, 26(27), pp. 7212–7221. doi: 10.1523/JNEUROSCI.1450-06.2006.

Qian, Buza-Vidas, Hyland, Jensen, Antonchuk, Månsson, Thoren, Ekblom, Alexander and Jacobsen (2007) 'Critical Role of Thrombopoietin in Maintaining Adult Quiescent Hematopoietic Stem Cells', *Cell Stem Cell*, 1(6), pp. 671–684. doi: 10.1016/j.stem.2007.10.008.

Qu, Zaba, Giresi, Li, Longmire, Kim, Greenleaf and Chang (2015) 'Individuality and Variation of Personal Regulomes in Primary Human T Cells', *Cell Systems*, 1(1), pp. 51–61. doi: 10.1016/j.cels.2015.06.003.

Ramirez, El-Ali, Mager, Wyman, Conesa and Mortazavi (2017) 'Dynamic Gene Regulatory Networks of Human Myeloid Differentiation', *Cell Systems*, 4(4), p. 416–429.e3. doi: 10.1016/j.cels.2017.03.005.

Rando and Chang (2012) 'Aging, rejuvenation, and epigenetic reprogramming: Resetting the aging clock', *Cell*, pp. 46–57. doi: 10.1016/j.cell.2012.01.003.

Reynolds, Maurer and Kolesnick (2004) 'Ceramide synthesis and metabolism as a target for cancer therapy', *Cancer Letters*, pp. 169–180. doi: 10.1016/j.canlet.2003.08.034.

Rippo, Babini, Prattichizzo, Graciotti, Fulgenzi, Tomassoni Ardori, Olivieri, Borghetti, Cinti, Poloni, *et al.* (2013) 'Low FasL levels promote proliferation of human bone marrow-derived mesenchymal stem cells, higher levels inhibit their differentiation into adipocytes.', *Cell death & disease*, 4(4), p. e594. doi: 10.1038/cddis.2013.115.

Ross (2000) 'Inhibition of Adipogenesis by Wnt Signaling', *Science*, 289(5481), pp. 950–953. doi: 10.1126/science.289.5481.950.

Rossi, Bryder, Zahn, Ahlenius, Sonu, Wagers and Weissman (2005) 'Cell intrinsic alterations underlie hematopoietic stem cell aging', *Proceedings of the National Academy of Sciences*, 102(26), pp. 9194–9199. doi: 10.1073/pnas.0503280102.

Rossi, Jamieson and Weissman (2008) 'Stems Cells and the Pathways to Aging and Cancer', *Cell*, pp. 681–696. doi: 10.1016/j.cell.2008.01.036.

Schofield (1978) 'The relationship between the spleen colony-forming cell and the haemopoietic stem cell.', *Blood cells*, 4(1–2), pp. 7–25. doi: Chronic ischaemic mitral regurgitation. Current treatment results and new mechanism-based surgical approaches☆.

Schuurs-Hoeijmakers, Landsverk, Foulds, Kukolich, Gavrilova, Greville-Heygate, Hanson-Kahn, Bernstein, Glass, Chitayat, *et al.* (2016) 'Clinical delineation of the PACS1-related syndrome-Report on 19 patients', *American Journal of Medical Genetics, Part A*, 170(3), pp. 670–675. doi: 10.1002/ajmg.a.37476.

Schweitzer and Scaiano (2003) 'Selective binding and local photophysics of the fluorescent cyanine dye PicoGreen in double-stranded and single-stranded DNA', *Physical Chemistry Chemical Physics*, 5(21), p. 4911. doi: 10.1039/b305921a.

Segal and Widom (2009) 'What controls nucleosome positions?', *Trends in Genetics*, pp. 335–343. doi: 10.1016/j.tig.2009.06.002.

Seita and Weissman (2010) 'Hematopoietic stem cell: Self-renewal versus differentiation', *Wiley Interdisciplinary Reviews: Systems Biology and Medicine*, pp. 640–653. doi: 10.1002/wsbm.86.

Sensebé, Krampera, Schrezenmeier, Bourin and Giordano (2010) 'Mesenchymal stem cells for clinical application', *Vox Sanguinis*, pp. 93–107. doi: 10.1111/j.1423-0410.2009.01227.x.

Sethe, Scutt and Stolzing (2006) 'Aging of mesenchymal stem cells', *Ageing Research Reviews*, pp. 91–116. doi: 10.1016/j.arr.2005.10.001.

Shah, Donahue, Otte, Capell, Nelson, Cao, Aggarwala, Cruickshanks, Rai, McBryan, *et al.* (2013) 'Lamin B1 depletion in senescent cells triggers large-scale changes in gene expression and the chromatin landscape', *Genes and Development*, 27(16), pp. 1787–1799. doi: 10.1101/gad.223834.113.

Shi, Liu and Wang (2011) 'Immunomodulatory properties and therapeutic application of mesenchymal stem cells', *Clinical and Experimental Immunology*, pp. 1–8. doi: 10.1111/j.1365-2249.2011.04327.x.

Shu, Chen, Bo and Wang (2011) 'Genome-wide analysis of the relationships between DNaseI HS, histone modifications and gene expression reveals distinct modes of chromatin domains', *Nucleic Acids Research*, 39(17), pp. 7428–7443. doi: 10.1093/nar/gkr443.

Shuler, Aris and Tsuchiya (1972) 'Hydrodynamic focusing and electronic cell-sizing techniques.', *Applied microbiology*, 24(3), pp. 384–388.

Sidney, Branch, Dunphy, Dua and Hopkinson (2014) 'Concise review: Evidence for CD34 as a common marker for diverse progenitors', *Stem Cells*, pp. 1380–1389. doi: 10.1002/stem.1661.

Siebold, Banerjee, Tie, Kiss, Moskowitz and Harte (2010) 'Polycomb Repressive Complex 2 and Trithorax modulate Drosophila longevity and stress resistance', *Proceedings of the National Academy of Sciences*, 107(1), pp. 169–174. doi: 10.1073/pnas.0907739107.

Siersbaek, Nielsen and Mandrup (2010) 'PPARgamma in adipocyte differentiation and metabolism--novel insights from genome-wide studies.', *FEBS letters*, 584(15), pp. 3242–9. doi: 10.1016/j.febslet.2010.06.010.

Signer, Montecino-Rodriguez, Witte, McLaughlin and Dorshkind (2007) 'Age-related defects in B lymphopoiesis underlie the myeloid dominance of adult leukemia', *Blood*, 110(6), pp. 1831–1839. doi: 10.1182/blood-2007-01-069401.

Siminovitch, McCulloch and Till (1963) 'The distribution of colony-forming cells among spleen colonies', *Journal of Cellular and Comparative Physiology*, 62(3), pp. 327–336. doi: 10.1002/jcp.1030620313.

Simmons, Masinovsky, Longenecker, Berenson, Torok-Storb and Gallatin (1992) 'Vascular cell adhesion molecule-1 expressed by bone marrow stromal cells mediates the binding of hematopoietic progenitor cells.', *Blood*, 80(2), pp. 388–95.

Simon and Kingston (2013) 'Occupying Chromatin: Polycomb Mechanisms for Getting to Genomic Targets, Stopping Transcriptional Traffic, and Staying Put', *Molecular Cell*, pp. 808–824. doi: 10.1016/j.molcel.2013.02.013.

Stenderup, Justesen, Clausen and Kassem (2003) 'Aging is associated with decreased maximal life span and accelerated senescence of bone marrow stromal cells', *Bone*, 33(6), pp. 919–926. doi: 10.1016/j.bone.2003.07.005.

Stier, Ko, Forkert, Lutz, Neuhaus, Grunewald, Cheng, Dombkowski, Calvi, Rittling, *et al.* (2005) 'Osteopontin is a hematopoietic stem cell niche component that negatively regulates stem cell pool size', *J Exp Med*, 201(11), pp. 1781–1791. doi: jem.20041992 [pii] 10.1084/jem.20041992.

Sudo, Ema, Morita and Nakauchi (2000) 'Age-associated characteristics of murine hematopoietic stem cells.', *The Journal of experimental medicine*, 192(9), pp. 1273–1280. doi: 10.1084/jem.192.9.1273.

Sun, Luo, Jeong, Rodriguez, Xia, Hannah, Wang, Le, Faull, Chen, *et al.* (2014) 'Epigenomic profiling of young and aged HSCs reveals concerted changes during aging that reinforce self-renewal', *Cell Stem Cell*, 14(5), pp. 673–688. doi: 10.1016/j.stem.2014.03.002.

Sutherland, Eaves, Eaves, Dragowska and Lansdorp (1989) 'Characterization and partial purification of human marrow cells capable of initiating long-term hematopoiesis in vitro', *Blood*, 74(5), pp. 1563–

1570.

Till and McCulloch (1961) ‘A Direct Measurement of the Radiation Sensitivity of Normal Mouse Bone Marrow Cells’, *Radiation Research*, 14(2), p. 213. doi: 10.2307/3570892.

Tonks (2006) ‘Protein tyrosine phosphatases: from genes, to function, to disease’, *Nat Rev Mol Cell Biol*, 7(11), pp. 833–846. doi: 10.1038/nrm2039.

Tsurumi and Li (2012) ‘Global heterochromatin loss: A unifying theory of aging?’, *Epigenetics*, 7(7), pp. 680–688. doi: 10.4161/epi.20540.

Tuljapurkar, Mcguire, Brusnahan, Jackson, Garvin, Kessinger, Lane, O’Kane and Sharp (2011) ‘Changes in human bone marrow fat content associated with changes in hematopoietic stem cell numbers and cytokine levels with aging’, *Journal of Anatomy*, 219(5), pp. 574–581. doi: 10.1111/j.1469-7580.2011.01423.x.

Ucar, Márquez, Chung, Marches, Rossi, Uyar, Wu, George, Stitzel, Palucka, *et al.* (2017) ‘The chromatin accessibility signature of human immune aging stems from CD8 $^{+}$ T cells’, *The Journal of Experimental Medicine*, p. jem.20170416. doi: 10.1084/jem.20170416.

Vaca Jacome, Rabilloud, Schaeffer-Reiss, Rompais, Ayoub, Lane, Bairoch, Van Dorsselaer and Carapito (2015) ‘N-terminome analysis of the human mitochondrial proteome’, *Proteomics*, 15(14), pp. 2519–2524. doi: 10.1002/pmic.201400617.

Verovskaya, Campbell and Passegué (2017) ‘Bone marrow niches and HSC fates’, *Nature Reviews Immunology*, Poster.

Wagner, Ansorge, Wirkner, Eckstein, Schwager, Blake, Miesala, Selig, Saffrich, Ansorge, *et al.* (2004) ‘Molecular evidence for stem cell function of the slow-dividing fraction among human hematopoietic progenitor cells by genome-wide analysis’, *Blood*, 104(3), pp. 675–686. doi: 10.1182/blood-2003-10-3423.

Wagner, Bork, Horn, Krunic, Walenda, Diehlmann, Benes, Blake, Huber, Eckstein, *et al.* (2009) ‘Aging and replicative senescence have related effects on human stem and progenitor cells’, *PLoS ONE*, 4. doi: 10.1371/journal.pone.0005846.

Wagner, Feldmann, Seckinger, Maurer, Wein, Blake, Krause, Kalenka, Bürgers, Saffrich, *et al.* (2006) ‘The heterogeneity of human mesenchymal stem cell preparations--evidence from simultaneous analysis of proteomes and transcriptomes.’, *Experimental hematology*, 34, pp. 536–548. doi: 10.1016/j.exphem.2006.01.002.

Wagner, Roderburg, Wein, Diehlmann, Frankhauser, Schubert, Eckstein and Ho (2007) ‘Molecular and secretory profiles of human mesenchymal stromal cells and their abilities to maintain primitive hematopoietic progenitors.’, *Stem cells*, 25, pp. 2638–2647. doi: 2007-0280 [pii]\n10.1634/stemcells.2007-0280.

Wagner, Saffrich and Ho (2008) ‘The stromal activity of mesenchymal stromal cells’, *Transfusion Medicine and Hemotherapy*, pp. 185–193. doi: 10.1159/000128956.

Walenda, Bork, Horn, Wein, Saffrich, Diehlmann, Eckstein, Ho and Wagner (2010) ‘Co-culture with mesenchymal stromal cells increases proliferation and maintenance of haematopoietic progenitor cells’, *Journal of Cellular and Molecular Medicine*, 14(1–2), pp. 337–350. doi: 10.1111/j.1582-4934.2009.00776.x.

Wang, Hisha, Taketani, Adachi, Li, Cui, Cui, Wang, Song, Mizokami, *et al.* (2006) ‘Characterization of mesenchymal stem cells isolated from mouse fetal bone marrow.’, *Stem cells (Dayton, Ohio)*, 24(3), pp. 482–93. doi: 10.1634/stemcells.2005-0219.

Wanka, Steinbach and Rieger (2012) ‘Tp53-induced glycolysis and apoptosis regulator (TIGAR) protects glioma cells from starvation-induced cell death by up-regulating respiration and improving cellular redox homeostasis’, *Journal of Biological Chemistry*, 287(40), pp. 33436–33446. doi: 10.1074/jbc.M112.384578.

Wasserman and Sandelin (2004) ‘Applied bioinformatics for the identification of regulatory elements’, *Nature Reviews Genetics*, 5(4), pp. 276–287. doi: 10.1038/nrg1315.

Weilbaecher, Weissman, Blume and Heimfeld (1991) ‘Culture of phenotypically defined hematopoietic stem cells and other progenitors at limiting dilution on Dexter monolayers.’, *Blood*, 78(4), pp. 945–52.

Wilson and Trumpp (2006) ‘Bone-marrow haematopoietic-stem-cell niches.’, *Nature reviews. Immunology*, 6, pp. 93–106. doi: 10.1038/nri1779.

Winnefeld and Lyko (2012) ‘The aging epigenome: DNA methylation from the cradle to the grave.’, *Genome biology*, 13(7), p. 165. doi: 10.1186/gb4033.

Yang (2009) ‘Krüppel-like factors in cancers’, in *The Biology of Krüppel-like Factors*, pp. 205–219. doi: 10.1007/978-4-431-87775-2-16.

Yang, Han, Suarez Saiz and Minden (2007) ‘A tumor suppressor and oncogene: the WT1 story.’, *Leukemia : official journal of the Leukemia Society of America, Leukemia Research Fund, U.K*, 21(5), pp. 868–876. doi: 10.1038/sj.leu.2404770.

Yoshihara, Arai, Hosokawa, Hagiwara, Takubo, Nakamura, Gomei, Iwasaki, Matsuoka, Miyamoto, *et al.* (2007) ‘Thrombopoietin/MPL Signaling Regulates Hematopoietic Stem Cell Quiescence and Interaction with the Osteoblastic Niche’, *Cell Stem Cell*, 1(6), pp. 685–697. doi: 10.1016/j.stem.2007.10.020.

Zepeda-Moreno, Taubert, Hellwig, Hoang, Pietsch, Lakshmanan, Wagner and Ho (2011) ‘Innovative method for quantification of cell-cell adhesion in 96-well plates.’, *Cell adhesion & migration*, 5(3), pp. 215–219. doi: 10.4161/cam.5.3.14648.

Zhang, Liu, Meyer, Eeckhoute, Johnson, Bernstein, Nussbaum, Myers, Brown, Li, *et al.* (2008) ‘Model-based Analysis of ChIP-Seq (MACS)’, *Genome Biology*, 9(9), p. R137. doi: 10.1186/gb-2008-9-9-r137.

Zhang, Niu, Ye, Huang, He, Tong, Ross, Haug, Johnson, Feng, *et al.* (2003) ‘Identification of the haematopoietic stem cell niche and control of the niche size’, *Nature*, 425(6960), pp. 836–841. doi: 10.1038/nature02041.

Zhao, Duan, Reyes, Keene, Verfaillie and Low (2002) ‘Human bone marrow stem cells exhibit neural phenotypes and ameliorate neurological deficits after grafting into the ischemic brain of rats.’, *Experimental neurology*, 174(1), pp. 11–20. doi: 10.1006/exnr.2001.7853.

Zhou, Greenberger, Epperly, Goff, Adler, Leboff and Glowacki (2008) ‘Age-related intrinsic changes in human bone-marrow-derived mesenchymal stem cells and their differentiation to osteoblasts’, *Aging Cell*, 7(3), pp. 335–343. doi: 10.1111/j.1474-9726.2008.00377.x.

7. Supplementary Material

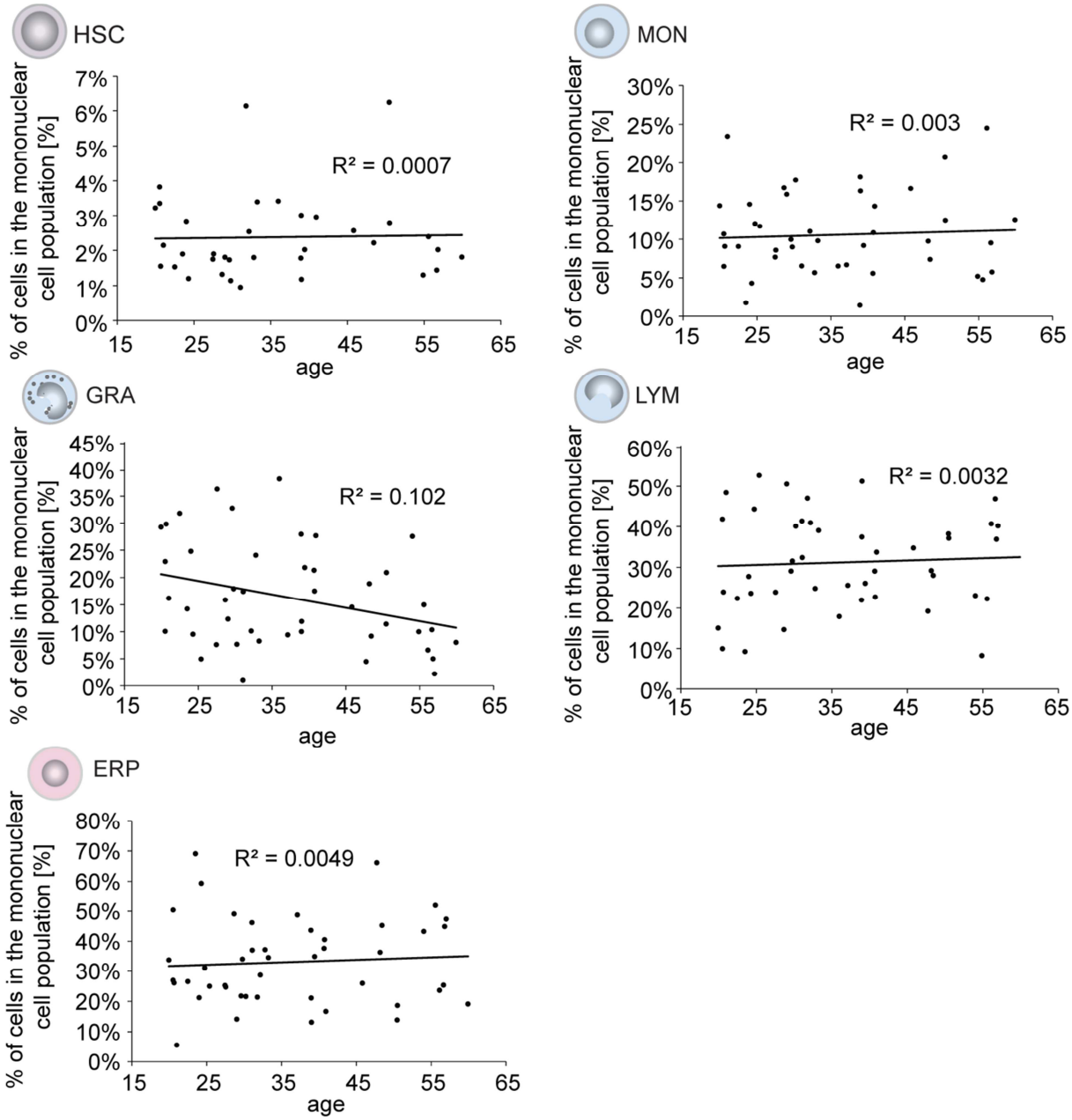

Figure 1 The relative percentages of cell types HSC, LYM, MON, GRA and ERP in the mononuclear cell population are not linearly correlated with age of the donor. The numbers of the analyzed samples are n=35 for HSC, n=45 for LYM, n=40 for MON, n=44 for GRA and n=45 for ERP. The coefficients of determination R^2 of the linear correlation test are shown for each cell type. ERP, erythroid precursors; MON, monocytes, macrophages and restricted precursors; GRA, granulocytic precursors; LYM, lymphocytes and restricted precursors; HSC, hematopoietic stem cells.

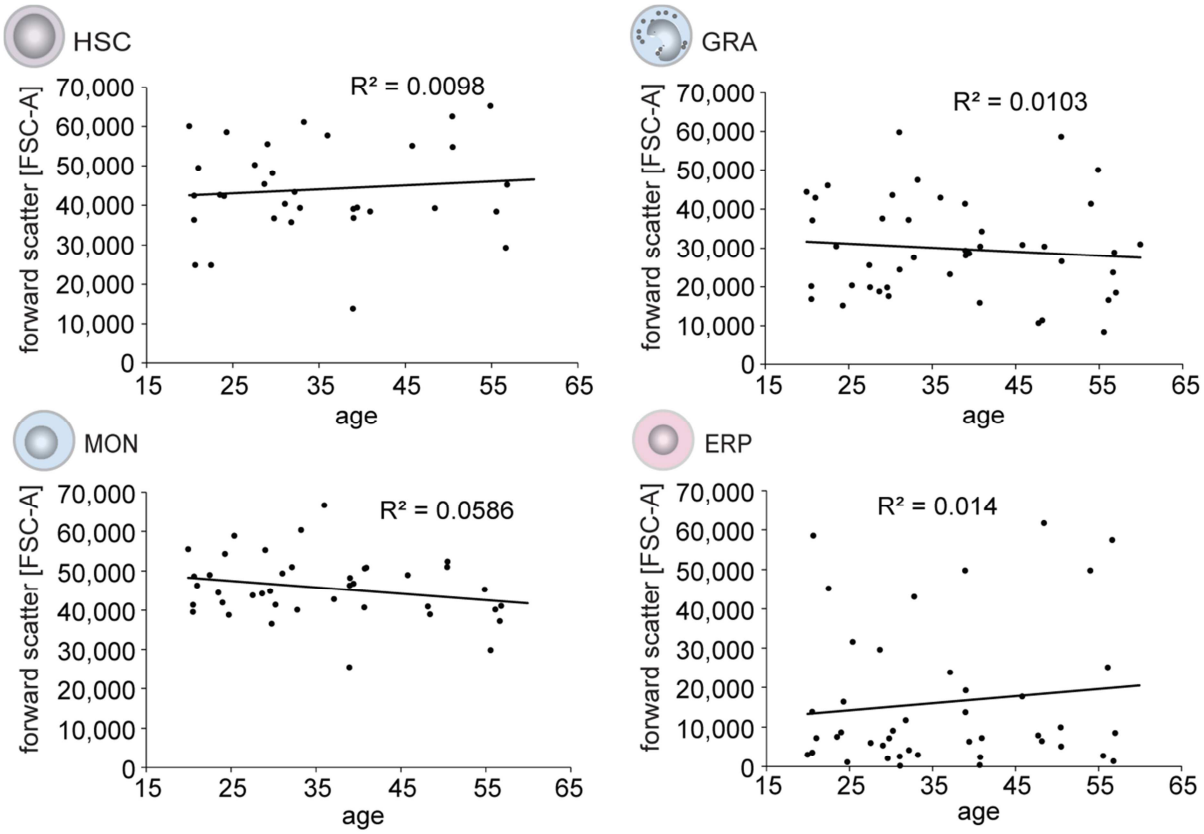

Figure 2 The relative cell sizes of cell types HSC, MON, GRA and ERP in the mononuclear cell population are not linearly correlated with age of the donor. The numbers of the analyzed samples are n=33 for HSC, n=40 for MON, n=44 for GRA and n=43 for ERP. The coefficients of determination R^2 of the linear correlation test are shown for each cell type. ERP, erythroid precursors; MON, monocytes, macrophages and restricted precursors; GRA, granulocytic precursors; LYM, lymphocytes and restricted precursors; HSC, hematopoietic stem cells.

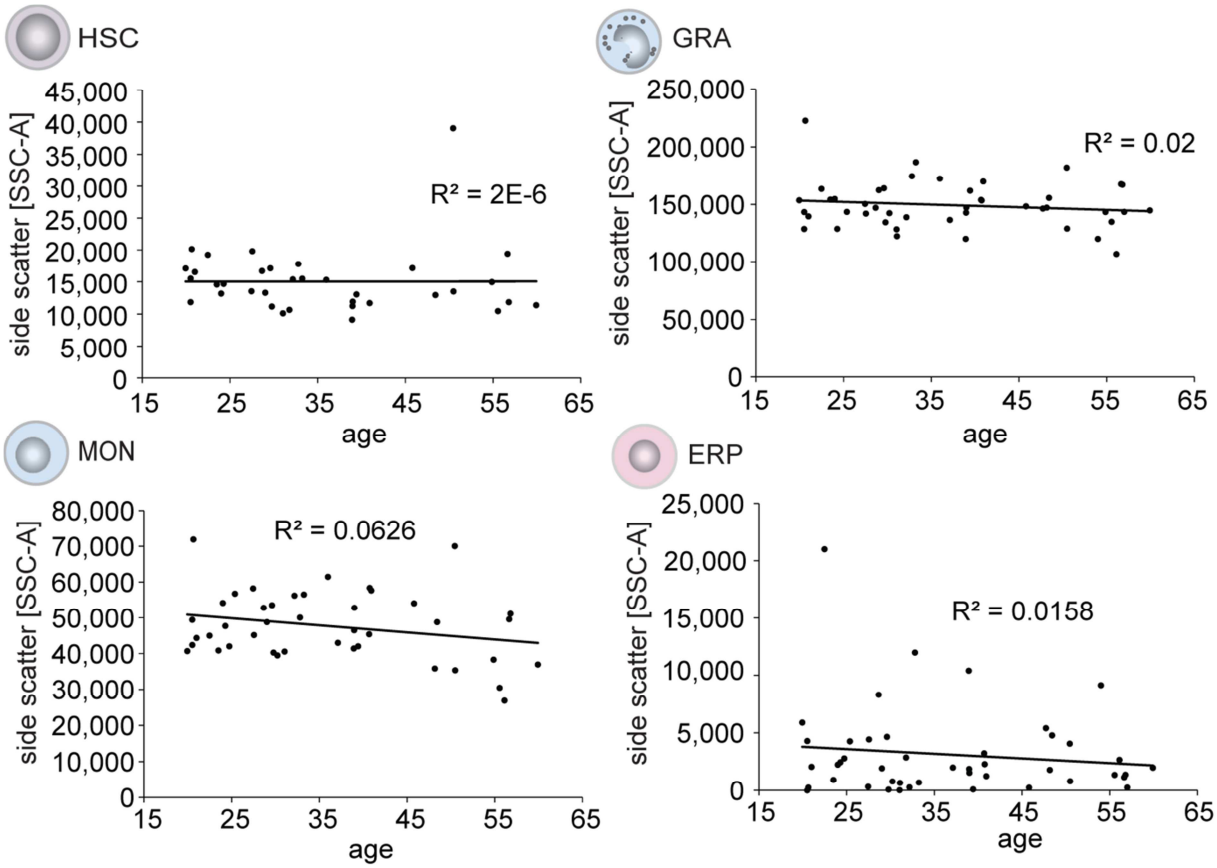

Figure 3 The relative cell granularity of cell types HSC, MON, GRA and ERP in the mononuclear cell population are not linearly correlated with age of the donor. The numbers of the analyzed samples are n=33 for HSC, n=40 for MON, n=44 for GRA and n=43 for ERP. The coefficients of determination R^2 of the linear correlation test are shown for each cell type. ERP, erythroid precursors; MON, monocytes, macrophages and restricted precursors; GRA, granulocytic precursors; LYM, lymphocytes and restricted precursors; HSC, hematopoietic stem cells.

Table 1 Spearman correlation test of the myeloid to lymphoid ratios with age of the donors. The p-values of Spearman's rank correlation were indicated here suggesting a non-correlation of the variables with donor age (p-value <0.01).

myeloid to lymphoid ratio	0.18
normalized myeloid to lymphoid ratio	0.49

Table 2 Spearman correlation test of the relative proportion, cell size, and granularity with age of the donors. The p-values of Spearman's rank correlation were indicated here suggesting a non-correlation of the variables with donor age (p-value <0.01).

	HSC	LYM	MON	GRA	ERP
Relative proportions	0.95	0.63	0.82	0.02	0.82
Relative cell size	0.84	N/A	0.28	0.58	0.77
Relative cell granularity	0.12	N/A	0.29	0.91	0.61

Table 3 Gene ontology (GO) and KEGG enrichment analysis. An enrichment analysis was carried out on a total set of 3,580 genes annotated to differential ATAC-seq peaks. The ID of the GO-term, the term description, the p-value, the percentage of associated genes and the number of genes are indicated by the table.

GO-term	Description	Term p-value	% of associated genes	Number of genes
GO:0007399	nervous system development	5.9E-26	21.6	510
GO:0009653	anatomical structure morphogenesis	2.5E-21	20.5	523
GO:2000026	regulation of multicellular organismal development	1.3E-19	21.6	392
GO:0050793	regulation of developmental process	9.3E-19	20.3	486
GO:0045595	regulation of cell differentiation	2.5E-18	21.8	353
GO:0000975	regulatory region DNA binding	1.3E-07	20.7	175
GO:0000981	RNA polymerase II transcription factor activity	1.9E-07	21.2	156
GO:0003690	double-stranded DNA binding	2.7E-07	20.7	167
GO:0022836	gated channel activity	3.2E-07	24.7	83
GO:0004714	transmembrane receptor protein tyrosine kinase activity	1.1E-06	37.7	26
GO:0004390	Hippo signaling pathway	1.1E-05	32.2	47
GO:0005200	Pathways in cancer	4.4E-05	25.8	94

GO:0004350	TGF-beta signaling pathway	1.7E-04	35.5	27
GO:0004510	Focal adhesion	3.6E-04	28.0	52

Table 4 The top 50 significant ATAC-seq peaks located in promoter regions ranked by p-value as well as median ATAC-seq signal intensity.

PeakID	P-value	Median signal intensity	Gene Name
chr6_167412488_167412988	0	323.4997317	FGFR1OP
chr12_4430025_4430525	0	284.5970705	TIGAR
chr2_166810129_166810629	0	181.9555041	TTC21B
chr2_169312476_169312976	0	157.4173981	CERS6
chr20_18118279_18118779	0	92.95253727	PET117
chr3_18486479_18486979	0	74.64841193	SATB1-AS1
chr11_17756345_17756845	0	48.35672059	KCNC1
chr6_166401439_166401939	0	45.50989939	LINC00473
chr2_47797830_47798814	0	41.98973171	KCNK12
chr11_117699307_117699807	0	35.27716776	FXYD2
chr9_27529534_27530034	0	34.14140805	MOB3B
chr7_8301489_8301989	0	30.35618571	ICA1
chr3_238823_239323	0	25.48554366	CHL1
chr3_68981497_68981997	0	22.60781782	FAM19A4
chr4_3578362_3578862	0	22.18336648	LINC00955
chr9_68455180_68455680	0	18.42118489	FRG1JP
chr1_144994687_144995187	0	18.07891226	PDE4DIP
chr6_62995941_62996441	0	16.32934011	KHDRBS2
chr4_190579577_190580077	0	16.32934011	LINC01262
chr7_63505541_63506041	0	10.50791044	ZNF727
chr11_92702622_92703122	0.000131956	20.09583806	MTNR1B
chr1_231298130_231298630	0.000134053	29.18864011	TRIM67
chr12_131355991_131356491	0.000134332	150.0296102	RAN
chr2_71127513_71128013	0.000141291	91.26859785	VAX2
chr6_11044326_11044826	0.000158056	30.0150118	ELOVL2
chr22_34316954_34317454	0.000163652	169.2844816	LARGE
chr3_12329296_12329796	0.000185944	29.87373204	PPARG
chr11_57227851_57228351	0.000199059	29.10231199	RTN4RL2
chr17_38574020_38574520	0.000211472	96.80965922	TOP2A
chr11_115630573_115631073	0.000248984	25.60605604	LINC00900
chr20_29611600_29612100	0.000266491	65.37872211	FRG1BP

chr12_9217103_9217603	0.000284935	60.12859862	LINC00612
chr1_6480542_6481042	0.000284935	17.49572154	HES2
chr20_17207223_17207723	0.000293714	37.94523214	PCSK2
chr11_115374977_115375477	0.0003215	52.07581907	CADM1
chr7_158497441_158497941	0.000359942	309.6742713	NCAPG2
chr9_103189251_103189751	0.000396524	58.32490542	MSANTD3
chr20_33759525_33760025	0.000460685	92.76361948	PROCR
chr3_192958713_192959213	0.000468462	57.79350741	HRASLS
chr6_146864518_146865018	0.000469786	282.2643076	RAB32
chr17_46018600_46019100	0.000481451	81.08584411	PNPO
chr7_73038649_73039149	0.000490928	23.01707925	MLXIPL
chr12_44199888_44200388	0.000494501	98.22030298	TWF1
chr2_14772516_14773016	0.00051887	132.2979562	FAM84A
chr2_211341234_211341734	0.000525976	135.4352901	LANCL1
chr10_123356608_123357108	0.000617643	14.56316781	FGFR2
chr7_86688723_86689223	0.000620645	61.23502541	KIAA1324L
chr6_90121699_90122199	0.000628877	25.464523	RRAGD
chr1_211307313_211307813	0.000635654	132.5164261	KCNH1
chr7_3340439_3340939	0.000635654	93.40364835	SDK1